2015

Ligh Extraction and Nanomaterials for III-Nitride Based White Light-Emitting Diode

Peifen Zhu
Lehigh University

Light Extraction and Nanomaterials for III-Nitride Based White Light-Emitting Diodes

by

Peifen Zhu

Presented to the Graduate and Research Committee

of Lehigh University

in Candidacy for the Degree of

Doctor of Philosophy

in

Electrical Engineering

Lehigh University

January 2015

Copyright Page

DISSERTATION SIGNATURE SHEET

Approved and recommended for acceptance as a dissertation in partial fulfillment of the requirements for the degree of Doctor of Philosophy.

Date

Prof. Nelson Tansu, PhD Advisor

Accepted Date

Committee Members:

Prof. Nelson Tansu, Chair

Prof. David Richard Decker

Prof. Daniel Ou-Yang

Prof. Chao Zhou

Acknowledgement

I would like to express my sincerest gratitude to my Ph.D. advisor, Prof. Nelson Tansu, for providing me with the opportunity and great environment to pursue my Ph.D. studies in his group. His remarkable ideas lead me into the field of light-emitting diode (LED). His continuous support, invaluable guidance and inspiration enable me to complete my research project. I am truly indebted to him for helping me in my professional development.

I am also deeply grateful to Prof. David Richard Decker, and Prof. Daniel Ou-Yang, Prof. Chao Zhou for serving in my Ph.D. committee and providing valuable comments. I am also indebted to Prof . Weiping Qin at Jilin University for his advices and support during my early stage of Ph.D. pursuit.

I would like to express my sincere gratitude to my research mates for their assistance during my Ph.D. studies at Lehigh: Dr. Mohammad Jamil, Dr. Guangyu Liu (Intel), Prof. Jing Zhang (Rochester Institute of Technology), Dr. Te Li, Chee-Keong Tan, and Wei Sun, Guosong Zeng. I am proud to be part of the team with them. I am also grateful to Anthony Jeffers, our cleanroom manager for the cleanroom training and for the maintenance of the facilities and equipment. I also want to thank all the faculties, research fellows and staffs who taught me, trained me and helped me at Lehigh

I would also like to thank the professors at Lehigh University: Prof. Yujie Ding, Prof. David Richard Decker, Prof. James D. Gunton, and Prof. Michael J. Stavola. They provided me strong knowledge about mathematics, physics, semiconductor devices, and photonics. Without the knowledge I learned from their class, I could not accomplish my Ph.D. study.

I am very grateful for the professors and friends at Lehigh University, who has been helping me, supporting me for long time. Without their support and help, I could not finish my Ph.D. study.

Most importantly, I am deeply indebted to my parents, sisters and brothers for their unconditional love, everlasting faith in me, and encouraging support for many years of pursuit of academic career. Special thanks go to my husband Hongyang Zhu, My daughter Lily Zhu and my parents in law, Jieliang Zhu and Qinghua Zhang for their everlasting support, continuous encouragement, who gave me strength to overcome the innumerable obstacles that I encountered during my Ph.D. study.

Table of Contents

List of Figures

Abstract

The importance of having low-cost and practical technology for improving the efficiency of solid-state lighting is key for the practical implementation of this technology for general illumination market. The thin-film flip-chip (TFFC) LED has been pursued as the state-of-the-art LED technology, which has been shown to have improved extraction by 1.6 times over the conventional planar LED technology. The combination of the thin-film concept with flip-chip technology provided surface brightness and flux output advantages over conventional LED, and currently the TFFC LEDs are widely used in industry for improved performance. To improve the light extraction further in TFFC LEDs, both surface roughness and photonic crystal methods had been implemented.

In this thesis, the use of self-assembled colloidal microlens arrays with rapid convective deposition (RCD) method will be demonstrated in both GaN and organic LEDs. The use of rapid convective deposition method enables roll-to-roll printing process of microsphere and nanosphere arrays on large wafer area applicable for manufacturing of large area LED technology. Comprehensive studies were carried out to analyze the light extraction efficiency of conventional top-emitting III-Nitride LEDs with microsphere arrays and TFFC LEDs with microsphere arrays deposited via rapid convective deposition process. The device structure was engineered to achieve optimum light extraction by varying refractive indices of spheres, the diameters of spheres, packing density and packing geometry of microsphere arrays. The optimized device structure is TFFC LED with hexagonal close-packed TiO_2 sphere arrays. The use of hexagonal close-packed monolayer of TiO_2 microsphere arrays on TFFC LED results in light extraction of 75%, which is 3.6 times higher than that of TFFC LEDs with planar surface. Further optimization by using microlens arrays on TFFC LED results in light extraction efficiency of 86%, which is 1.3 times higher than that of state-of-the-art TFFC LED with surface roughness approach. The key advantage of the self-assembled colloidal process is the ability for implementation of roll-to-roll printing method for large wafer scale manufacturing process.

Chapter 1 Introduction

1.1 III-Nitride based Light-emitting Diode for Solid-State Lighting

Group III Nitride semiconductors have three different crystal structures: wurtzite, zinc blend, and rock salt [1]. Among these three structures, the wurtzite structure is thermodynamically stable. The wurzite structure is of hexagonal unit cell and it contains six atoms of each type. The space group is $P6_3mc$. The wurtzite structure consists of two interpenetrating hexagonal close-packed sublattices, each with one type of lattices, offset along the c-axis by 5/8 of the cell height.

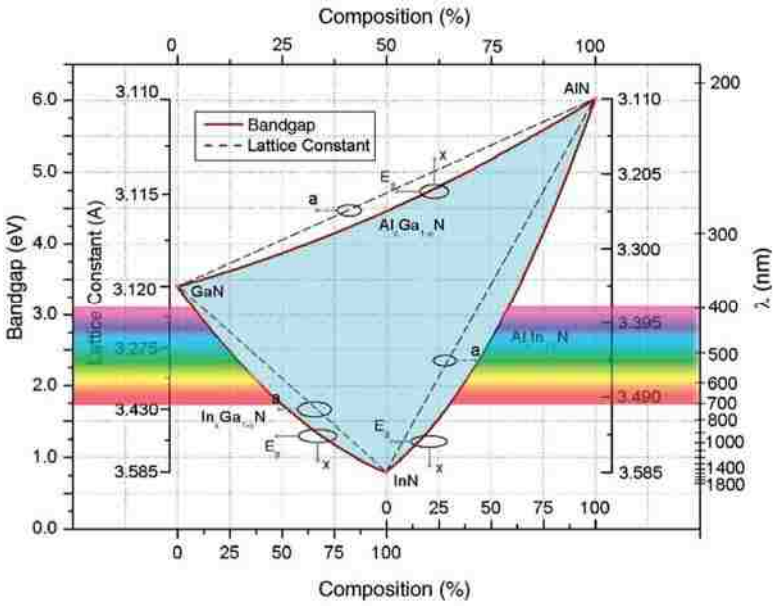

Figure 1-1. The band gap and lattice constant of $In_xGa_{1-x}N$, $Al_xIn_{1-x}N$, and $Al_xGa_{1-x}N$ with various compositions [1].

GaN, InN and AlN as well as their ternary and quaternary alloys are considered as one of the most important groups of semiconductor after Si for their various applications in general illumination, displays, consumer electronics, lasers, detectors, solar cells due to their excellent optical, electronic properties, as well as their tunable band gap from 0.7 eV to 6 eV as shown in Figure 1-1[1].

Solid-state lighting (SSL) is a lighting technology which uses semiconductor light-emitting diode, organic light-emitting diode and polymer light-emitting diode as source of illumination instead of electrical filaments, plasma and gas. In recent years, it has emerged as a promising new lighting technology that could fundamentally improve lighting system and has the potential to reduce the energy consumption by one half. SSL is controllable and directional, with the potential to change the way we illuminate buildings and outdoor areas by putting the light where it is needed, when it is needed, while eliminating the wasted light and drawing just a fraction of power used by traditional light sources.

Light-emitting diode (LED) directly converts the electricity to light. It is a p-n junction device and it converts electrical power into visible light through spontaneous emission, the wavelength of which is determined by the bandgap of semiconductor and the photons emitted in random directions. The advent of bright-blue LEDs based on InGaN materials in the mid-1990s is a landmark achievement in SSL [2]. White-light sources based on InGaN LEDs have a promising future in general illumination with the advantages over conventional light sources (e.g., incandescent, fluorescence and high intensity discharge lamps), as they are energy-saving, compact, and environmentally friendly. There are three approaches to generate white light [2, 3]: 1) blue LED pumps yellow phosphors or green and red phosphors, 2) UV LED pumps blue and yellow phosphors or blue, green and red phosphors [4-6], and 3) multi-chip approach that combines blue, green, and red LEDs. The first two approaches bases on phosphor-converted LEDs with advantage of low cost, high efficiency and color stability over a wide range of temperatures. White light based on the blue LEDs is commonly used as a simple long-life white-light source due to its efficiency and stability. Among them, the most popular approach for commercial white LEDs is made by coating an InGaN blue LED with a yellow-emitting phosphors, which has led to its wide use in the various outdoor lighting applications. The first as well as the most

widely used yellow phosphor is Ce^{3+}-doped $Y_3Al_5O_{12}$ (YAG: Ce^{3+}) owing to its many favorable properties such as strong absorption of blue light (~420-480 nm), broad emission band in the visible region (500-700 nm), fast luminescence decay time (<100 ns), high external quantum efficiency (~90% under blue LED excitation) [7], remarkable chemical and thermal stability and easy to synthesize. Due to these advantages, white LEDs made of the blue LED and YAG: Ce^{3+} phosphors are currently the mainstream in the LED market and are being widely used in not only point light sources, but also wide-illumination equipment, back-lighting of liquid-crystal TVs and high-power automotive headlights. However, the color rendering index of YAG: Ce^{3+} is ~70, which is lower than the desired value for general illumination and the correlated color temperature is 4,000 K, which is too high [8]. Thus, developing the new green and red phosphor which can be used in the InGaN-based LED will advance the SSL technology.

1.2 Research Work Accomplished

1.2.1 FDTD Calculation of Light Extraction Efficiency of Top-Emitting LED

The Finite-Difference Time-Domain (FDTD) method was employed to calculate the light extraction efficiency of top-emitting GaN-based LEDs with sphere arrays. Specifically, the refractive index and diameter of spheres were optimized to achieve high light extraction. The results shows that the diameter and refractive index of sphere have significant effect on the light extraction efficiency. The optimized device structure is the LED with 400-nm anatase TiO_2 sphere arrays, which resulted in the 2.4 times enhancement in the light extraction efficiency.

1.2.2 Deposition of Monolayer, Submonolayer, and Multilayer Sphere Arrays

The low-cost, large-scale rapid convective deposition (RCD) method was employed to deposit spheres with various refractive indices and diameters to form sphere arrays. The monolayer, submonolayer, and multilayer sphere arrays have been obtained by

tuning the deposition speed, suspension concentration, humidity, temperature et.al. The hexagonal close-packed sphere arrays with diameter of 100 nm, 250 nm, 400 nm, and 1 μm have been obtained. The deposition of binary sphere arrays was also carried out and the microlens arrays with various aspect ratio has been achieved by tuning thermal annealing time.

1.2.3 Implementation of TiO_2 Sphere Arrays on the Top-Emitting LED

The anatase TiO_2 as well as amorphous TiO_2 sphere arrays was implemented on the top-emitting GaN LED, which results in 1.8 times enhancement in the output power. This is attributed to the enlarged light escape cone and reduced Fresnel reflection. The use of 'refractive-index' matched layer enables a strong coupling of light from the GaN layer into the TiO_2 scattering layer, which in turn results in optimum extraction structure.

1.2.4 Overcome the Fundamental Limit of Light Extraction Efficiency of TFFC LED by Self-assembly Colloidal Microlens Arrays

GaN-based Thin-Film Flip-Chip (TFFC) LED is the state-art of LED technology, which is used in combination with green and red phosphors, to generate white light for general illumination and display technologies. However, the low efficiency and high fabrication cost have been hindering the widely adoption of white LED. Cost-effective method is required to improve the overall efficiency of TFFC LED. The extraction efficiency of TFFC LED is significantly enhanced by employing the self-assembly microsphere or microlens arrays on the top of LED. The light extraction efficiency of 75% has been achieved by employing hexagonal-close packed 400-nm anataseTiO_2 sphere arrays. Further enhancement is achieved by forming the microlens arrays on the LED. The light extraction efficiency of 86% has been achieved by embedding 400-nm TiO_2 sphere arrays in 75 nm polystyrene layers on the TFFC LED, which is 1.3 times higher than that of the TFFC LED

with surface roughness. This result represents a state-of-the-art method to achieve improved light extraction efficiency in nitride-based LEDs with cost-effective manner.

1.2.5 Implementation of Microlens Arrays on the Organic Light-Emitting Diode (OLED)

The self-assembly 500-nm and 1-μm sphere arrays deposited by RCD method were employed as imprinting template to fabricate OLED with corrugated structures, which results in 1.8 times enhancement in output power compared to that of conventional planar OLED. This is attributed to the whisper gallery mode due to the Mie scattering of individual grating structure and Bragg diffraction resulted from the periodical arrangement of structures.

The light extraction efficiency of OLED with corrugated structures was computed for OLED employing 400-nm and 300-nm SiO_2/PS microlens arrays with various aspect ratio as template. The use of microlens arrays as imprinting template to fabricate OLED results in significant enhancement in light extraction efficiency. The light extraction efficiency depends on both the sphere diameter and aspect ratio of microlens arrays. Specifically, the use of 400-nm SiO_2/PS microlens arrays as template results in light extraction efficiency of 59%. The use of 300-nm SiO_2/PS microlens arrays results in the light extraction efficiency of 91%. Both the diameter of sphere and aspect ratio of microlens have significant effect on the light extraction. The optimized device structure is OLED employing 300-nm SiO_2/PS microlens arrays with depth of 100 nm from the top. The use of microlens and imprinting method in OLED with colloidal method results in 3-times enhancement in power conversion efficiency over traditional OLED.

1.2.6 Eu^{3+}-doped TiO_2 Nanospheres for GaN-based White LED

The monodisperse TiO_2 spheres were prepared by mixed-solvent method; ammonia plays an important role in forming the spherical TiO_2 particles. The ratio of acetonitrile to

acetone is the key factor to form monodisperse TiO_2 particles. In the presence of ammonia, we obtained monodisperse spherical TiO_2 particles when the ratio of acetonitrile to acetone is 3:1. The size of TiO_2 particles can be tuned by changing the precursor's concentration and reaction temperature. We have also demonstrated that these spherical TiO_2 particles could be converted from amorphous to anatanse and then to rutile by annealed at elevated temperatures. The optical properties of Eu^{3+}-doped TiO_2 was investigated, we found that there are some strong absorption in blue region and emit red light. Especially for the anatase TiO_2. This leads to potential applications for the Eu^{3+}-doped TiO_2 in high efficiency LED devices.

1.3 Dissertation Organization

This dissertation report comprises of nine chapters. The brief introduction of III-nitride materials and their applications will be presented in Chapter 1. The current challenges of III-based LED for high power and high efficiency solid-state lighting applications will be discussed in Chapter 2. The numerical calculation of light extraction efficiency of LED based on finite-difference time-domain (FDTD) method will be discussed in Chapter 3.

After providing the motivation for the device engineering, the report will move on to the discussion of experimental works. Chapter 4 will introduce self-assembly microlens arrays by the rapid convective deposition method (RCD). The deposition condition was investigated and hexagonal close-packed monolayer sphere arrays were obtained by tuning the suspension concentration, deposition speed. Chapter 5 will show device applications of self-assembly sphere arrays by RCD method. The deposition of anatase TiO_2 microsphere arrays on the LED was demonstrated, which results in significant enhancement in light extraction efficiency.

In chapter 6, we implemented the colloidal microsphere arrays on state of art of LED technology, the thin-film flip-chip (TFFC) LED, to advance the solid-state lighting technology. The refractive index of microsphere arrays, the quantum well position, and the cavity thickness were tuned to achieve maximum light extraction efficiency. The microlens arrays was also implemented on the TFFC LED to further improve the light extraction efficiency. In chapter 7, I will show that the applications of self-assembly microlens arrays on the OLED structures and it is resulted in 1.8 times enhancement in light extraction efficiency.

In chapter 8, I will show the high efficiency white LED can be realized by implementing Eu^{3+}-doped TiO_2 nanospheres on the top of LED, which not only can serve as red component of white light emission but also can improve the light extraction efficiency of LED. In chapter 8, the research work is summarized, and the future outlook for III-Nitride base solid-state lighting is discussed and presented.

References

[1] H. Morkoç, *Nitride Semiconductor Devices: Fundamentals and Applications*: John Wiley & Sons, 2013.

[2] N. C. George, K. A. Denault, and R. Seshadri, "Phosphors for Solid-State White Lighting," *Annu Rev Mater Res,* vol. 43, pp. 481-501, 2013.

[3] S. Ye, F. Xiao, Y. X. Pan, Y. Y. Ma, and Q. Y. Zhang, "Phosphors in phosphor-converted white light-emitting diodes Recent advances in materials, techniques and properties," *Mater. Sci. Eng. R-Rep.,* vol. 71, pp. 1-34, Dec 2010.

[4] K. C. Mishra, A. Setlur, H. Yamamoto, J. Collins, and M. Bettinelli, "Preface to the Special Issue on Luminescent Materials for Solid State Lighting," *ECS J. Solid State Sci. Technol.,* vol. 2, pp. Y2-Y2, 2013.

[5] J. McKittrick, M. E. Hannah, A. Piquette, J. K. Han, J. I. Choi, M. Anc*, et al.*, "Phosphor Selection Considerations for Near-UV LED Solid State Lighting," *ECS J. Solid State Sci. Technol.,* vol. 2, pp. R3119-R3131, 2013.

[6] J. S. Wang, H. Y. Zhu, C. L. Ma, X. X. Wu, J. Zhang, D. M. Li*, et al.*, "High-Pressure Behaviors of SrF2 Nanocrystals with Two Morphologies," *Journal of Physical Chemistry C,* vol. 117, pp. 615-619, Jan 10 2013.

[7] V. Bachmann, C. Ronda, and A. Meijerink, "Temperature Quenching of Yellow Ce3+ Luminescence in YAG:Ce," *Chem Mater,* vol. 21, pp. 2077-2084, May 26 2009.

[8] R. J. Xie, N. Hirosaki, M. Mitomo, K. Takahashi, and K. Sakuma, "Highly efficient white-light-emitting diodes fabricated with short-wavelength yellow oxynitride phosphors," *Appl Phys Lett,* vol. 88, Mar 6 2006.

Chapter 2 III-Nitride LEDs for Solid-State Lighting

2.1 Device Physics of GaN Light-Emitting Diode

LED is a semiconductor device in which the light emission originates from a very thin crystalline layer composed of semiconductor compounds, such as InGaN, AlGaN, AlInN when an electrical current is flowing through it. The thin active layer materials formed by InGaN material, which is sandwiched between the p-GaN and n-GaN, is called quantum well. The typical top-emitting LED device structure is shown in Figure 2-1. The n-GaN is grown on the sapphire substrate with buffer layer and followed by InGaN/GaN quantum wells and p-GaN growth. The metal contacts are deposited on the n-GaN and p-GaN by e-beam metal evaporation. When the p-n junction is connected to an electrical power source, current flows from the p side to the n side. The electrons are injected into the InGaN/GaN quantum well from n-GaN and holes are injected from the p-GaN. The electrons and holes are located in the different energy levels in the quantum well region separated by E_g. The energy is released in the form of a photon with the energy equivalent to the band gap energy when the electrons and holes meet and recombine subsequently. The color emitted by LED depends on the materials used to make the diode. The emission of color can be tuned by composition and thickness of quantum well [1].

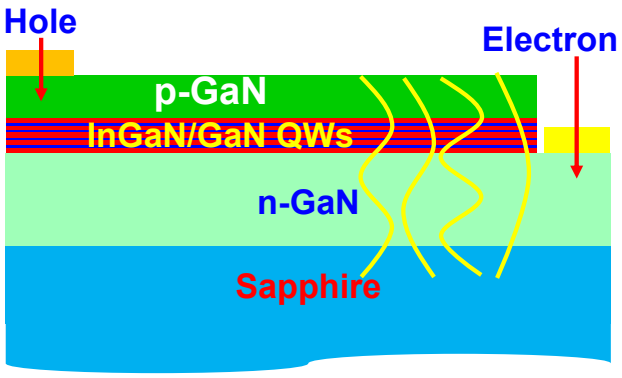

Figure 2-1. Schematics of conventional top-emitting LED device structure.

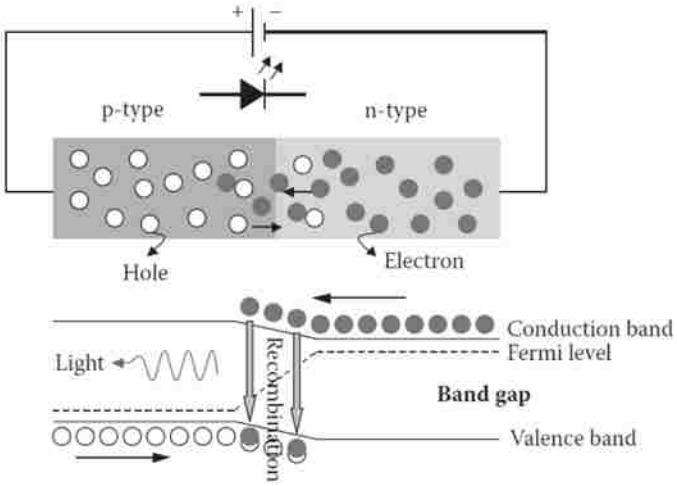

Figure 2-2. Schematic diagram of a light-emitting diode [2].

The light generated in the quantum well region escapes from the LED to the free space, which can be used for general illumination and display technology. The quantum efficiency of LED depends on the three factors [3]: 1) injection efficiency, which is defined as the ratio of current injected into the quantum well region to the current injected into the device; 2) radiative efficiency, which is defined as the ratio of radiative recombination rate to total recombination rate; 3) light extraction efficiency, which is defined as the ratio of light escaped from the device to light generated in quantum well region.

The electrical efficiency of LED is defined as the ratio of energy of emitted photon to the applied voltage, which can be expressed as the following [4]:

$$\eta_{wall\_plug} = \eta_{el} \cdot \eta_{ext} = \eta_{el} \cdot \eta_{extr} \cdot \eta_{inj} \cdot \eta_{\text{int}} = \frac{E_{photon}}{qV} \cdot \eta_{extr} \cdot \eta_{inj} \cdot \frac{\kappa_{rad}}{\kappa_{rad} + \kappa_{non}} \qquad (2.1).$$

The improvement in light extraction efficiency in LED devices is critical in determining power conversion efficiency. The progress in both injection and radiative efficiencies in LED technologies have been accomplished in the past 5 years, and the key limitation in achieving high extraction efficiency with cost-effective method remains important.

2.2 Low Light Extraction Efficiency

2.2.1 Introduction and Possible Causes

The III-Nitride materials have a considerable amount of device applications, such as solid-state lighting [5-12], thermoelectrics [13, 14], diode lasers [15, 16], transistors [17-19], solar cells and solar hydrogen [20-22]. Among these applications, GaN-based light-emitting diodes (LEDs) have been attracted tremendous attention due to various advantages over the conventional light sources. However, the quantum efficiency is still low and fabrication cost is high at current stage, which is hindering the widely adoption of LED. Thus, quantum efficiency of LED needs to be further improved for realizing the next generation high efficiency and high power LED devices. The internal quantum efficiency and light extraction efficiency are the two main factors that have great impact on the quantum efficiency [4]. The internal quantum efficiency has been increased to the limit by optimizing the active region and growth conditions in the past few years [23-29]. However, the light extraction efficiency of conventional LED is still low due to large refractive index contrast between GaN and free space as shown in Figure 2-3.

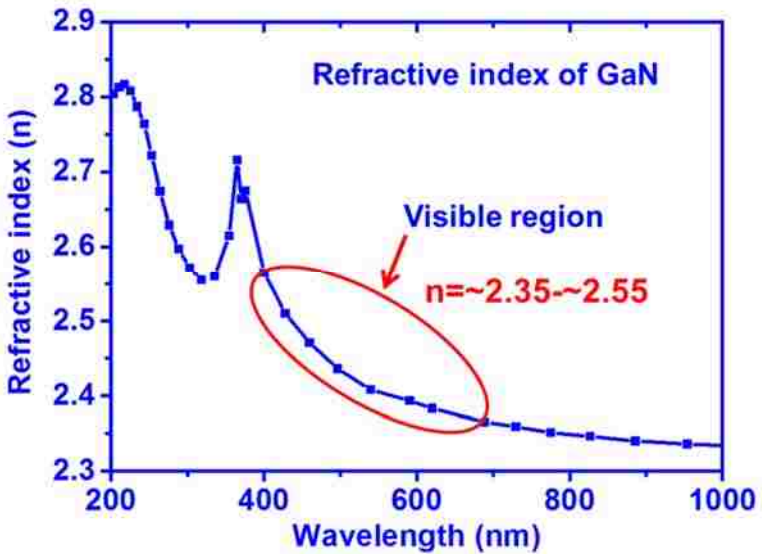

Figure 2-3. The refractive index of GaN as a function of wavelength.

As shown in Figure 2-3, the refractive index of GaN is 2.5 in the visible region and the refractive index of free space is 1. Assuming that the angle of incidence in the semiconductor at the semiconductor-air interface is given by θ_s. Then angle of the refracted ray, θ_{air}, can be obtained by Snell's law

$$n_s \sin\theta_s = n_{air} \sin\theta_{air} \tag{2.2}.$$

The critical angle of for total internal reflection is obtained by setting $\theta_{air} = 90^o$. According to the Snell' law, the critical angle can be expressed as

$$\sin\theta_c = \frac{n_{air}}{n_s}\sin 90^o = \frac{n_{air}}{n_s} \tag{2.3},$$

and

$$\theta_c = \arcsin\frac{n_{air}}{n_s} \tag{2.4}.$$

For the GaN-based LED, the critical angle can be determined as 23.5^o. The light emitted into the light escape cone can partly escape from GaN, whereas light emitted outside the escape cone will be totally reflected back to LED devices.

For the light emitted into the light escape cone, part of light can escape from the LED device to free space, and part of light will be reflected back to the device, which can be described by Fresnel reflection. For s-polarized light, the reflection can be expressed as

$$R_s = \left[\frac{n_s\cos\theta_{air} - n_{air}\sqrt{1-\left(\frac{n_s}{n_{air}}\sin\theta_s\right)^2}}{n_s\cos\theta_s + n_{air}\sqrt{1-\left(\frac{n_s}{n_{air}}\sin\theta_s\right)^2}}\right]^2 \tag{2.5},$$

and for p-polarized light, it can be expressed as

$$R_p = \left[\frac{n_s \sqrt{1 - \left(\frac{n_s}{n_{air}} \sin\theta_s \right)^2} - n_{air} \cos\theta_s}{n_s \sqrt{1 - \left(\frac{n_s}{n_{air}} \sin\theta_s \right)^2} + n_{air} \cos\theta_s} \right]^2 \quad (2.6).$$

For the case of light emitted from the GaN to free space, the reflectivity as a function of incidence angle is plotted in Figure 2-4 for TE (s-polarized) and TM (p-polarized) polarized lights.

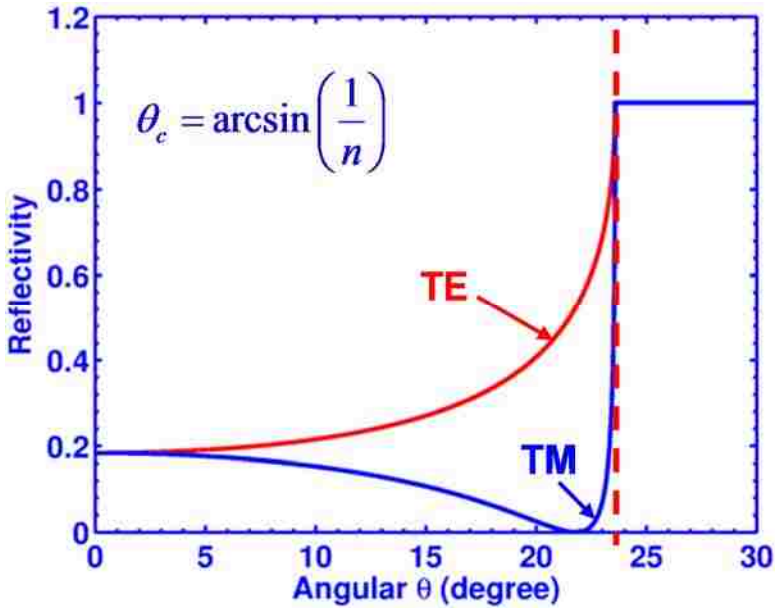

Figure 2-4. The reflectivity at GaN and free space interface for both TE polarized light and TM polarized light.

The light extraction efficiency of LED is calculated as the ratio of light emitted into free space to the total light emitted by the quantum well, which can be expressed as

$$\eta_{extr} = \frac{\int_0^{\arcsin(1/n)} p(\theta) 2\pi \sin(\theta) d\theta}{\int_0^{\pi} 2\pi \sin(\theta) d\theta} \quad (2.7).$$

The light emitted from the conventional hetero structures is isotropic, thus the light extraction efficiency can be calculated as ratio of surface area of the spherical cone with radius of r to the surface areas of whole spheres. As shown in Figure 2-5, the surface area is expressed as

$$A = \int dA = \int_{\phi=0}^{\phi_c} 2\pi r \sin\phi r d\phi = 2\pi r^2 \left(1 - \cos\phi_c\right) \tag{2.8}.$$

Assume that light is emitted from a point source in LED with a total power of P_{source} . The power that can escaped from LED is given by

$$P_{escape} = P_{source} \frac{2\pi r^2 \left(1 - \cos\theta_c\right)}{4\pi r^2} \tag{2.9},$$

and the light extraction can be expressed as

$$\eta_{extr} = \frac{P_{escape}}{P_{source}} = \frac{1}{2}\left(1 - \cos\phi_c\right) \tag{2.10}.$$

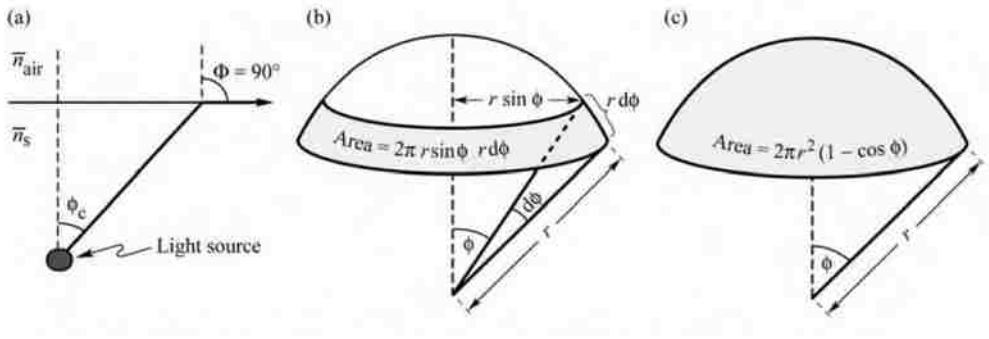

Figure 2-5. (a) Definition of the escape cone. (b) Area element Da. (c) Area of calotte-shaped section of the sphere defined by radius and angle ϕ_c [30].

Due to the small critical angle for the high refractive index materials, the cosine term can be expanded into power series using Taylor' expansion. By neglecting the higher order terms, the light extraction efficiency can be expressed as

$$\eta_{extr} = \frac{P_{escape}}{P_{source}} = \frac{1}{2}(1-\cos\phi_c) \approx \frac{1}{2}\left[1-\left(1-\frac{\phi_c^2}{2}\right)\right] = \frac{1}{4}\phi_c^2 = \frac{1}{4}\frac{n_{air}^2}{n_s^2} \quad (2.11).$$

For the GaN-based conventional top-emitting LED devices, only 4% of light generated in the quantum well region can be extracted out. Thus the light extraction efficiency needs to be improved. This limitation in extraction efficiency is critical in limiting the efficiency of the LED devices, and the use of microphotonics and nanophotonics structures are required to address the low extraction issue. Another important consideration for achieving high extraction method is related to the need for cost consideration in achieving improved structure.

2.2.2 Approaches for Enhancing Light Extraction Efficiency

Tremendous efforts have been devoted to improving the light extraction efficiency of GaN-based LED: 1) surface roughing [31-35], 2) sapphire microlenses [36], 3) oblique mesa sidewall [37], 4) nanopyramid [38], 5) photonic crystals [39-43], 6) graded refractive index [44], 7) self-assembled lithography p-GaN patterning [45], 8) GaN micro-domes [46, 47], and 9) TiO_2 micro-pillars [48]. The surface roughening approach utilizes chemical etching, which causes non-uniform surface. The photonic crystals and sapphire microlens approaches require the use of e-beam lithography or holography lithography [36], which leads to more expensive and / or complex fabrication process. Therefore, other low-cost and large area scalable method is highly desirable for implementation for low-cost and practical LEDs technologies.

2.2.3 Self-Assembly Colloidal Microlens Arrays to Improve Light Extraction Efficiency

The rapid convective deposition method developed in our laboratory is self-assembly microsphere arrays under capillary force and electrostatic force [49-51]. The deposition of 500-nm SiO_2 microsphere arrays on the LED has been resulted in significant

enhancement in light extraction efficiency for GaN-based LED [52-54]. Further enhancement of light extraction efficiency was achieved by deposition of 1-μm SiO_2/PS binary sphere arrays on the LED, followed by thermal annealing process to form microlens arrays with various aspect ratios [55]. The thickness of PS layer was tuned by adjusting the annealing time. The results show that the aspect ratio of microlens arrays have significant effect on the light extraction efficiency. The optimum light extraction efficiency of GaN-based LED has been achieved by tuning the thickness of PS layer.

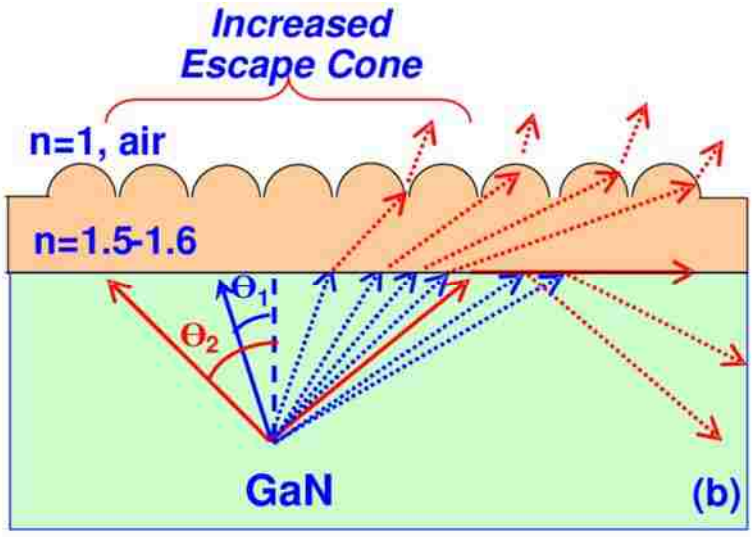

Figure 2-6. Schematic diagram of enhancement of light extraction efficiency of GaN-based LED with microlens arrays [54].

2.3 Challenges in Red Emitters

Solid-state lighting sources based on the GaN-based white LED have advantages over conventional light sources, such as incandescent lamp, and fluorescence lamps due to the high efficiency. The white light emission requires three color emitters. High efficient orange and red LEDs can be obtained using AlGaInP materials and the blue/violet LED can be obtained using InGaN materials. The strong charge separation and poor material quality for red emitter InGaN LEDs result in challenges in achieving practical red emitters with the conventional InGaN QW technology. The difficulty in growing high quality InGaN

materials with high In-content results in additional limitation in achieving high performance red emitters. The integration of InGaN-based LEDs with red or yellow phosphors become critical for achieving practical white LED emitters.

References

[1] C. J. Humphreys, "Solid-state lighting," *MRS Bull.,* vol. 33, pp. 459-470, Apr 2008.

[2] R.-J. Xie, *Nitride phosphors and solid-state lighting*: CRC/Taylor & Francis, 2011.

[3] E. F. Schubert, T. Gessmann, and J. K. Kim, "Inorganic Semiconductors for Light-emitting Diodes," in *Organic Light Emitting Devices*, ed: Wiley-VCH Verlag GmbH & Co. KGaA, 2006, pp. 1-33.

[4] A. I. Zhmakin, "Enhancement of light extraction from light emitting diodes," *Physics Reports-Review Section of Physics Letters,* vol. 498, pp. 189-241, Feb 2011.

[5] S. H. Park, "Radiative Efficiency Enhancement in Blue Saw-Like InGaN/GaN Light-Emitting Diodes," *Appl. Phys. Express,* vol. 6, May 2013.

[6] Y. K. Ee, J. M. Biser, W. J. Cao, H. M. Chan, R. P. Vinci, and N. Tansu, "Metalorganic Vapor Phase Epitaxy of III-Nitride Light-Emitting Diodes on Nanopatterned AGOG Sapphire Substrate by Abbreviated Growth Mode," *Ieee J Sel Top Quant,* vol. 15, pp. 1066-1072, Jul-Aug 2009.

[7] N. F. Gardner, G. O. Muller, Y. C. Shen, G. Chen, S. Watanabe, W. Gotz*, et al.*, "Blue-emitting InGaN--GaN double-heterostructure light-emitting diodes reaching maximum quantum efficiency above 200 A/cm[sup 2]," *Appl. Phys. Lett.,* vol. 91, pp. 243506-3, 12/10/ 2007.

[8] H. P. Zhao, J. Zhang, G. Y. Liu, and N. Tansu, "Surface plasmon dispersion engineering via double-metallic Au/Ag layers for III-nitride based light-emitting diodes," *Appl. Phys. Lett.,* vol. 98, Apr 2011.

[9] X. Li, S. G. Bishop, and J. J. Coleman, "GaN epitaxial lateral overgrowth and optical characterization," *Appl. Phys. Lett.,* vol. 73, pp. 1179-1181, Aug 1998.

[10] I. H. Brown, P. Blood, P. M. Smowton, J. D. Thomson, S. M. Olaizola, A. M. Fox*, et al.*, "Time evolution of the screening of piezoelectric fields in InGaN quantum wells," *IEEE J. Quantum Electron.,* vol. 42, pp. 1202-1208, Nov-Dec 2006.

[11] J. H. Ryou, P. D. Yoder, J. P. Liu, Z. Lochner, H. Kim, S. Choi*, et al.*, "Control of Quantum-Confined Stark Effect in InGaN-Based Quantum Wells," *Ieee J Sel Top Quant,* vol. 15, pp. 1080-1091, Jul-Aug 2009.

[12] X. Li, H. Y. Liu, X. Ni, U. Ozgur, and H. Morkoc, "Effect of carrier spillover and Auger recombination on the efficiency droop in InGaN-based blue LEDs," *Superlattices Microstruct.,* vol. 47, pp. 118-122, Jan 2010.

[13] B. N. Pantha, I. W. Feng, K. Aryal, J. Li, J. Y. Lin, and H. X. Jiang, "Erbium-Doped AlInGaN Alloys as High-Temperature Thermoelectric Materials," *Appl. Phys. Express,* vol. 4, May 2011.

[14] J. Zhang, H. P. Zhao, and N. Tansu, "Large optical gain AlGaN-delta-GaN quantum wells laser active regions in mid-and deep-ultraviolet spectral regimes," *Appl. Phys. Lett.,* vol. 98, pp. -, Apr 25 2011.

[15] M. X. Feng, J. P. Liu, S. M. Zhang, D. S. Jiang, Z. C. Li, K. Zhou*, et al.*, "High efficient GaN-based laser diodes with tunnel junction," *Appl. Phys. Lett.,* vol. 103, Jul 22 2013.

[16] J. Zhang and N. Tansu, "Optical Gain and Laser Characteristics of InGaN Quantum Wells on Ternary InGaN Substrates," *IEEE Photonics J.,* vol. 5, p. 11, Apr 2013.

[17] J. Lu, D. Denninghoff, R. Yeluri, S. Lal, G. Gupta, M. Laurent*, et al.*, "Very high channel conductivity in ultra-thin channel N-polar GaN/(AlN, InAlN, AlGaN) high electron mobility hetero-junctions grown by metalorganic chemical vapor deposition," *Appl. Phys. Lett.,* vol. 102, Jun 10 2013.

[18] L. Lugani, J. F. Carlin, M. A. Py, D. Martin, F. Rossi, G. Salviati*, et al.*, "Ultrathin InAlN/GaN heterostructures on sapphire for high on/off current ratio high electron mobility transistors," *J. Appl. Phys.,* vol. 113, Jun 7 2013.

[19] F. Shahedipour-Sandvik, J. Leathersich, R. P. Tompkins, P. Suvarna, M. Tungare, T. A. Walsh*, et al.*, "Enhanced performance of an AlGaN/GaN high electron mobility transistor on Si by means of improved adatom diffusion length during MOCVD epitaxy," *Semicond. Sci. Technol.,* vol. 28, Jul 2013.

[20] Z. W. Ren, L. Chao, X. Chen, B. J. Zhao, X. F. Wang, J. H. Tong*, et al.*, "Enhanced performance of InGaN/GaN based solar cells with an In0.05Ga0.95N ultra-thin inserting layer between GaN barrier and In0.2Ga0.8N well," *Opt. Express,* vol. 21, pp. 7118-7124, Mar 25 2013.

[21] J. Benton, J. Bai, and T. Wang, "Enhancement in solar hydrogen generation efficiency using a GaN-based nanorod structure," *Appl. Phys. Lett.,* vol. 102, Apr 29 2013.

[22] B. AlOtaibi, M. Harati, S. Fan, S. Zhao, H. P. T. Nguyen, M. G. Kibria*, et al.*, "High efficiency photoelectrochemical water splitting and hydrogen generation using GaN nanowire photoelectrode," *Nanotechnology,* vol. 24, May 3 2013.

[23] H. P. Zhao, G. Y. Liu, J. Zhang, J. D. Poplawsky, V. Dierolf, and N. Tansu, "Approaches for high internal quantum efficiency green InGaN light-emitting diodes with large overlap quantum wells," *Opt. Express,* vol. 19, pp. A991-A1007, Jul 4 2011.

[24] R. A. Arif, Y. K. Ee, and N. Tansu, "Polarization engineering via staggered InGaN quantum wells for radiative efficiency enhancement of light emitting diodes," *Appl. Phys. Lett.,* vol. 91, Aug 27 2007.

[25] S. H. Park, D. Ahn, and J. W. Kim, "High-efficiency staggered 530 nm InGaN/InGaN/GaN quantum-well light-emitting diodes," *Appl. Phys. Lett.,* vol. 94, Jan 2009.

[26] C. T. Liao, M. C. Tsai, B. T. Liou, S. H. Yen, and Y. K. Kuo, "Improvement in output power of a 460 nm InGaN light-emitting diode using staggered quantum well," *J. Appl. Phys.,* vol. 108, Sep 2010.

[27] U. Ozgur, H. Y. Liu, X. Li, X. F. Ni, and H. Morkoc, "GaN-Based Light-Emitting Diodes: Efficiency at High Injection Levels," *Proc. IEEE,* vol. 98, pp. 1180-1196, Jul 2010.

[28] H. P. Zhao, G. Y. Liu, J. Zhang, R. A. Arif, and N. Tansu, "Analysis of Internal Quantum Efficiency and Current Injection Efficiency in III-Nitride Light-Emitting Diodes," *Journal of Display Technology,* vol. 9, pp. 212-225, Apr 2013.

[29] G. Y. Liu, J. Zhang, C. K. Tan, and N. Tansu, "Efficiency-Droop Suppression by Using Large-Bandgap AlGaInN Thin Barrier Layers in InGaN Quantum-Well Light-Emitting Diodes," *Ieee Photonics J,* vol. 5, p. 11, Apr 2013.

[30] E. F. Schubert, T. Gessmann, and J. K. Kim, *Light emitting diodes*: Wiley Online Library, 2005.

[31] C. C. Kao, H. C. Kuo, K. F. Yeh, J. T. Chu, W. L. Peng, H. W. Huang*, et al.*, "Light-output enhancement of nano-roughened GaN laser lift-off light-emitting diodes formed by ICP dry etching," *IEEE Photonics Technol. Lett.,* vol. 19, pp. 849-851, May-Jun 2007.

[32] C. Huh, K. S. Lee, E. J. Kang, and S. J. Park, "Improved light-output and electrical performance of InGaN-based, light-emitting diode by microroughening of the p-GaN surface," *J. Appl. Phys.,* vol. 93, pp. 9383-9385, Jun 1 2003.

[33] T. Fujii, Y. Gao, R. Sharma, E. L. Hu, S. P. DenBaars, and S. Nakamura, "Increase in the extraction efficiency of GaN-based light-emitting diodes via surface roughening," *Appl. Phys. Lett.,* vol. 84, pp. 855-857, Feb 2004.

[34] C. F. Lin, Z. H. Yang, J. H. Zheng, and J. H. Dai, "Enhanced light output in nitride-based light-emitting diodes by roughening the mesa sidewall," *IEEE Photonics Technol. Lett.,* vol. 17, pp. 2038-2040, Oct 2005.

[35] H. W. Huang, J. T. Chu, C. C. Kao, T. H. Hseuh, T. C. Lu, H. C. Kuo*, et al.*, "Enhanced light output of an InGaN/GaN light emitting diode with a nano-roughened p-GaN surface," *Nanotechnology,* vol. 16, pp. 1844-1848, Sep 2005.

[36] H. W. Choi, C. Liu, E. Gu, G. McConnell, J. M. Girkin, I. M. Watson*, et al.*, "GaN micro-light-emitting diode arrays with monolithically integrated sapphire microlenses," *Appl. Phys. Lett.,* vol. 84, pp. 2253-2255, Mar 2004.

[37] J. S. Lee, J. Lee, S. Kim, and H. Jeon, "Fabrication of reflective GaN mesa sidewalls for the application to high extraction efficiency LEDs," *physica status solidi (c),* vol. 4, pp. 2625-2628, 2007.

[38] J. Q. Xi, H. Luo, A. J. Pasquale, J. K. Kim, and E. F. Schubert, "Enhanced light extraction in GaInN light-emitting diode with pyramid reflector," *IEEE Photonics Technol. Lett.,* vol. 18, pp. 2347-2349, Nov-Dec 2006.

[39] E. Matioli, B. Fleury, E. Rangel, T. Melo, E. Hu, J. Speck*, et al.*, "High Extraction Efficiency GaN-Based Photonic-Crystal Light-Emitting Diodes: Comparison of Extraction Lengths between Surface and Embedded Photonic Crystals," *Appl. Phys. Express,* vol. 3, 2010.

[40] J. J. Wierer, A. David, and M. M. Megens, "III-nitride photonic-crystal light-emitting diodes with high extraction efficiency," *Nat Photonics,* vol. 3, pp. 163-169, Mar 2009.

[41] J. Jewell, D. Simeonov, S. C. Huang, Y. L. Hu, S. Nakamura, J. Speck*, et al.*, "Double embedded photonic crystals for extraction of guided light in light-emitting diodes," *Appl. Phys. Lett.,* vol. 100, p. 4, Apr 2012.

[42] C. Wiesmann, K. Bergenek, N. Linder, and U. T. Schwarz, "Photonic crystal LEDs - designing light extraction," *Laser Photonics Rev.,* vol. 3, pp. 262-286, May 2009.

[43] M. Fujita, S. Takahashi, Y. Tanaka, T. Asano, and S. Noda, "Simultaneous inhibition and redistribution of spontaneous light emission in photonic crystals," *Science,* vol. 308, pp. 1296-1298, May 27 2005.

[44] J. Q. Xi, M. F. Schubert, J. K. Kim, E. F. Schubert, M. F. Chen, S. Y. Lin*, et al.*, "Optical thin-film materials with low refractive index for broadband elimination of Fresnel reflection," *Nat Photonics,* vol. 1, pp. 176-179, Mar 2007.

[45] S. Chhajed, W. Lee, J. Cho, E. F. Schubert, and J. K. Kim, "Strong light extraction enhancement in GaInN light-emitting diodes by using self-organized nanoscale patterning of p-type GaN," *Appl. Phys. Lett.,* vol. 98, Feb 14 2011.

[46] P. Zhao, L. Han, M. R. McGoogan, and H. Zhao, "Analysis of TM mode light extraction efficiency enhancement for deep ultraviolet AlGaN quantum wells light-emitting diodes with III-nitride micro-domes," *Opt. Mater. Express,* vol. 2, pp. 1397-1406, 10/01 2012.

[47] P. Zhao and H. P. Zhao, "Analysis of light extraction efficiency enhancement for thin-film-flip-chip InGaN quantum wells light-emitting diodes with GaN micro-domes," *Opt. Express,* vol. 20, pp. A765-A776, Sep 2012.

[48] M. Ma, J. Cho, E. F. Schubert, Y. Park, G. B. Kim, and C. Sone, "Strong light-extraction enhancement in GaInN light-emitting diodes patterned with TiO2 micro-pillars with tapered sidewalls," *Appl. Phys. Lett.,* vol. 101, Oct 1 2012.

[49] P. Kumnorkaew, Y. K. Ee, N. Tansu, and J. F. Gilchrist, "Investigation of the Deposition of Microsphere Monolayers for Fabrication of Microlens Arrays," *Langmuir,* vol. 24, pp. 12150-12157, Nov 2008.

[50] P. Kumnorkaew and J. F. Gilchrist, "Effect of Nanoparticle Concentration on the Convective Deposition of Binary Suspensions," *Langmuir,* vol. 25, pp. 6070-6075, Jun 2009.

[51] P. Kumnorkaew, A. L. Weldon, and J. F. Gilchrist, "Matching Constituent Fluxes for Convective Deposition of Binary Suspensions," *Langmuir,* vol. 26, pp. 2401-2405, 2010/02/16 2009.

[52] Y. K. Ee, R. A. Arif, N. Tansu, P. Kumnorkaew, and J. F. Gilchrist, "Enhancement of light extraction efficiency of InGaN quantum wells light emitting diodes using SiO_2/polystyrene microlens arrays," *Appl. Phys. Lett.,* vol. 91, Nov 2007.

[53] Y. K. Ee, P. Kumnorkaew, R. A. Arif, H. Tong, J. F. Gilchrist, and N. Tansu, "Light extraction efficiency enhancement of InGaN quantum wells light-emitting diodes with polydimethylsiloxane concave microstructures," *Opt. Express,* vol. 17, pp. 13747-13757, Aug 2009.

[54] Y. K. Ee, P. Kumnorkaew, R. A. Arif, H. Tong, H. P. Zhao, J. F. Gilchrist*, et al.*, "Optimization of Light Extraction Efficiency of III-Nitride LEDs With Self-Assembled

Colloidal-Based Microlenses," *Ieee J Sel Top Quant,* vol. 15, pp. 1218-1225, Jul-Aug 2009.

[55] H. C. Chang, K. Y. Lai, Y. A. Dai, H. H. Wang, C. A. Lin, and J. H. He, "Nanowire arrays with controlled structure profiles for maximizing optical collection efficiency," *Energy & Environmental Science,* vol. 4, pp. 2863-2869, Aug 2011.

Chapter 3 Light Extraction Efficiency of Top-Emitting Light-Emitting Diode

3.1 Light Extraction of Light-Emitting Diodes

The III-Nitride materials have a huge applications for addressing device technologies applicable in solid state lighting [1-4], thermoelectrics [5-10], diode lasers [11-14], and solar cells and solar hydrogen [15-17]. Among them, GaN-based light-emitting diodes (LEDs) have drawn tremendous attention in recent years for a variety of applications in flat-panel displays, mobile electronics, automobiles, traffic signals, large outdoor displays, and general lighting. However, for the next generation of applications of high-efficiency LEDs, further improvement of quantum efficiency of LEDs is required. The quantum efficiency depends on the internal quantum efficiency and light extraction efficiency [18]. The advances in active region optimization and growth methods have led to improvement in internal quantum efficiency in recent years [19, 20]. However, the light extraction efficiency of conventional LED is still low due to large refractive index contrast between GaN (~2.5 in the visible region) and free space. Therefore, various of methods have been employed to improve the light extraction efficiency of LEDs: 1) surface roughing [21-25], 2) sapphire microlenses [26], 3) oblique mesa sidewall [27], 4) nanopyramid [28], 5) photonic crystals [29-34], 6) graded refractive index [35], 7) self-assembled lithography p-GaN patterning [36], 8) GaN micro-domes [37, 38], and 9) TiO_2 micro-pillars [39]. The surface roughing approach utilizes chemical etching, which causes non-uniform surface. The photonic crystals and sapphire microlens approaches require the use of e-beam lithography or holography lithography [40], which lead to more expensive and complex fabrication process. Therefore, other low-cost and large area scalable method is highly desirable for implementation for cost-effective and practical LEDs technologies.

Previously, we have demonstrated the use of SiO_2 microsphere arrays and SiO_2 / PS microlens arrays, deposited via rapid convective deposition (RCD) method, leads to improvement in light extraction efficiency in III-Nitride LEDs [41-44]. The use of RCD method leads to the ability for deposition of large area (wafer scale) microspheres (and / or microlens) arrays structures on top of LEDs device structures [45-47]. Recently, this colloidal lithography method have been used as imprinting template for forming concave microstructure arrays for light extraction enhancement in GaN-based LEDs [42] and organic-based LEDs [48, 49]. The selection of SiO_2 as the microspheres in our previous works had been primarily motivated from the ease in obtaining the silica-based spheres with wide range of dimensions commercially. However, the material choices (ie. refractive indices) and dimensions of the spheres are design parameters that need to be optimized for maximizing the light extraction efficiency from nitride-based LEDs. In addition, the selection of spheres with various refractive indices and dimensions will also affect the far-field radiation pattern of the LEDs over wide angular distribution.

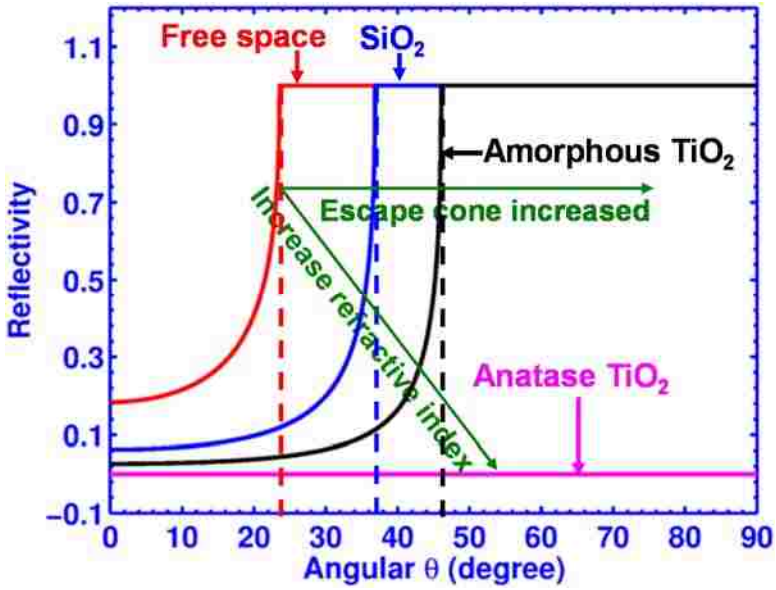

Figure 3-1. Angular dependent reflectivity at the interface of GaN and free space, SiO_2, amorphous TiO_2 and anatase TiO_2 for TE polarized light.

According to Snell's law, the total internal reflection takes place when the light travels from high refractive index material to low refractive index materials. The critical angle decreases with the increase in the refractive index difference. Based on the equation(2.5), the reflectivity at the interface between the GaN and free space, SiO_2, amorphous TiO_2, and anatase TiO_2 are plotted in Figure 3-1. The refractive index has significant effect on the reflectivity and higher refractive index material will decrease the reflectivity. Based on this consideration, in this work, we present the numerical simulation studies based on finite-difference time-domain (FDTD) method for analyzing the light extraction efficiency of III-Nitride LEDs employing microsphere arrays with various refractive indices and dimensions. Specifically, the light extraction characteristics of III-Nitride LEDs with anatase-TiO_2 and amorphous-TiO_2 microsphere arrays will be compared with those of III-Nitride LEDs with SiO_2 microsphere arrays. The refractive indices of anatase-TiO_2 and amorphous-TiO_2 microsphere arrays are higher than that of SiO_2 microsphere, which will lead to the improved extraction characteristics for III-Nitride LEDs employing the TiO_2 microsphere arrays. The comparison of the light extraction efficiency enhancement for LEDs employing lower refractive index sphere SiO_2, medium refractive index sphere amorphous-TiO_2, and higher refractive index sphere anatase-TiO_2 with various diameters will be presented. The current study will be limited to the optimization of the LEDs employing only the microsphere arrays, and note that the fabrication of the microlens arrays can be formed by embedding the microsphere arrays with polystyrene (PS) materials (ie. SiO_2 / PS microlens arrays [38-41]).

3.2 FDTD Calculation of Light Extraction Efficiency

The InGaN/GaN multiple quantum wells (MQWs) LED device structure analyzed in this study is shown in Figure 3-2. The n-GaN template was grown on sapphire substrate and followed by the growth of active region with total thickness of 12 nm. Then 0.1 μm p-

doped GaN layer was grown on top. Afterwards, the hexagonal close-packed (HCP) microsphere arrays were deposited on top of LED by employing rapid convective deposition (RCD) method [38-42]. The deposition of the microspheres or nanospheres can be performed with high uniformity in close-packed 2-D hexagonal pattern, and the scanning electron microscopy of the 100-nm diameter nanosphere arrays are shown in Figure 3-2.

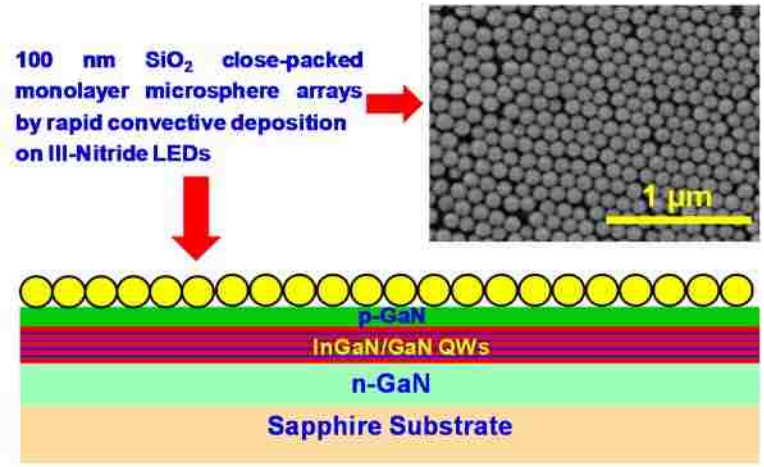

Figure 3-2. Schematic side view of the simulated microsphere LED device, and the corresponding SEM images of 100-nm SiO_2 sphere arrays.

The LED devices were treated as 3-D structures solved by taking into consideration of appropriate boundary conditions for ensuring efficient computation time. The 3-D FDTD method requires a large amount of memory and computation time. Therefore, the size of the simulation volume has to be reduced. Perfect matched layers boundary (PML) conditions were applied on the boundaries in order to avoid unnecessary reflection of light at the boundaries of domain as well as reduce the domain size. To reduce the size of the calculation, we have taken the simulation domain to be 5.5 μm x 5.5 μm. The thickness of n-GaN reduced to 0.1 μm and sapphire substrate was reduced to 0.2 μm.

A single dipole source within a finite computational domain was chosen and positioned in the center of x-y plane and also in the center of the InGaN/GaN active layer

in the vertical direction. In addition, inhomogeneous mesh was used during the simulation; the grid size was 10 nm in the bulk and 2.4 nm in the interface. The refractive index of GaN and InGaN layer is set as 2.5 and 2.6, respectively. The absorption coefficient of InGaN was chosen to be 2000 cm^{-1} [15]. The emission wavelength used in all our computation is set as λ = 500 nm. The light extraction efficiency was calculated as the ratio of the optical output power radiated through the microlens array to the total output power generated in the InGaN/GaN MQWs active region. The numerical simulation formulation of the light extraction efficiency were performed by calculating the ratio of the power collected by the detector placed above the devices to the total power generated from the dipole sources.

3.3 Effect of Refractive Index on the Light Extraction Efficiency

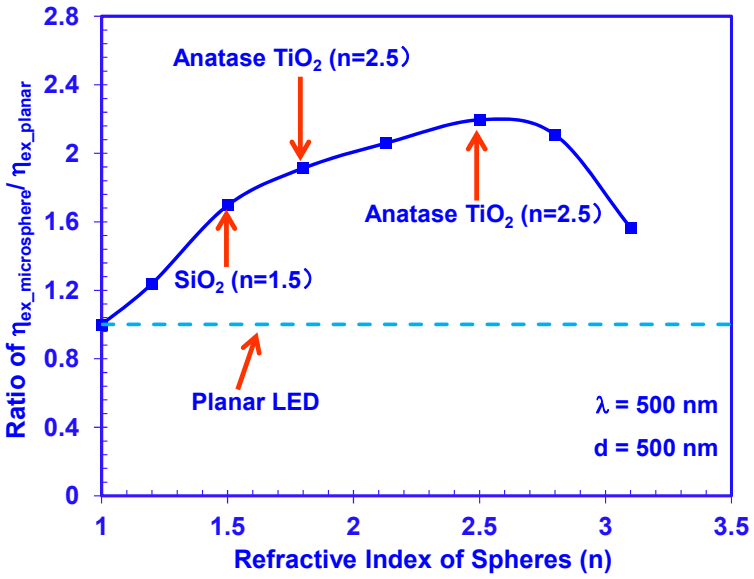

Figure 3-3. Ratio of light extraction efficiency of microsphere array LED with various refractive index to that of planar LED.

To investigate the effect of the refractive index of microsphere arrays on the light extraction efficiency of III-nitride LEDs, light extraction efficiency of GaN LEDs with microsphere ($d_{microsphere}$ = 500 nm) arrays and planar LED were calculated for various

refractive indices. The ratios of the light extraction efficiencies of the LEDs with microsphere arrays to those of the planar LED are shown in Figure 3-3. Light extraction efficiency increases with the increase in refractive index of microsphere, and ~2.2 times enhancement is achieved when the refractive index of microsphere matched with that of GaN.

The enhancement started to decrease with further increase in the refractive index of the microspheres, which is expected due to the increased light trapping in microspheres (for n > 2.5). To compare suitable microsphere materials applicable for the experiments, the following microspheres were investigated as follow 1) SiO_2 (n~1.5), 2) amorphous TiO_2 (n~1.8), and 3) anatase TiO_2 (n~2.5). The computational analysis indicated that the use of SiO_2 microsphere arrays (d_{SiO2} = 500 nm) leads to an increase of 1.7-times in the light extraction efficiency of the devices, which is in good agreement with the experimental results (~1.69 times increase) [39] and the simulation results employing ray tracing method (1.75 times enhancement) [39]. Note that simulation results using FDTD method is much closer to the experimental results compared to that of using ray tracing method. By using amorphous and anatase TiO_2 microsphere arrays, the light extraction efficiencies of the LEDs increase by1.91-times and 2.19-times over that of planar LEDs. As the microsphere refractive indices increase beyond n > 2.5, the light trapping in the microspheres leads to reduction in the light extraction to free space.

The increase in the refractive indices of the microspheres up to n ~ 2.5 provides minimal Fresnel reflection between the GaN and spheres and results in light captured in the spheres, which will then extracted out efficiently by the increased escape cone from the strong curvature surfaces introduced by microsphere arrays.

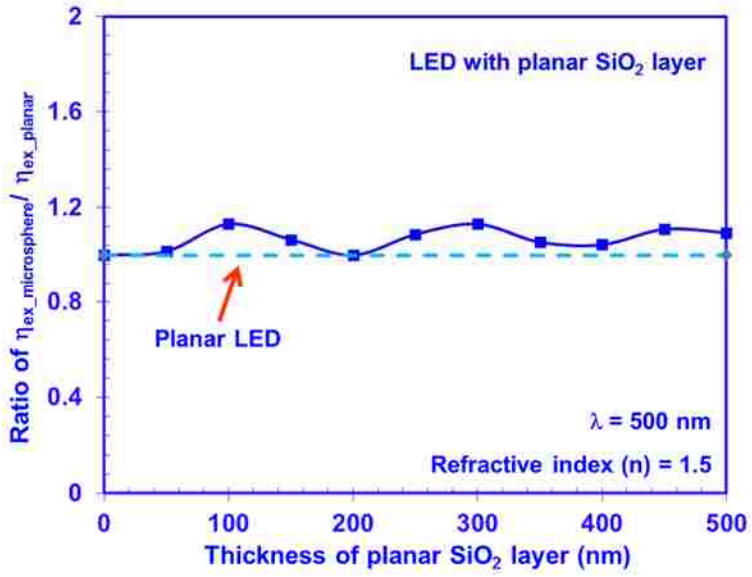

Figure 3-4. Ratio of light extraction efficiency of LED with 500-nm planar SiO_2 layer to that of planar LED.

As an comparison, anti-reflection layer was deposited on the GaN LED to reduce the Fresnel reflection [50]. The ratio of light extraction efficiency of LED with planar SiO_2 anti-reflection layer to that of planar LED was plotted in Figure 3-4. The planar SiO_2 layer deposited on the LEDs as antireflection coatings reduces the Fresnel reflection and increases the light extraction efficiency. Maximum enhancement of 1.2 times is achieved for LED with planar SiO_2 layer, which is much lower than that of LED with SiO_2 spheres (1.7 times). Following the Snell's law, the critical angles are 23.5^o, 36.9^o, and 41.8^o for the light emission from GaN to free space, from GaN to SiO_2 film, and from the SiO_2 film to free space, respectively. However, the overall critical angle for the light emission from GaN to air is 23.5^o, the same as that without SiO_2 film. The role of the microsphere or nanosphere arrays is to provide strong scattering centers to extract light out beyond the critical angle, which in turn results in the increase in light extraction efficiency for the microsphere LEDs over LEDs with only planar SiO_2 anti-reflecting film.

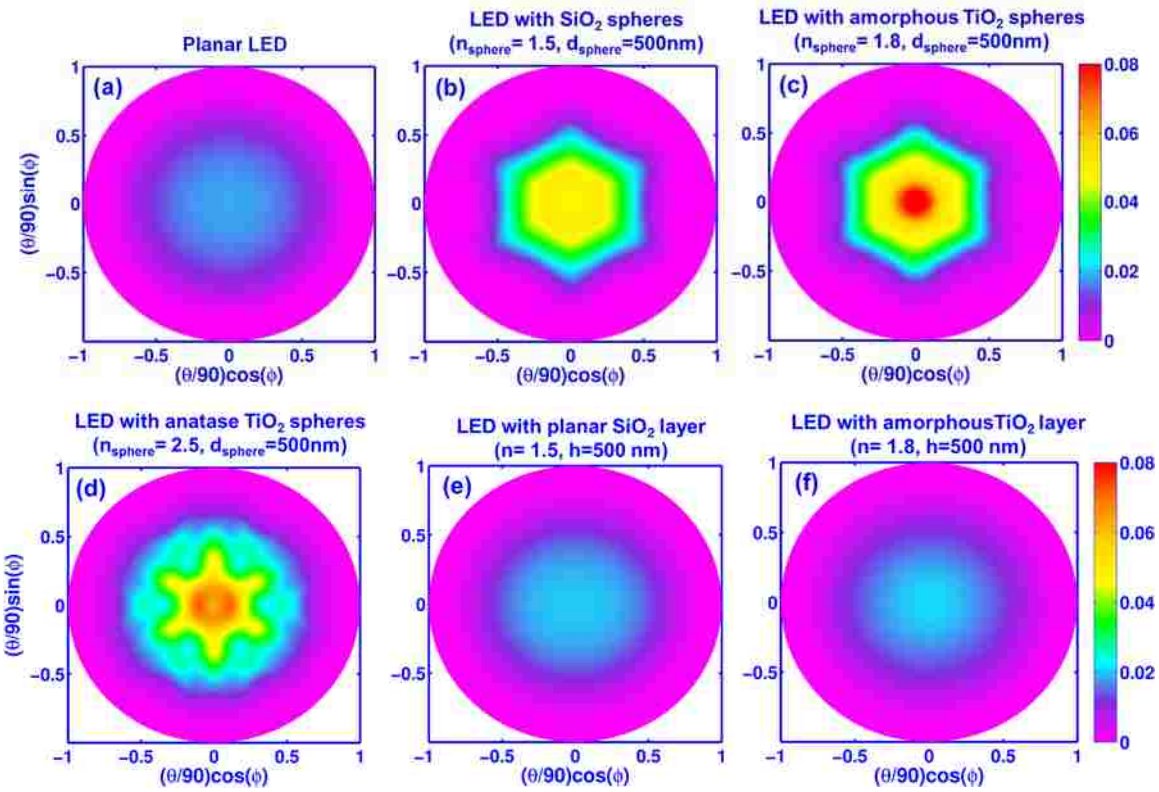

Figure 3-5. Contour plot of far-field radiation patterns of (a) planar LED, (b) LED with SiO_2 microsphere arrays, (c) LED with amorphous TiO_2 microsphere arrays, and (d) LED with anatase TiO_2 microsphere arrays, (e) LED with 500-nm planar SiO_2 layer, and (f) LED with 500-nm planar amorphous TiO_2 layers.

To investigate the effect of microsphere arrays on the light emission, the far-field radiation patterns were calculated for the LED with 500-nm SiO_2 sphere arrays [Figure 3-5 (b)], LED with 500-nm amorphous TiO_2 sphere arrays [Figure 3-5 (c)], LED with 500-nm anatase TiO_2 sphere arrays [Figure 3-5(d)]. The far-field emission patterns of planar LED [Figure 3-5 (a)], LED with 500-nm planar SiO_2 layer [Figure 3-5(e)], and LED with 500-nm planar amorphous TiO_2 layer [Figure 3-5(f)] were also calculated as comparison. The far-field radiation pattern for planar LEDs, as expected, exhibited Lambertian radiation pattern with only angular (θ) dependent, while the symmetrically azimuthal (ϕ) distribution. The light emission intensity is weak in both normal direction and large angular directions, which results in the low light extraction efficiency. The intensity slightly increases for the LED

deposited with 500-nm planar SiO_2 layer and 500-nm planar amorphous TiO_2 layer, which leads to slightly increase in light extraction efficiency. Note that the far-field radiation patterns still shows perfect circular shape, which is same as that of planar LED. As expected, significant increase in light emission is observed for the LED with microsphere arrays [see Figure 3-5 (b), (c) and (d)] and the far-field radiation patterns exhibit both angular (θ) and azimuthal (ϕ) dependent. The significantly higher intensity in both the normal and large angular distribution result in improved light extraction efficiency for these LEDs. Note that the comparison of the light extraction efficiency ratio for the microsphere LEDs and planar LEDs were carried out by taking the total output power integrated in all angular (θ) and azimuthal (ϕ) directions.

To provide a quantitative comparison, the far-field radiation patterns for these LEDs are plotted at a particular azimuthal direction of $\phi = 0$ [as shown in Figure 3-6(a)]. The angular dependent (in θ direction) power density comparison data for microsphere LEDs and planar LED are also plotted for comparison purpose [as shown in Figure 3-6(b)]. The microsphere array LEDs exhibit significant increase in the far-field emission for all angular directions. More importantly, the contribution of the large angular θ component in the far-field radiation pattern is significantly increased for anatase TiO_2 microsphere arrays LEDs, which results in increase in power density extracted from this microsphere LEDs.

Note that the choice of the refractive indices of the materials (SiO_2, amorphous TiO_2, and anatase TiO_2) strongly affects the radiation pattern, extraction efficiency, and power density profile at large angular direction. The studies presented in Figure 3-5 and Figure 3-6 assume identical diameters for all the microspheres investigated. However, both the refractive indices and diameters of the spheres are important as optimization parameters in LEDs extraction.

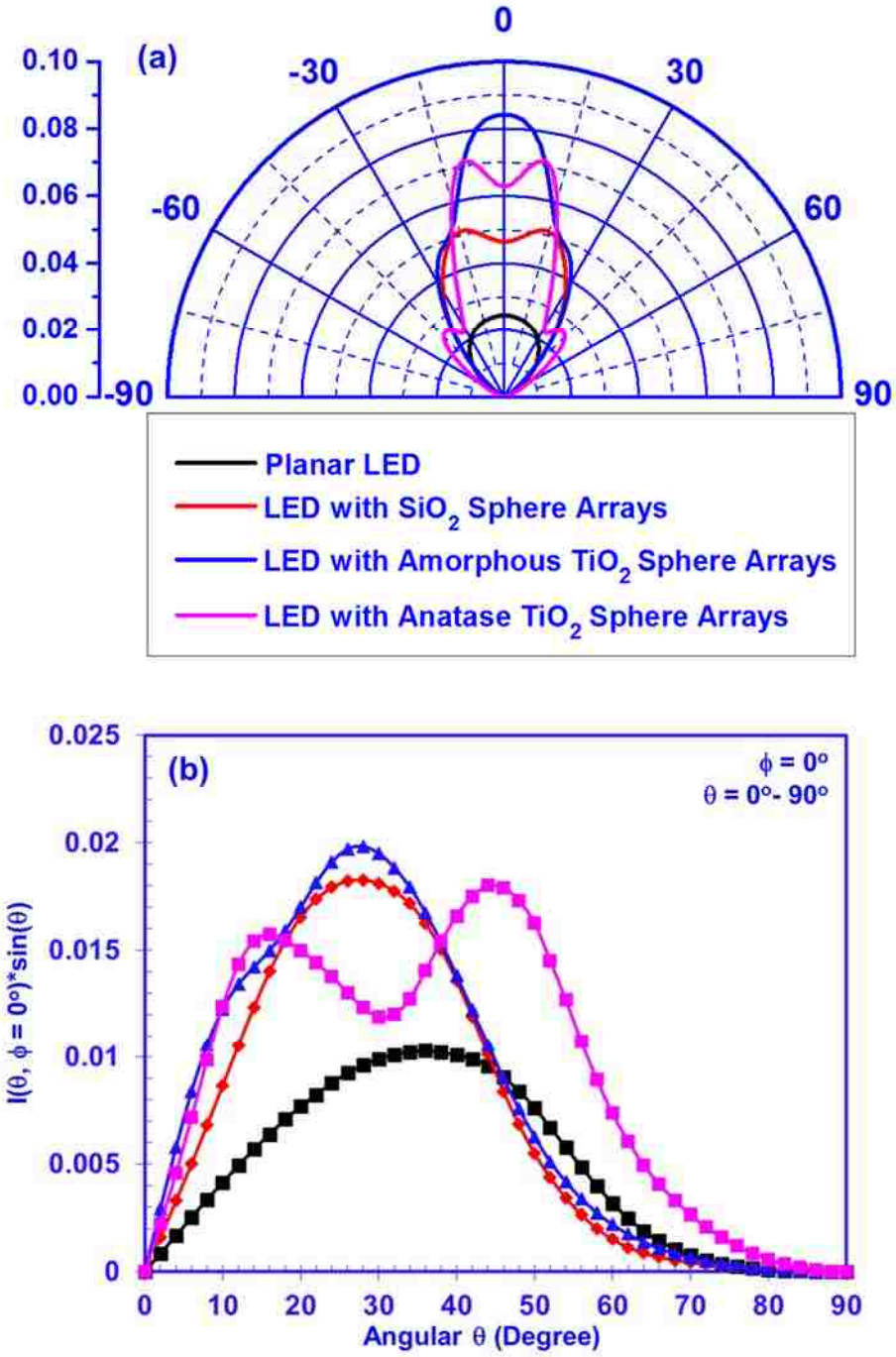

Figure 3-6. (a) Polar plot of far-field intensities of microsphere LEDs with various refractive indices, and (b) angular dependent power density of microsphere array LED with various refractive indices.

3.4 Effect of Sphere Diameters on the Light Extraction Efficiency

In order to further optimize the light extraction efficiency of LEDs with microsphere arrays, the effect of diameter of spheres on the light extraction efficiency of microsphere LEDs was also investigated [as shown in Figure 3-7(a), (b), and (c)]. Figure 3-7(a) shows the light extraction efficiency enhancement of LEDs with SiO_2 (n~1.5) microsphere arrays as a function of diameters of spheres at λ = 500 nm. All the three microsphere LEDs exhibited strong dependency on the diameter of the microsphere arrays employed in the structures. The optimum dimensions for each types of sphere materials occur at different dimensions resulting in maximum allowed extraction enhancement in the microsphere LEDs. The comparison of the light extraction efficiencies for microsphere LEDs were carried out with that of planar LEDs serving as reference LEDs.

For the case of SiO_2-based microsphere LEDs, the maximum extraction enhancement of 1.85 times is expected for diameter of ~ 1 μm. Large range of SiO_2 microsphere diameter exists for enhancement in extraction efficiency by ~ 1.6 times of higher. Specifically, the diameters in the range of 0.4 μm up to 1.2 μm are expected to result in relatively favorable increase in light extraction in LEDs.

For the case of amorphous TiO_2 microsphere LEDs, the increase up to 2.1 times is observed for LEDs using optimum diameter d ~ 0.8μm. The use of amorphous TiO_2 microspheres with diameters ranging from 0.4 μm up to 0.9 μm is expected to result in increased extraction efficiency by 1.9 times or higher. By using the anatase TiO_2 microsphere arrays, the optimum diameter for this structure was obtained as d ~ 0.4 μm. The use of this optimum anatase TiO_2 microsphere arrays with d ~ 0.4 μm results in 2.4 times increase in light extraction efficiency over that of planar LEDs.

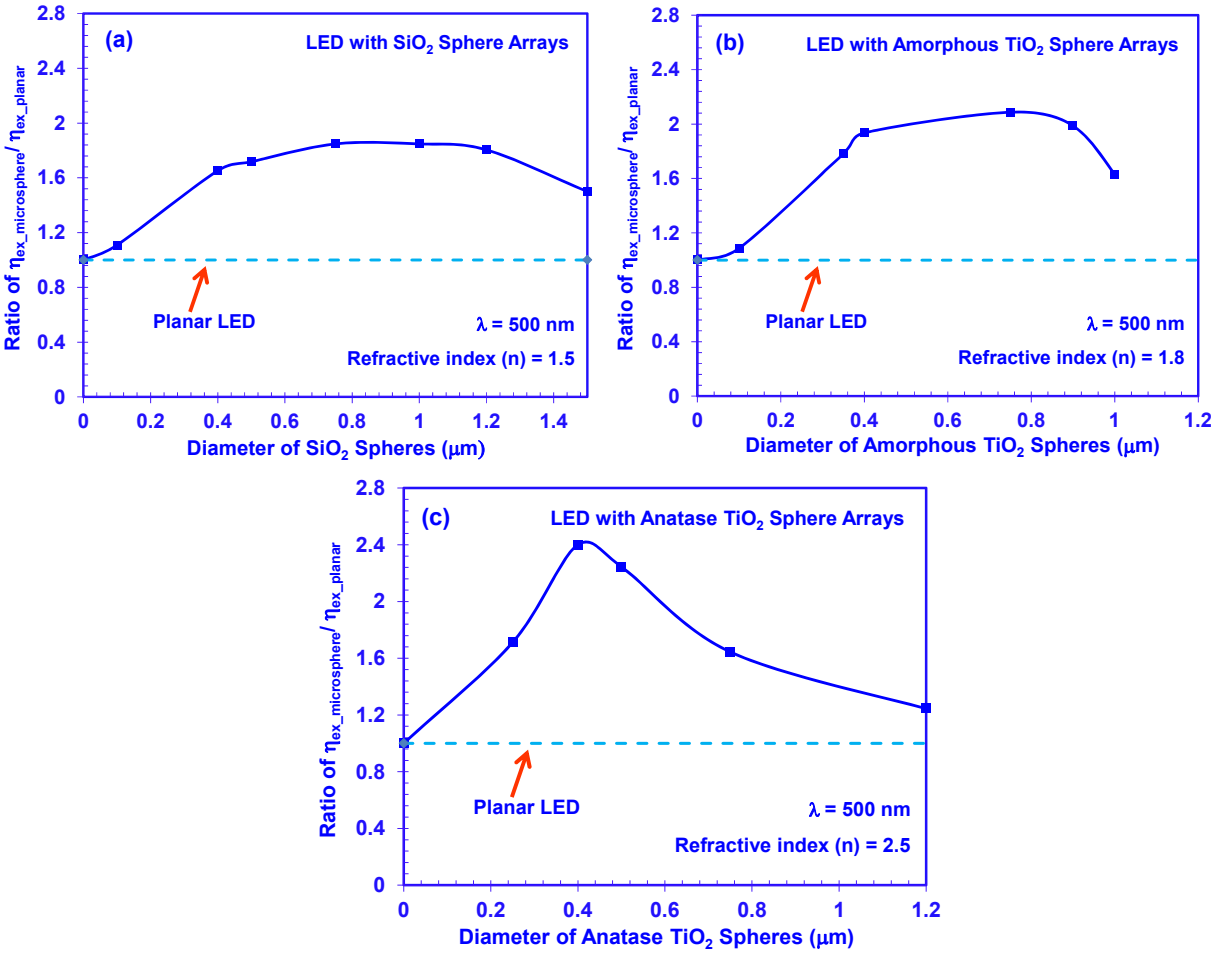

Figure 3-7. Ratio of the light extraction efficiency of microsphere LEDs with various diameters to that of planar LED: (a) LEDs with SiO_2 microsphere arrays; (b) LEDs with amorphous TiO_2 microsphere arrays and (c) LEDs with anatase TiO_2 microsphere arrays.

From our finding, the optimum diameter range for high extraction efficiency for each type of microsphere arrays reduces, as the refractive indices increas to n ~ 2.5 (n_{GaN}). However, the maximum light extraction enhancement for the LEDs can be obtained from the microspheres with the refractive index closest to n ~ 2.5 (anatase TiO_2).

To further investigate the effect of sphere diameter on the device performance, the far-field radiation patterns were calculated. Figure 3-8 shows the far-field radiation patterns of LED with SiO_2 sphere arrays with various sphere diameters. The far-field radiation pattern of planar led is plotted in the same figure as comparison. For the planar

LED, the far-field radiation pattern shows perfect circular symmetry due to the large refractive index contrast between the GaN and free space which leads to the Lambertian like radiation pattern. The light escape is very small, and only a small amount of light can be extracted out from the LED.

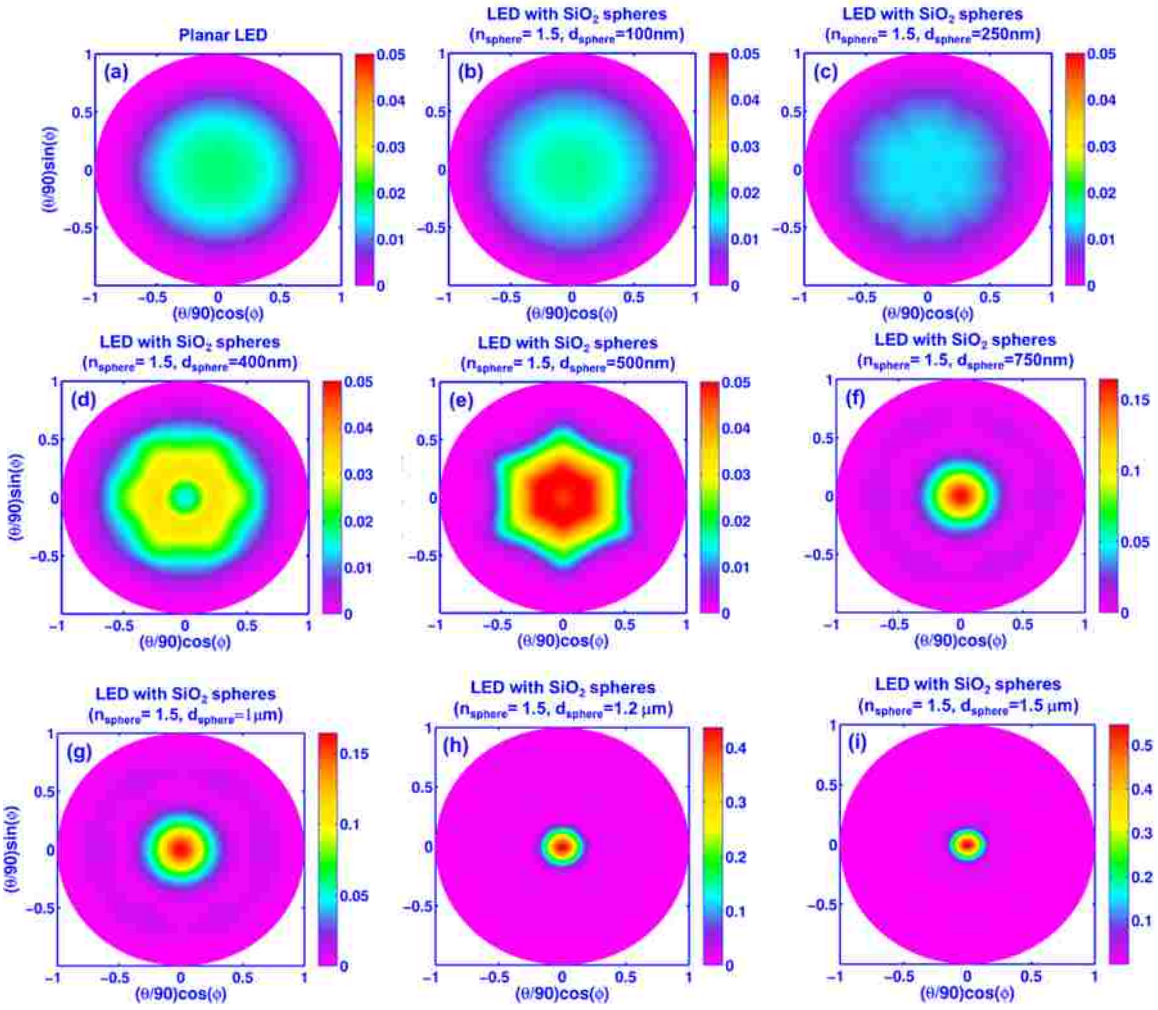

Figure 3-8. Far-field radiation pattern of LED with SiO_2 sphere arrays with diameter of (a) 0 nm, (b) 100 nm,(c) 400 nm, (d) 500 nm, (e) 750 nm, (f) 1μm, (g) 1.2 μm and (f) 1.5 μm.

When microsphere arrays are deposited on the top of LED, the scattered radiation pattern are seen and light emission spread over the entire surface. Note that the far-field radiation pattern strongly depends on the diameter of spheres. The far-field radiation pattern of LED with 100-nm sphere arrays is very similar with that of planar LED, which

results in the slightly enhancement in light extraction efficiency. The light emission in the large angular direction starts to increase when the sphere diameter increases to 250 nm, and further enhancement is achieved at sphere diameter of 400 nm. The dramatic increase in the light emission is observed at normal direction when sphere diameter increases to 500 nm and it keeps increasing with the increase in the sphere diameter.

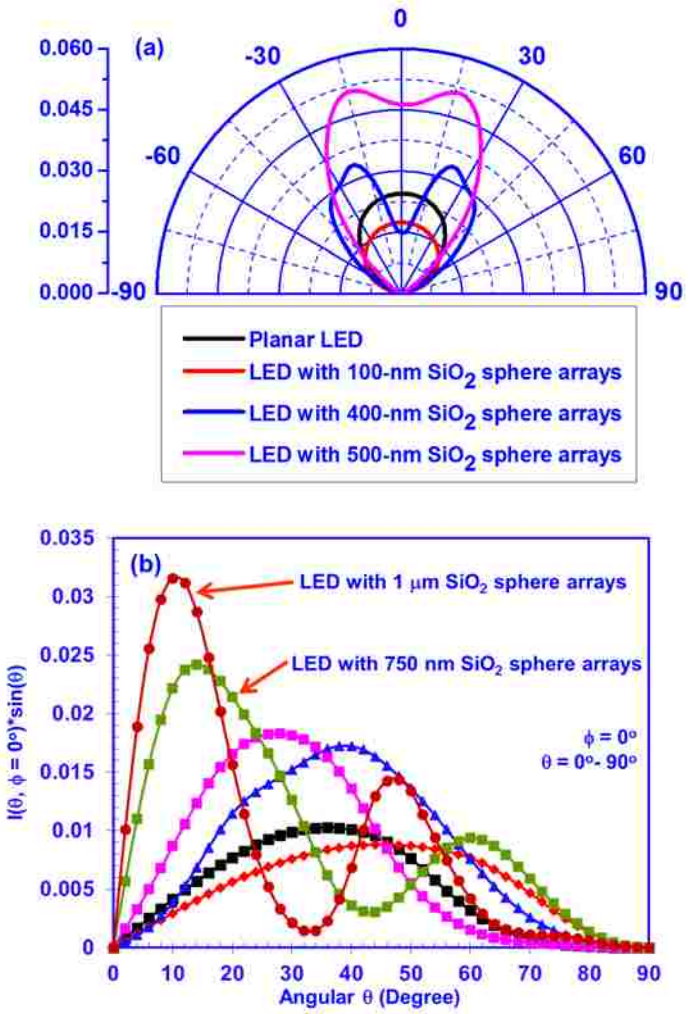

Figure 3-9. (a) Far-field radiation patterns of SiO_2 microsphere array LEDs with various SiO_2 sphere diameters. (b) Angular dependent power density comparison of SiO_2 microsphere array LEDs. The planar LED is included as reference.

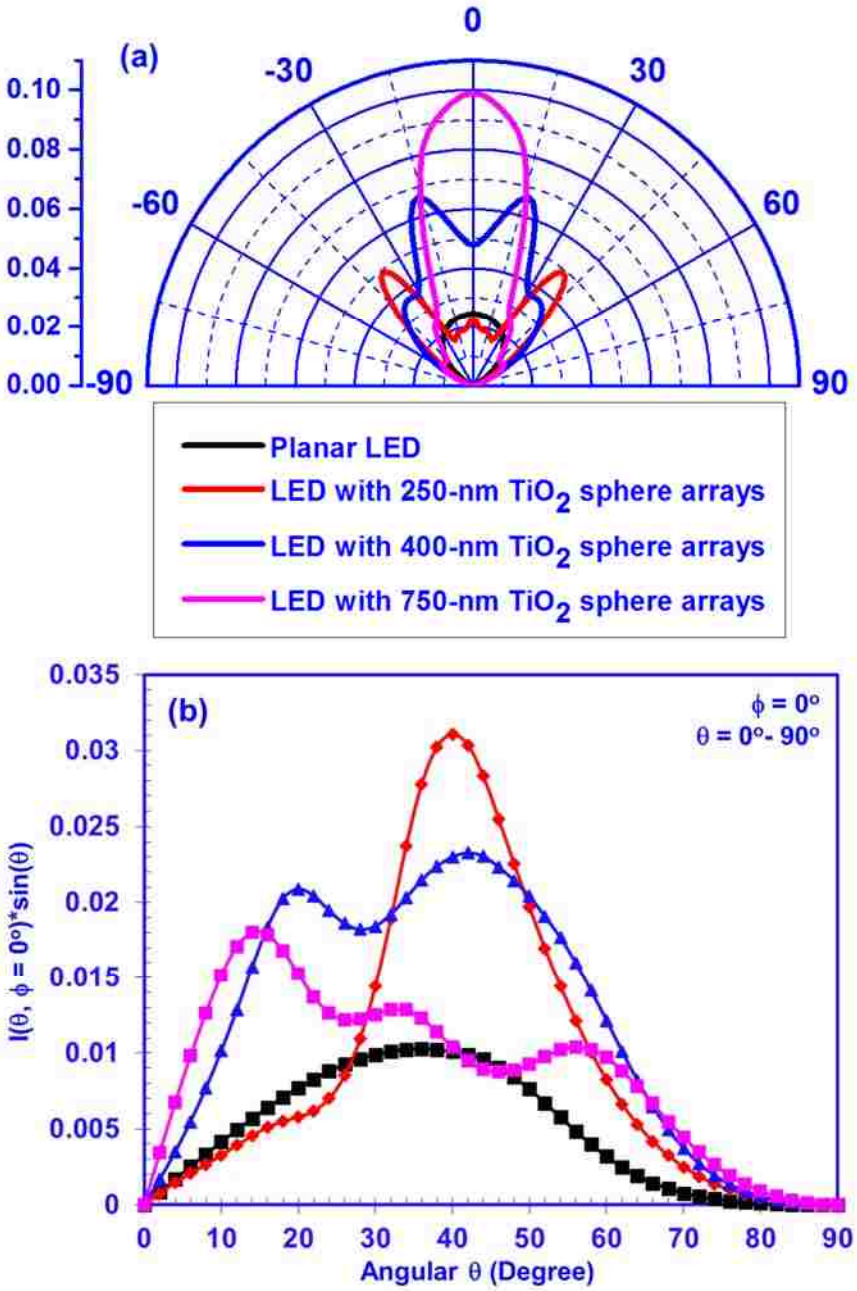

Figure 3-10. (a) Far-field radiation patterns of anatase TiO_2 microsphere array LEDs with various sphere diameters. (b) Angular dependent power density comparison of anatase TiO_2 microsphere array LEDs. The planar LED was included as reference.

The comparison of the far-field radiation patterns of the SiO_2 and anatase TiO_2 (as optimized material) microsphere arrays for various diameters are shown in Figure 3-9 and

Figure 3-10. The comparison of the far-field radiation patterns for both SiO_2 [Figure 3-9(a)] and TiO_2 [Figure 3-10(a)] microspheres were taken with azimuthal $\phi = 0$ direction, in order to provide quantitative comparison between the two materials with various diameters. The comparison of the angular power density distributions for both SiO_2 and TiO_2 microsphere LEDs for various diameters are also shown in figures Figure 3-9(b) and Figure 3-10(b), respectively (with azimuthal $\phi = 0$ direction).

In the case of SiO_2 microsphere array LEDs [Figure 3-9(a) and (b)], the microsphere diameters were varied from 0.1 μm, 0.4 μm, 0.5 μm, 0.75 μm and 1 μm. The use of small SiO_2 microsphere ($d_{SiO2} < 0.1$ μm) leads to an increased in light extraction at large angular component, while LEDs with larger sphere arrays ($d_{SiO2} > 0.5$ μm) results in significant increase in the output power in the normal direction. The large contribution of diffuse light output power can be attributed from the increased photon escape cone in the structure.

In the analysis of the anatase-TiO_2 microsphere array LEDs [Figure 3-10(a) and (b)], the diameters were varied from 0.25 μm, 0.4 μm, and 0.75 μm. As shown in Figure 3-10(b), the far-field radiation patterns for the anatase TiO_2 microsphere array LEDs were strongly enhanced in comparison to that of planar LEDs. Similar to the SiO_2 microsphere LEDs, the use of smaller anatase TiO_2 spheres resulted in strong enhancement in the large angular emission. In contrast, the dominant component leading to enhancement in extraction efficiency for larger anatase TiO_2 spheres can be attributed to the stronger normal light emission.

In summary, the effects of refractive indices, material choices, and sphere diameters were investigated for optimizing the far-field radiation patterns and light extraction efficiency in III-Nitride based LEDs with microsphere arrays. The analysis was carried out by using 3-D vectorial FDTD with PML boundary condition. The results show that the use

of microsphere arrays with high refractive index as favorably for achieving maximum light extraction efficiency in microsphere array LEDs. Specifically, the use of anatase TiO_2 microsphere arrays is expected to result in more than 2.4 times increase in light extraction efficiency over that of planar LEDs. The optimum diameters of the spheres are found to strongly affect the radiation patterns and light extraction efficiency in microsphere LEDs. The use of smaller spheres results in significant enhancement in light extraction at large angular component, while the larger sphere appears to result in stronger enhancement in normal light emission. The current work is limited to the optimization of LEDs with microsphere arrays, and this finding will serve as useful guide for optimizing the light extraction in microsphere array LEDs deposited by RCD method. Future works will also include the optimization of the microlens array LEDs, which can be formed by embedding the microsphere arrays in polystyrene (PS) materials (ie. SiO_2 / PS microlens arrays).

References

[1] M. H. Crawford, "LEDs for Solid-State Lighting: Performance Challenges and Recent Advances," *Ieee J Sel Top Quant,* vol. 15, pp. 1028-1040, Jul-Aug 2009.

[2] Y. K. Ee, J. M. Biser, W. J. Cao, H. M. Chan, R. P. Vinci, and N. Tansu, "Metalorganic Vapor Phase Epitaxy of III-Nitride Light-Emitting Diodes on Nanopatterned AGOG Sapphire Substrate by Abbreviated Growth Mode," *Ieee J Sel Top Quant,* vol. 15, pp. 1066-1072, Jul-Aug 2009.

[3] N. F. Gardner, G. O. Muller, Y. C. Shen, G. Chen, S. Watanabe, W. Gotz*, et al.*, "Blue-emitting InGaN--GaN double-heterostructure light-emitting diodes reaching maximum quantum efficiency above 200 A/cm[sup 2]," *Appl. Phys. Lett.,* vol. 91, pp. 243506-3, 12/10/ 2007.

[4] H. P. Zhao, J. Zhang, G. Y. Liu, and N. Tansu, "Surface plasmon dispersion engineering via double-metallic Au/Ag layers for III-nitride based light-emitting diodes," *Appl. Phys. Lett.,* vol. 98, Apr 2011.

[5] B. N. Pantha, R. Dahal, J. Li, J. Y. Lin, H. X. Jiang, and G. Pomrenke, "Thermoelectric properties of In(x)Ga(1-x)N alloys," *Appl. Phys. Lett.,* vol. 92, Jan 2008.

[6] B. N. Pantha, R. Dahal, J. Li, J. Y. Lin, H. X. Jiang, and G. Pomrenke, "Thermoelectric Properties of In(0.3)Ga(0.7)N Alloys," *J. Electron. Mater.,* vol. 38, pp. 1132-1135, Jul 2009.

[7] B. N. Pantha, I. W. Feng, K. Aryal, J. Li, J. Y. Lin, and H. X. Jiang, "Erbium-Doped AlInGaN Alloys as High-Temperature Thermoelectric Materials," *Appl. Phys. Express,* vol. 4, May 2011.

[8] J. Zhang, H. P. Zhao, and N. Tansu, "Large optical gain AlGaN-delta-GaN quantum wells laser active regions in mid-and deep-ultraviolet spectral regimes," *Appl. Phys. Lett.,* vol. 98, pp. -, Apr 25 2011.

[9] H. Tong, "Thermoelectric characteristics and measurements of ternary III-nitride semiconductors," Ph.D. 3419411, Lehigh University, United States -- Pennsylvania, 2010.

[10] H. Tong, J. Zhang, G. Y. Liu, J. A. Herbsommer, G. S. Huang, and N. Tansu, "Thermoelectric properties of lattice-matched AlInN alloy grown by metal organic chemical vapor deposition," *Appl. Phys. Lett.,* vol. 97, Sep 2010.

[11] J. Zhang and N. Tansu, "Optical Gain and Laser Characteristics of InGaN Quantum Wells on Ternary InGaN Substrates," *IEEE Photonics J.,* vol. 5, p. 11, Apr 2013.

[12] J. Zhang and N. Tansu, "Engineering of AlGaN-Delta-GaN Quantum-Well Gain Media for Mid- and Deep-Ultraviolet Lasers," *IEEE Photonics J.,* vol. 5, p. 9, Apr 2013.

[13] M. X. Feng, J. P. Liu, S. M. Zhang, D. S. Jiang, Z. C. Li, K. Zhou*, et al.*, "High efficient GaN-based laser diodes with tunnel junction," *Appl. Phys. Lett.,* vol. 103, Jul 22 2013.

[14] C. C. Chen, C. H. Chiu, S. P. Chang, M. H. Shih, M. Y. Kuo, J. K. Huang*, et al.*, "Large-area ultraviolet GaN-based photonic quasicrystal laser with high-efficiency green color emission of semipolar {10-11} In0.3Ga0.7N/GaN multiple quantum wells," *Appl. Phys. Lett.,* vol. 102, Jan 7 2013.

[15] N. G. Young, R. M. Farrell, Y. L. Hu, Y. Terao, M. Iza, S. Keller*, et al.*, "High performance thin quantum barrier InGaN/GaN solar cells on sapphire and bulk (0001) GaN substrates," *Appl. Phys. Lett.,* vol. 103, p. 5, Oct 2013.

[16] Z. W. Ren, L. Chao, X. Chen, B. J. Zhao, X. F. Wang, J. H. Tong*, et al.*, "Enhanced performance of InGaN/GaN based solar cells with an In0.05Ga0.95N ultra-thin inserting layer between GaN barrier and In0.2Ga0.8N well," *Opt. Express,* vol. 21, pp. 7118-7124, Mar 25 2013.

[17] C. F. Lin, K. T. Chen, S. H. Chen, C. C. Yang, W. C. Huang, and T. H. Hsieh, "InGaN-based solar cells with a tapered GaN structure," *J. Cryst. Growth,* vol. 370, pp. 97-100, May 1 2013.

[18] A. I. Zhmakin, "Enhancement of light extraction from light emitting diodes," *Physics Reports-Review Section of Physics Letters,* vol. 498, pp. 189-241, Feb 2011.

[19] H. P. Zhao, G. Y. Liu, J. Zhang, J. D. Poplawsky, V. Dierolf, and N. Tansu, "Approaches for high internal quantum efficiency green InGaN light-emitting diodes with large overlap quantum wells," *Opt. Express,* vol. 19, pp. A991-A1007, Jul 4 2011.

[20] R. A. Arif, Y. K. Ee, and N. Tansu, "Polarization engineering via staggered InGaN quantum wells for radiative efficiency enhancement of light emitting diodes," *Appl. Phys. Lett.,* vol. 91, Aug 27 2007.

[21] J. Ho Won, R. Seong Wook, Y. Hak Ki, L. Sanghan, and L. Jong-Lam, "The role of reflective p-contacts in the enhancement of light extraction in nanotextured vertical InGaN light-emitting diodes," *Nanotechnology,* vol. 21, p. 025203, 2010.

[22] C. C. Kao, H. C. Kuo, K. F. Yeh, J. T. Chu, W. L. Peng, H. W. Huang*, et al.*, "Light-output enhancement of nano-roughened GaN laser lift-off light-emitting diodes formed by ICP dry etching," *IEEE Photonics Technol. Lett.,* vol. 19, pp. 849-851, May-Jun 2007.

[23] C. F. Lin, Z. H. Yang, J. H. Zheng, and J. H. Dai, "Enhanced light output in nitride-based light-emitting diodes by roughening the mesa sidewall," *IEEE Photonics Technol. Lett.,* vol. 17, pp. 2038-2040, Oct 2005.

[24] H. W. Huang, J. T. Chu, C. C. Kao, T. H. Hseuh, T. C. Lu, H. C. Kuo*, et al.*, "Enhanced light output of an InGaN/GaN light emitting diode with a nano-roughened p-GaN surface," *Nanotechnology,* vol. 16, pp. 1844-1848, Sep 2005.

[25] T. Fujii, Y. Gao, R. Sharma, E. L. Hu, S. P. DenBaars, and S. Nakamura, "Increase in the extraction efficiency of GaN-based light-emitting diodes via surface roughening," *Appl. Phys. Lett.,* vol. 84, pp. 855-857, Feb 2004.

[26] H. W. Choi, C. Liu, E. Gu, G. McConnell, J. M. Girkin, I. M. Watson*, et al.*, "GaN micro-light-emitting diode arrays with monolithically integrated sapphire microlenses," *Appl. Phys. Lett.,* vol. 84, pp. 2253-2255, Mar 2004.

[27] J. S. Lee, J. Lee, S. Kim, and H. Jeon, "Fabrication of reflective GaN mesa sidewalls for the application to high extraction efficiency LEDs," *physica status solidi (c),* vol. 4, pp. 2625-2628, 2007.

[28] J. Q. Xi, H. Luo, A. J. Pasquale, J. K. Kim, and E. F. Schubert, "Enhanced light extraction in GaInN light-emitting diode with pyramid reflector," *IEEE Photonics Technol. Lett.,* vol. 18, pp. 2347-2349, Nov-Dec 2006.

[29] K. H. Li, K. Y. Zang, S. J. Chua, and H. W. Choi, "III-nitride light-emitting diode with embedded photonic crystals," *Appl Phys Lett,* vol. 102, p. 4, May 2013.

[30] Q. Ding, K. Li, M. Kong, L. Chen, and J. Zhao, "Improving Vertical Light Extraction Efficiency of GaN-based Thin-Film Flip-Chip LEDs with p-side Deep-Hole Photonic Crystals," *Display Technology, Journal of,* vol. PP, pp. 1-1, 2013.

[31] B. Zhang, X. X. Fu, X. N. Kang, J. Xu, C. Xiong, and G. Y. Zhang, "Lattice constant effects of photonic crystals on the extraction of guided mode of GaN based light emitting diodes," *Science China-Technological Sciences,* vol. 54, pp. 1-5, Jan 2011.

[32] G. M. Wu, C. C. Yen, H. W. Chien, H. C. Lu, T. W. Chang, and T. E. Nee, "Effects of nano-structured photonic crystals on light extraction enhancement of nitride light-emitting diodes," *Thin Solid Films,* vol. 519, pp. 5074-5077, 2011.

[33] X. Fu, B. Zhang, X. Kang, J. Xu, C. Xiong, and G. Zhang, "Lattice constant effects of photonic crystals on the extraction of guided mode of GaN based light emitting diodes," *SCIENCE CHINA Technological Sciences,* vol. 54, pp. 1-5, 2011.

[34] E. Matioli and C. Weisbuch, "Impact of photonic crystals on LED light extraction efficiency: approaches and limits to vertical structure designs," *J Phys D Appl Phys,* vol. 43, Sep 8 2010.

[35] J. Q. Xi, M. F. Schubert, J. K. Kim, E. F. Schubert, M. F. Chen, S. Y. Lin*, et al.*, "Optical thin-film materials with low refractive index for broadband elimination of Fresnel reflection," *Nat Photonics,* vol. 1, pp. 176-179, Mar 2007.

[36] S. Chhajed, W. Lee, J. Cho, E. F. Schubert, and J. K. Kim, "Strong light extraction enhancement in GaInN light-emitting diodes by using self-organized nanoscale patterning of p-type GaN," *Appl. Phys. Lett.,* vol. 98, Feb 14 2011.

[37] L. Han, T. A. Piedimonte, and H. Zhao, "Experimental exploration of the fabrication of GaN microdome arrays based on a self-assembled approach," *Opt. Mater. Express,* vol. 3, pp. 1093-1100, 08/01 2013.

[38] Y. T. Wang, Y. Chou, L. Y. Chen, Y. F. Yin, Y. C. Lin, and J. J. Huang, "On the Radiation Profiles and Light Extraction of Vertical LEDs With Hybrid Nanopattern and Truncated Microdome Surface Textures," *IEEE J. Quantum Electron.,* vol. 49, pp. 11-16, Jan 2013.

[39] M. Ma, J. Cho, E. F. Schubert, Y. Park, G. B. Kim, and C. Sone, "Strong light-extraction enhancement in GaInN light-emitting diodes patterned with TiO2 micro-pillars with tapered sidewalls," *Appl. Phys. Lett.,* vol. 101, Oct 1 2012.

[40] J. J. Wierer, A. David, and M. M. Megens, "III-nitride photonic-crystal light-emitting diodes with high extraction efficiency," *Nat Photonics,* vol. 3, pp. 163-169, Mar 2009.

[41] Y. K. Ee, R. A. Arif, N. Tansu, P. Kumnorkaew, and J. F. Gilchrist, "Enhancement of light extraction efficiency of InGaN quantum wells light emitting diodes using SiO_2/polystyrene microlens arrays," *Appl. Phys. Lett.,* vol. 91, Nov 2007.

[42] Y. K. Ee, P. Kumnorkaew, R. A. Arif, H. Tong, J. F. Gilchrist, and N. Tansu, "Light extraction efficiency enhancement of InGaN quantum wells light-emitting diodes with polydimethylsiloxane concave microstructures," *Opt. Express,* vol. 17, pp. 13747-13757, Aug 2009.

[43] Y. K. Ee, P. Kumnorkaew, R. A. Arif, H. Tong, H. P. Zhao, J. F. Gilchrist*, et al.*, "Optimization of Light Extraction Efficiency of III-Nitride LEDs With Self-Assembled Colloidal-Based Microlenses," *Ieee J Sel Top Quant,* vol. 15, pp. 1218-1225, Jul-Aug 2009.

[44] H. C. Chang, K. Y. Lai, Y. A. Dai, H. H. Wang, C. A. Lin, and J. H. He, "Nanowire arrays with controlled structure profiles for maximizing optical collection efficiency," *Energy & Environmental Science,* vol. 4, pp. 2863-2869, Aug 2011.

[45] P. Kumnorkaew, Y. K. Ee, N. Tansu, and J. F. Gilchrist, "Investigation of the Deposition of Microsphere Monolayers for Fabrication of Microlens Arrays," *Langmuir,* vol. 24, pp. 12150-12157, Nov 2008.

[46] P. Kumnorkaew and J. F. Gilchrist, "Effect of Nanoparticle Concentration on the Convective Deposition of Binary Suspensions," *Langmuir,* vol. 25, pp. 6070-6075, Jun 2009.

[47] P. Kumnorkaew, A. L. Weldon, and J. F. Gilchrist, "Matching Constituent Fluxes for Convective Deposition of Binary Suspensions," *Langmuir,* vol. 26, pp. 2401-2405, 2010/02/16 2009.

[48] K. K. Jang, P. Prabhakaran, D. Chandran, J.-J. Park, and K.-S. Lee, "Solution processable and photopatternable blue, green and red quantum dots suitable for full color displays devices," *Opt. Mater. Express,* vol. 2, pp. 519-525, 2012.

[49] W. Koo, W. Yun, P. Zhu, X. H. Li, N. Tansu, and F. So, "P ¡110: Light extraction of Phosphorescent OLEDs by Defective Hexagonal ¡Close ¡Packed Array," *SID Symposium Digest of Technical Papers,* vol. 43, pp. 1474-1476, 2012.

[50] J. Y. Cho, K. J. Byeon, and H. Lee, "Forming the graded-refractive-index antireflection layers on light-emitting diodes to enhance the light extraction," *Opt. Lett.,* vol. 36, pp. 3203-3205, Aug 15 2011.

Chapter 4 Rapid Convective Deposition of Microsphere Arrays

4.1 Introduction to Rapid Convective Deposition Method

Rapid convective deposition (see Figure 4-1), uses the horizontal deposition of a microliter droplet where a concentrated suspension is injected between the deposition blade and substrate. The small droplet of suspension is held by the capillary force between the blade and substrate. The substrate is then translated by linear motor. As the substrate is pulled away from the bulk suspension. The meniscus stretches out and sweeps across the substrate. The thickness of the meniscus gradually decreases from the bulk to the contact line where crystallization occurs.

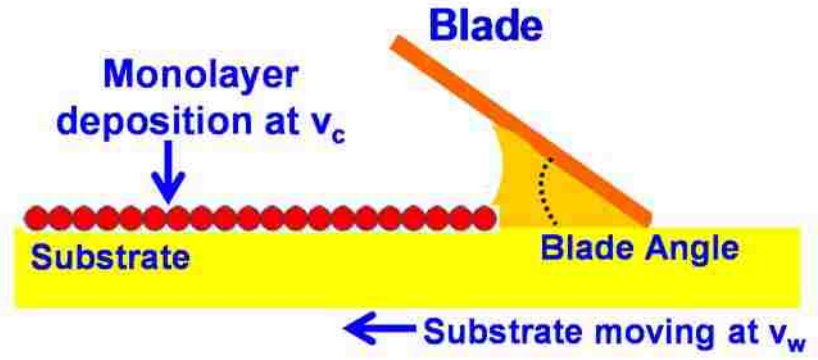

Figure 4-1. The schematic of rapid convective deposition process.

The 2D particle arrays were formed under the tradeoff between electrostatic and capillary forces [1-4]. The lateral capillary forces are capable of gathering particles into layered arrays [5-7]. When the spheres are partially immersed in a liquid on horizontal solid substrate, the meniscus are formed due to the deformations of liquid-gas interface (see Figure 4-2). The shape of meniscus depends on the distance between the particles S_1+S_2, the thickness of liquid l_0 and the contact angle α. This leads to the strong and long-range interparticle capillary forces [3, 8, 9].

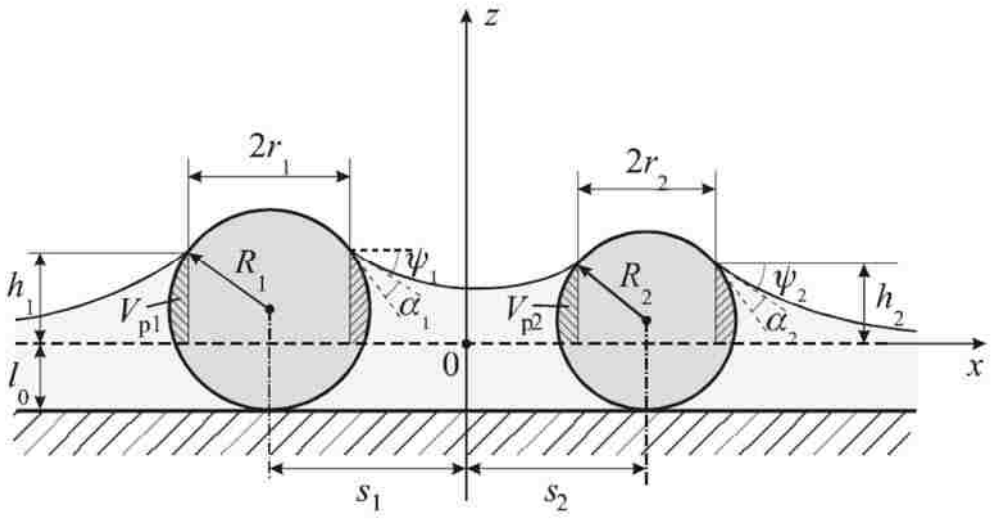

Figure 4-2. Schematics of two spheres partially immersed in a liquid layer a horizontal substrate. [9]

The inclination of the three-phase contact lines at the particle surface leads to two capillary effects: 1) pressure effect, which is caused by the higher hydrostatic pressure in the gas phase than the pressure in the liquid, this pressure difference contributes to the attraction of particles; 2) surface force effect: the slope of liquid surface varies along the contact line. The surface tension effect is much larger than then pressure effect for the micrometer-size and smaller particles [3, 8]. The capillary can be expressed as[5]

$$F \approx 2\pi\sigma r_c^2 \left(\sin^2 \Psi_c\right)\left(1/L\right) \tag{4.1}$$

Where δ is the surface tension of the liquid, r_c is the radius of three-phase contact line at the particle surface, Ψ_c is the mean meniscus slope angle at the contact line. From equation(4.1), liquid deformation increases with the decrease in thickness of film, which results in stronger inter-particle attraction.

The particles most possibly self-assemble into a hexagonal close-packed structure at the “crystal front” a result of large capillary force generated when the particles confined in the thin film near where the three phase of the air/liquid/substrate meet. The horizontal

component of the capillary forces results in the directional motion of particles towards the order arrays. The directional particle motion is attributed to the convective water flux which carriers along the particles toward the ordered phase. The convective transport of the particles can be speed up or slowed down by the increasing or decreasing the water evaporation rate. The level of water between the particles decreases with the increase in the water evaporation, which leads to increase in the curvature of the menisci. This increases the local sucking capillary pressure and drives the water influx to the ordered arrays. In the opposite, when water evaporation rate decreases due to high humidity of atmosphere, the pressure decreases, which results in the decrease in the particle convective influx. Further increase in the humidity will lead to complete stopping of the process of ordering and even to disintegration of the ordered arrays and restoration of the chaotic particle motion.

Thus, the following ways are able to control the ordering process: 1) control of the speed of convective flow by adjusting the rate of water evaporation. This can be realized by tuning the temperature and humidity of atmosphere; 2) control of profile of the liquid meniscus around the ordered arrays. This can be realized by adjust the suspension concentration.

Controlling the relative position of array's leading edge is the key in producing large-sized, homogenous particle arrays. Control of the acceleration or deceleration of the array production by changing environmental conditions, such as humidity, temperature, and particle volume fraction [10].

The homogenous formation of a monolayer or multilayer was successfully maintained by carefully withdrawing the substrate together with the already formed particle arrays from the suspension. The centimeter-sized monolayer particle arrays was obtained [10].

Convective transfer of particles from the bulk of the suspension to the thin wetting film due to water evaporation from the film surface and interactions between the particles that lead to the specific textures [10]. The primary driving force for the convective transfer of particles is the water evaporation from the freshly formed particle arrays.

$$v_w = v_c^k = \frac{\beta l j_e \varphi}{h(1-\varepsilon)(1-\varphi)} \tag{4.2}$$

where v_w is the substrate withdraw speed; v_c is the film growth speed; h is the height of the film; β is the interaction between the particle-particle and particle-substrate and should vary from 0 to 1. The stronger the interaction, the smaller the value of β. For nonadsorbing particles and dilute suspensions, β approaches 1. Therefore, we set β as 1; j_e is the water evaporation rate and it depends on the temperature and humidity; φ is the volume fraction of the particles; ϵ is the packing density of particles, which is 0.605 for the hexagonal-close-packed monolayer arrays and 0.52 for square closed packed monolayer arrays.

For the monolayer crystal growth, the contact line is assumed to be the crystal front. If the height of meniscus at the crystal front is less than the particle diameter, then the incoming particle will not form a close-packed structure. On the contrary, if the height of crystal is higher than the particle diameter, then the multilayer crystals are formed.

The interactions between particles confined in the thin films can be attributed to electrostatic and lateral capillary forces.

4.1.1 Optimization Parameters to Deposit Microsphere Arrays

According to equation(4.2), the growth rate of microsphere arrays depends on the particle volume fraction, φ, water evaporation rate, j_e, diameter of particles, thickness of layers, and an experimentally determined constant, the product βl.

Deposition Speed

The substrate moving speed has significant effect on the microsphere quality: 1) the multilayer sphere arrays will be formed if the substrate moving speed is lower than the film growth speed; 2) the monolayer sphere arrays will be formed if the substrate moving speed is equal to the film growth speed; 3) the submonolayer sphere arrays will be formed if the substrate moving speed is higher than the film growth speed.

Suspension Concentration

In order to deposit homogenous sphere arrays, the suspension concentration is an important parameter needed to be optimized. Our experiment results (see Figure 4-3) showed that optimized suspension concentration is different for different diameter of spheres. Suspension concentration increased with sphere diameters.

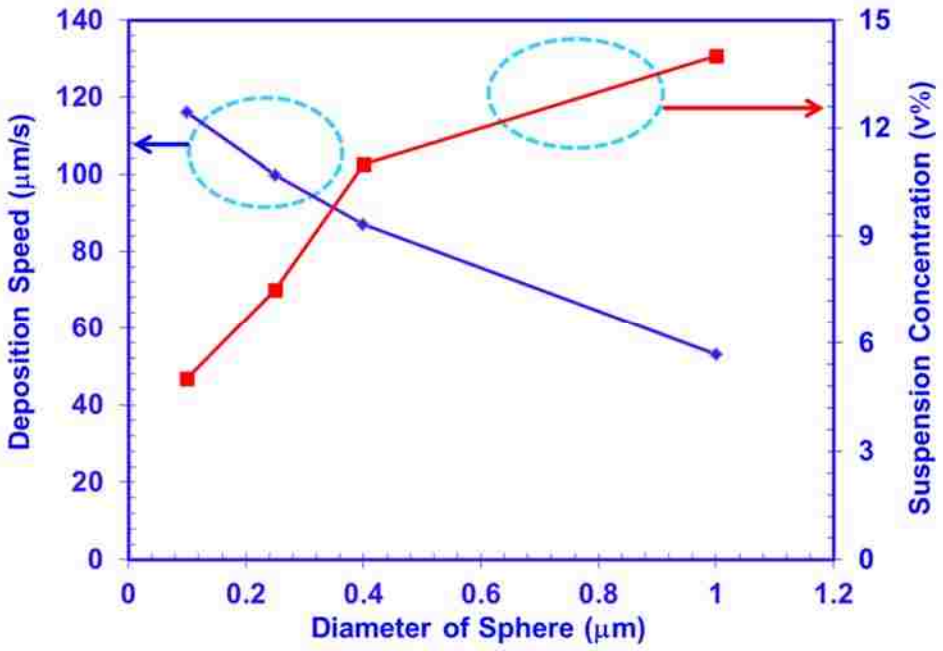

Figure 4-3. Deposition speed and suspension concentration as a function of sphere diameters for forming hexagonal closed monolayer sphere arrays.

Figure 4-3 shows the deposition speed and suspension concentration as a function of sphere diameter for the monolayer sphere arrays deposition. Forming monolayer sphere arrays for the bigger sphere requires lower deposition speed and high volume fraction of suspension.

4.1.2 Comparison of RCD Method and Spin-Coating Method

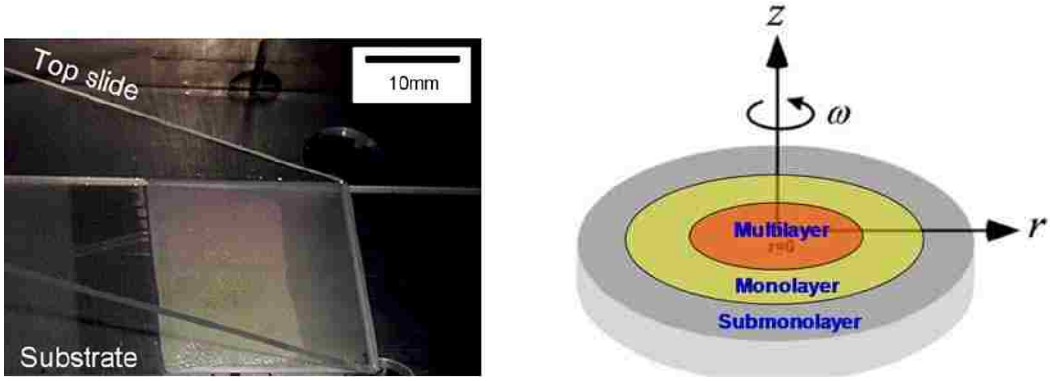

Figure 4-4. Comparison between rapid convective deposition method (left) and spin-coating method (right).

Spin coating is another method which is used to self-assemble sphere arrays. The comparison of RCD method and spin-coating method is shown in Figure 4-4 (a) and (b). The deposition speed is constant across the whole substrate for the RCD method. However, for the case of spin-coating method, the deposition speed can be expressed as

$$v = \omega r \tag{4.3}$$

Thus the deposition speed is radius dependent, which leads to: 1) multi-layer sphere array deposition in the center region of wafer due to lower deposition speed; 2) monolayer sphere deposition in an mm x mm region of wafer [see Figure 4-4 (b)]; 3) sub-monolayer sphere array deposition at the edge of the wafer resulted from the high deposition speed. The large-area sphere coverage cannot be obtained due to the non-homogenous speed across the whole wafer [11].

4.2 RCD Deposition of Microsphere Arrays

4.2.1 Suspension preparation:

The colloidal suspensions used in this work were purchased from the Polysciences Incorporation. The silica spheres are dispersed in deionized (DI) water. The concentration of silica spheres in suspension was tuned by adjusting the ratio of silica spheres to the DI water. The suspension is dispersed using an ultrasonic machine (fisher scientific) and stirred for 10 min using standard vortex mixer (fisher scientific).

4.2.2 Substrate preparation:

Plain microscope slides with dimension of 25 mm x 75 mm x 1.0 mm from Fisher Scientific are used as the deposition blade and substrate. All the glass slides are immersed in a piranha solution with 5:1 of sulfuric acid to hydrogen peroxide overnight and then rinsed with DI water. After that, they are immersed in DI water. The back and bottom of glass deposition blade were added with a thin coating parafilm from fisher scientific to make them hydrophobic. The angle between the blade and substrate keeps as 45^{o}. The 7 μL droplet was add between the blade and substrate.

4.2.3 Deposition:

The experimental setup is shown in Figure 4-1. The deposition was carried out at room temperature. The deposition blade was placed 10 μm above the substrate. 1μm suspension was injected between and bladed and substrate. The microsphere arrays were formed as the substrate was pulled away by the linear motor.

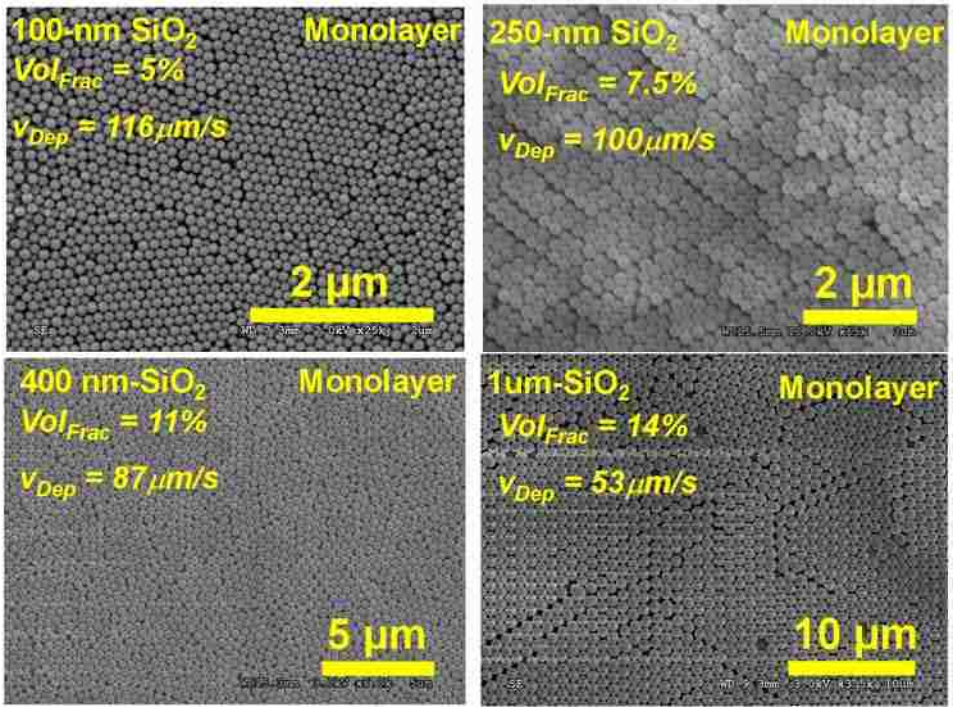

Figure 4-5. SEM images of hexagonal sphere arrays deposited by rapid convective deposition method

The comprehensive studies were carried out to investigate the deposition conditions of monolayer sphere arrays for SiO_2 sphere with various diameters. The concentration of suspension and deposition speed were tuned while the blade angle, temperature and humidity keep constant. We found that the monolayer sphere arrays can only be formed at specific volume fraction and deposition speed for a specific diameter of spheres. The deposition condition for 100-nm sphere arrays are volume fraction of 5% and deposition speed of 116μm/s. The deposition conditions for 250-nm sphere arrays are volume fraction of 7.5% and deposition speed of 100μm/s. The deposition conditions for 400-nm sphere arrays are volume fraction of 11% and deposition speed of 87μm/s. The deposition conditions of 1-μm microsphere arrays are volume fraction of 14% and deposition speed of 53 μm/s.

4.3 RCD Deposition of Binary Microsphere Arrays

For the deposition of SiO_2/PS sphere arrays, the SiO_2 and PS spheres were mixed in DI water and SiO_2/PS suspension was formed. 7μL suspension was injected between the substrate and plain glass slides forming a wedge with the substrate at the angle of 45° or 55° and then the blade swept across the substrate at a certain speed to achieve monolayer deposition.

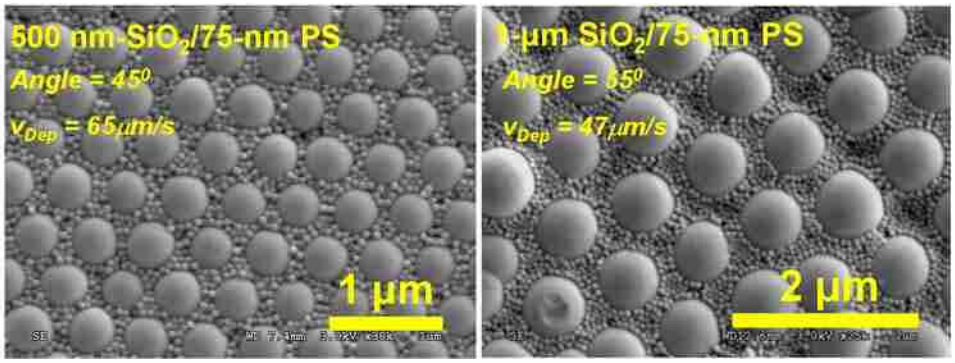

Figure 4-6. SEM images of hexagonal close-packed binary sphere arrays:1) 500-nm SiO_2/75-nm PS binary sphere arrays, 2) 1-μm SiO_2/75-nm PS binary sphere arrays.

Comprehensive study was carried out to investigate the deposition conditions of monolayer binary sphere arrays for sphere with various diameters. We found that in addition to the atmosphere temperature, humidity, deposition speed and concentration of SiO_2 spheres, the ratio of SiO_2 concentration to PS concentration, and the ratio of the SiO_2 diameter to PS diameter have significant effect on the formation of hexagonal close packed sphere arrays.

We investigated the deposition conditions of 1-μm SiO_2 and 500-nm SiO_2/ PS binary sphere arrays. For the 1-μm SiO_2 spheres, to form hexagonal close packed monolayer sphere arrays, the ratio of SiO_2 to PS should be 14% to 4%, and the deposition speed is 47μm/s with the blade angle of 55°. For the 500-μm SiO_2 spheres, the optimized conditions are deposition speed of 65μm, blade angle of 45° and SiO_2/PS ratio of 14%/4%. The SEM

images of hexagonal close packed monolayer of 500-nm sphere arrays and -μm sphere arrays embedded in the PS are shown in Figure 4-6.

The deposition for 400-nm/75 nm PS binary sphere arrays requires more optimization due to the smaller SiO_2 / PS diameter ratios (400 nm versus 75 nm) and larger variation in SiO_2 diameter distribution. The optimized deposition conditions are volume fraction of 8.8% for 400-nm SiO2 spheres and volume fraction of 3.5% for 75-nm PS spheres.

The microlens arrays were obtained by heat treatment of SiO_2/PS binary sphere arrays which resulted in the hexagonal-close packed monolayer SiO_2 sphere arrays embedded in the planar PS layer (see Figure 4-7). The PS thickness was tuned by adjusting the annealing time at annealing temperature of 140°C, which resulted in the microlens arrays with various aspect ratio.

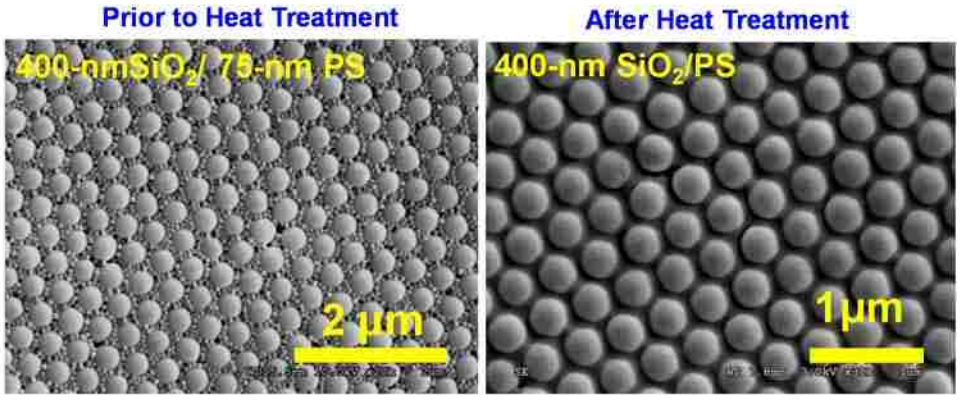

Figure 4-7. The SEM images of 400-nm SiO_2/75-nm PS binary sphere arrays and the 400-nm SiO_2/PS microlens arrays.

4.4 Light Extraction Efficiency Enhancement of LED with Microsphere and Microlens Arrays [12-16]

The enhancement of light extraction efficiency of InGaN quantum wells LEDs employing SiO_2/PS microlens arrays deposited by RCD method was demonstrated

experimentally [12]. The use of microlens arrays on the top of InGaN quantum well LED increased the light escape cone and reduced the Fresnel reflection.

The schematic device structure of InGaN quantum well LED is shown in Figure 4-8. The 1-μm SiO_2/PS microsphere arrays were deposited on the top of InGaN QW LED structure [12]. The refractive index of GaN in the visible region is 2.5, while the refractive indices of SiO_2 and PS are 1.46 and 1.58, respectively. The SiO_2 spheres are embedded in the planar PS layer, which forms close-packed microlens arrays. The utilization of these lens arrays increases the light escape cone due to the curvature formed between the SiO_2 and free space.

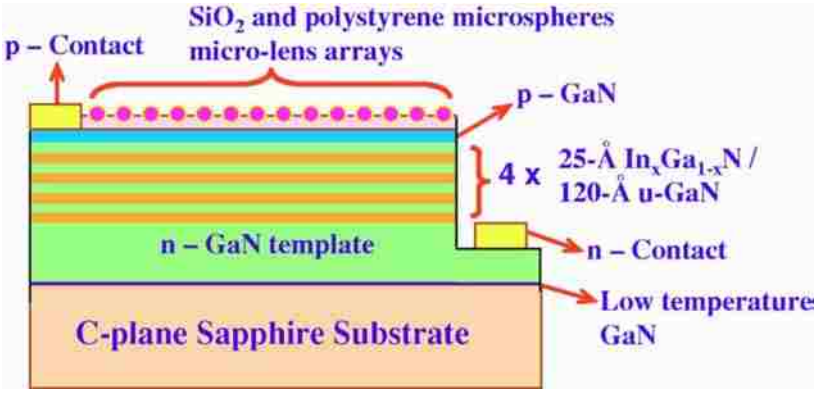

Figure 4-8. Schematic of InGaN QWs LEDs structure with SiO_2/PS microsphere or microlens arrays [12].

Electroluminescence measurement shows that the use of microlens arrays has resulted in increased light output from the top of LED as shown in Figure 4-9. The output power as a function of driving current for up to 100 mA for both LED with and without microlens arrays was measured. The results show that output power of LED with microlens arrays is 219% higher than that of planar LED. The significant enhancement in the light extraction efficiency is attributed to the enlarged escape cone. In addition, the use of intermediate refractive index materials, SiO_2 and PS reduces the Fresnel reflection between GaN and free space.

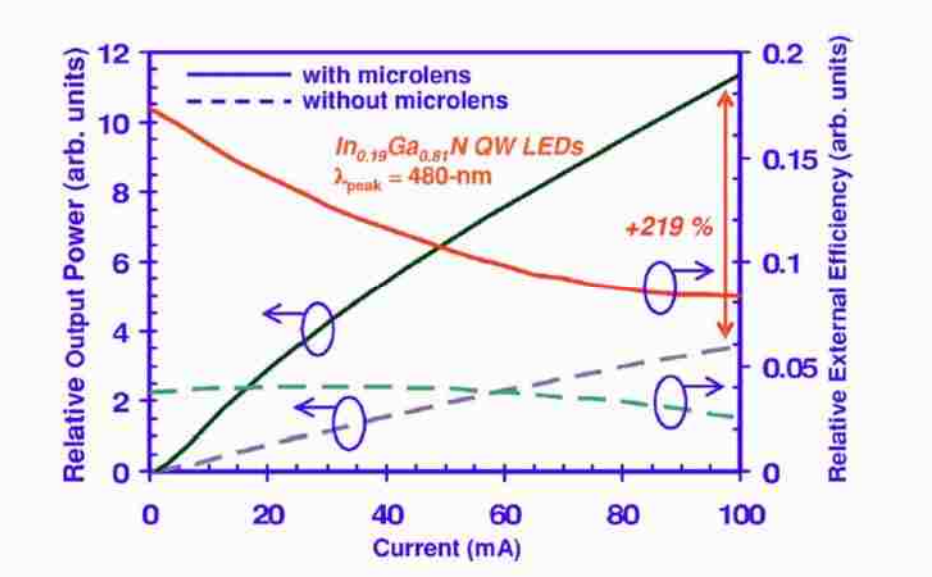

Figure 4-9. Electroluminescence of InGaN LED with and without SiO_2/PS microlens arrays [12].

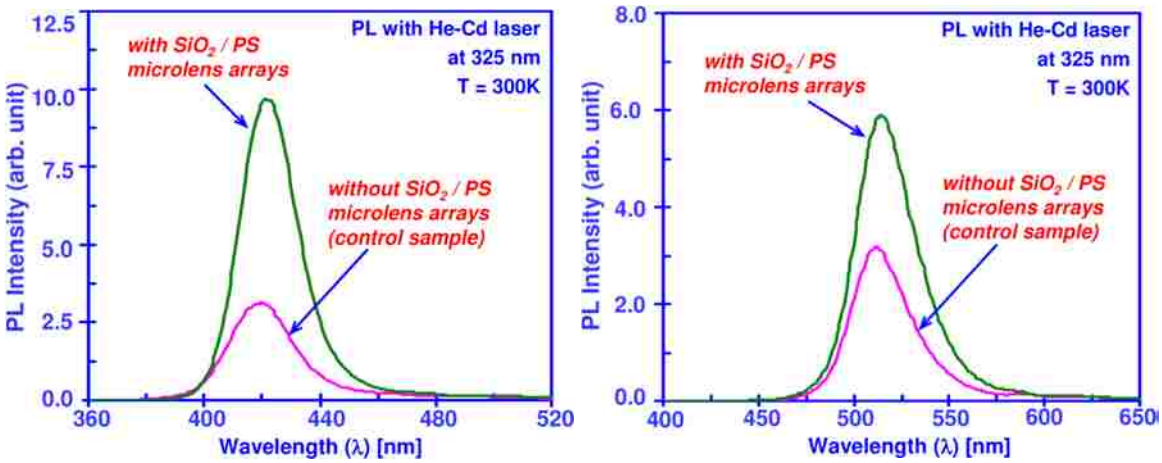

Figure 4-10. (Left) Photoluminescence intensity of LED with and without 1.0μm SiO_2/PS microlens arrays. (Right) Photoluminescence intensity of LED with and without 0.5 μm SiO_2/PS microlens arrays.[12]

To further enhance the light extraction efficiency of InGaN QW LED. The device structure of LED with SiO_2/PS microsphere/microlens arrays was engineered by tuning diameter of SiO_2 spheres [13]. The results shows that the size of SiO_2 spheres has significant effect on the light extraction. The deposition of 0.5-μm sphere arrays on the LED results in 1.69 times enhancement in light extraction efficiency while the use of 1$-\mu$m

sphere arrays leads to 2.00 times enhancement in output power compared to that of planar LED [13].

The effect of aspect ratio of microlens on the light extraction efficiency of LED with 1−μm SiO_2/PS microlens arrays was also investigated [17].

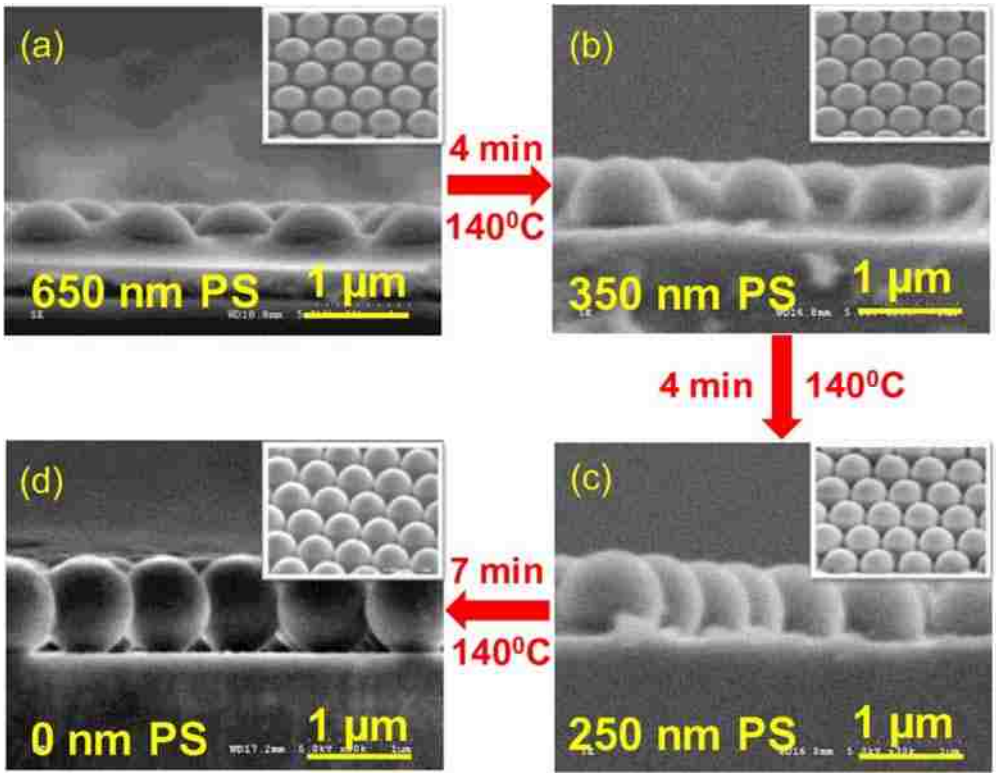

Figure 4-11. SEM images of 1.0-μm SiO_2/PS microlens arrays LEDs with PS thickness of (a) 650 nm, (b) 350 nm, (c) 250 nm, (d) 0 nm. [17]

The deposition of SiO_2/PS microlens arrays were carried out on GaN-based top-emitting LED device by using RCD method. The obtained the SiO_2/PS binary sphere arrays was annealed at 140°C to melt the PS nanospheres. This leads to forming a planar PS layer surrounding the SiO_2 microspheres. The thickness of PS is tuned by adjusting the annealing time. The SiO_2/PS microlens arrays with various aspect ratio are obtained by tuning the annealing time.

The effect of aspect ratio of microlens on the light extraction was investigated by measuring the electroluminescence of microlens LED with various aspect ratio which is compared to that of planar LED.

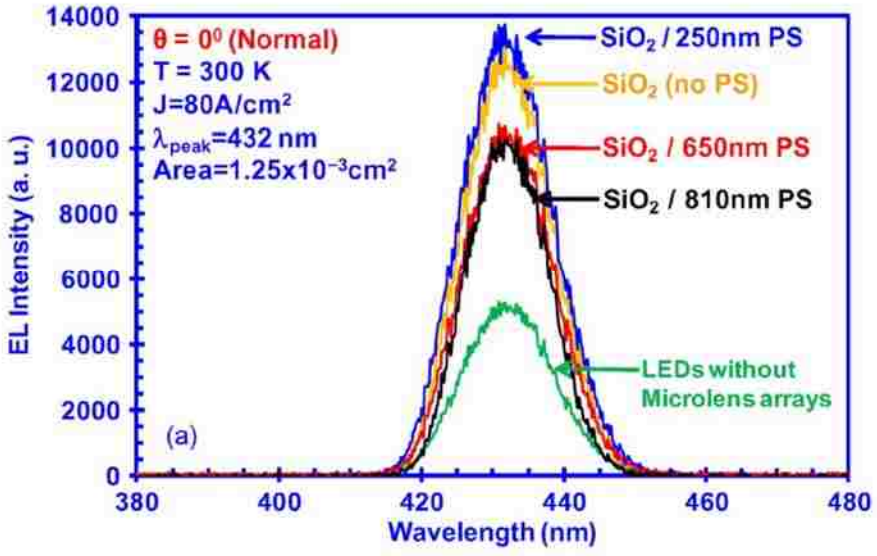

Figure 4-12. Electroluminescence spectra of InGaN quantum well microlens arrays LED with various PS thickness and planar LED for normal at angle of 0°. [17]

Figure 4-12 is the EL spectra at normal direction of LED with microlens arrays and planar LED at current density of 80 A/cm^2. 2.40, 2.60, 2.03, and 1.96 times enhancement in output power has been achieved for microlens LED with PS thickness of 0 nm, 250 nm, 650 nm, and 810 nm.

To investigate the effect of microlens aspect ratio on the output power, the output power was plotted as a function of PS thickness. Figure 4-13 shows the total output power versus PS thickness of SiO_2/PS microlens arrays LED at current density of 80mA/cm^2. The implementation of the optimized PS layer thickness in the SiO_2/PS microlens arrays leads to enhancement in the output power. The controllability of PS thickness is critical in the extracting the light from the LED devices.

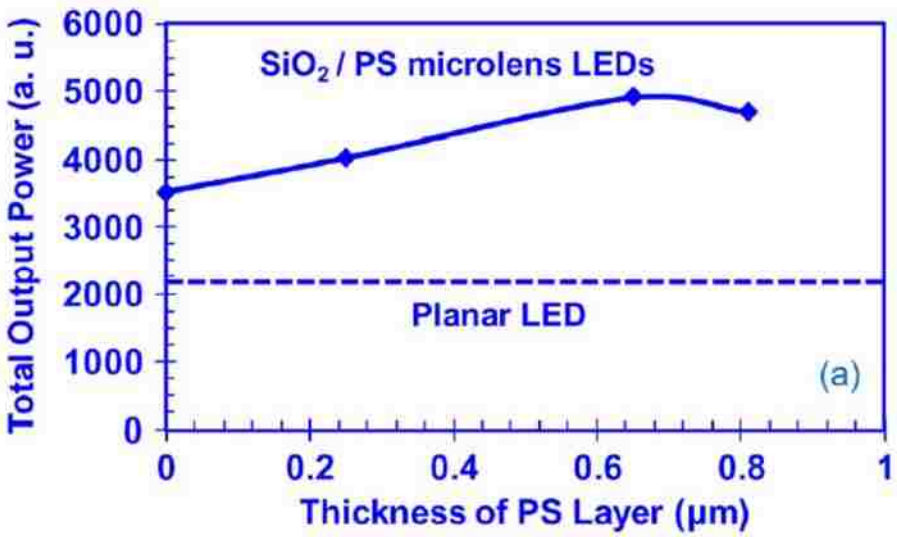

Figure 4-13. Total output power as a function of PS thickness of LED with SiO_2/PS microlens arrays. [17]

4.5 Light Extraction Efficiency of LED with Concave Structures[18]

The enhancement in light extraction of GaN LED using polydimethylsiloxane (PDMS) concave microstructures arrays was also demonstrated.

The process flow of forming PDMS concave structures is shown in Figure 4-14. The SiO_2/PS microlens arrays deposited via RCD method was employed as template for forming concave structures on PDMS via soft-lithography. The PDMS was deposited on the top of LED. The PDMS-coated LED wafer was then imprinted by the monolayer SiO_2 microsphere arrays template. The PDMS-coated wafer was heated to a temperature of 80^{o}C for 45 minutes to cure the PDMS layer.

The electroluminescence measurements were conducted for the LED with and without PDMS concave microstructure arrays. The output power of InGaN MQWs LED, with the inject current density ranging from 0 to 80 A/cm^2 are shown in Figure 4-15. The results show that 1.60 times enhancement in the output power has been achieved for LED with concave structures compared to that of planar LED.

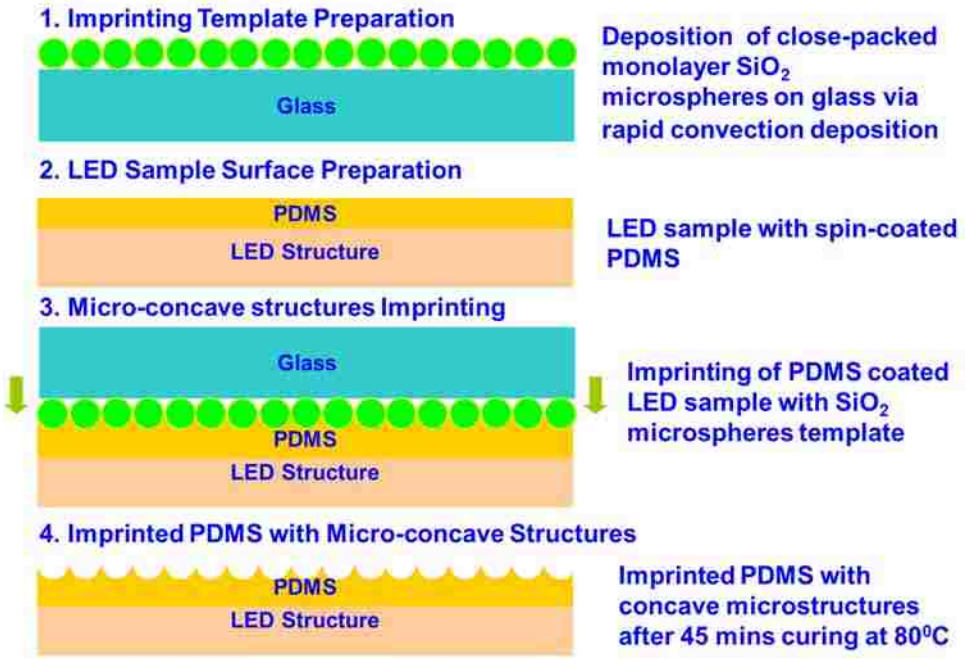

Figure 4-14. Process flow of depositing PDMS concave microstructures arrays on InGaN QWs LEDs.[18]

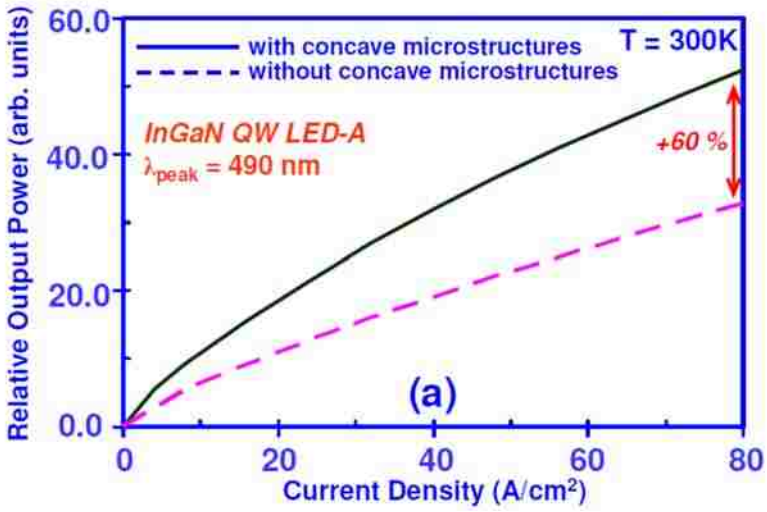

Figure 4-15. Comparison of electroluminescence intensity of InGaN QW LEDs with and without 3.0 μm thick PDMS layer. [18]

4.6 Implementation of Self-Assembled Microlens Arrays on Organic Light-Emitting Diode [19-21]

The microsphere arrays deposited via RCD method was also used as imprinting template to form corrugated structures on the organic light-emitting diodes (OLEDs) to extract waveguide modes [19, 22].

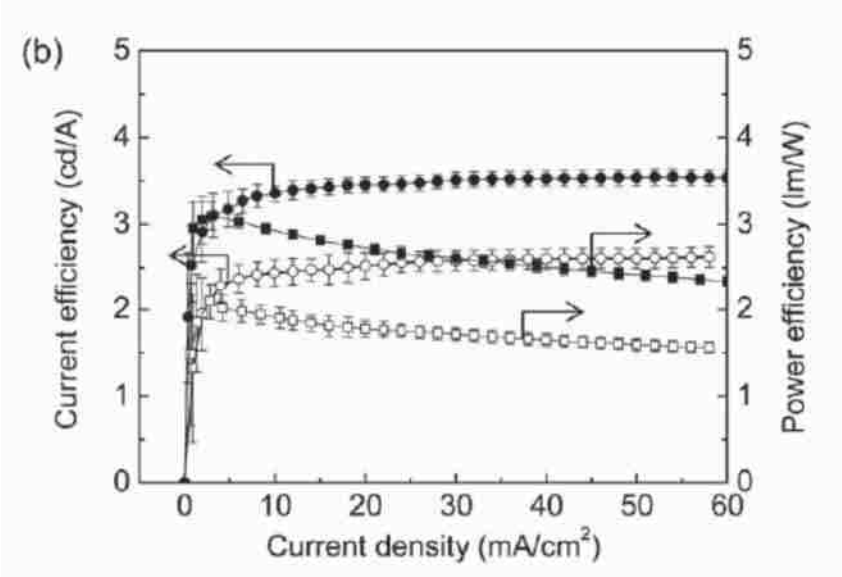

Figure 4-16. Current efficiency and power efficiency for 1.0 μm grating (filled symbols) and reference (open symbols) devices. [20]

The SiO_2 sphere arrays were fabricated by depositing SiO_2 spheres and 100-nm PS spheres on glass substrate by RCD method. After deposition, the sample was heated at 140°C to melt the PS spheres, and the microlens arrays was formed. The obtained microlens arrays were used as template on which the PDMS was deposited and cured to form the PDMS replica. To fabricate the resin coated substrates, a drop of resin was placed on the resin-coated substrates. Then the silica sphere array patterns of PDMS replica were transferred to UV-curable resin layer.

The use of 0.5 μm grating (Figure 4-16) and 1.0 μm grating resulted in 70% and 90% enhancement in power efficiency.

In summary, the comprehensive study were carried out to investigate deposition of microsphere or microlens arrays by using rapid convective deposition method. The results showed that monolayer, submonolayer, and multilayer sphere arrays can be obtained by tuning deposition speed, suspension concentration, temperature, humidity, and blade angle. The rapid deposition method can be used to deposit microsphere arrays with various diameters and refractive indices. The use of microsphere or microlens arrays resulted in significant enhancement in light extraction for both GaN-based LED and organic LED.

References

[1] P. Pieranski, L. Strzelecki, and B. Pansu, "Thin Colloidal Crystals," *Physical Review Letters,* vol. 50, pp. 900-903, 1983.

[2] C. A. Murray and D. H. Vanwinkle, "Experimental-Observation of 2-Stage Melting in a Classical Two-Dimensional Screened Coulomb System," *Physical Review Letters,* vol. 58, pp. 1200-1203, Mar 23 1987.

[3] P. A. Kralchevsky, V. N. Paunov, I. B. Ivanov, and K. Nagayama, "Capillary Meniscus Interaction between Colloidal Particles Attached to a Liquid-Fluid Interface," *J. Colloid Interface Sci.,* vol. 151, pp. 79-94, Jun 1992.

[4] P. A. Kralchevsky and K. Nagayama, "Capillary Forces between Colloidal Particles," *Langmuir,* vol. 10, pp. 23-36, Jan 1994.

[5] N. D. Denkov, O. D. Velev, P. A. Kralchevsky, I. B. Ivanov, H. Yoshimura, and K. Nagayama, "Mechanism of Formation of 2-Dimensional Crystals from Latex-Particles on Substrates," *Langmuir,* vol. 8, pp. 3183-3190, Dec 1992.

[6] C. D. Dushkin, H. Yoshimura, and K. Nagayama, "Nucleation and Growth of 2-Dimensional Colloidal Crystals," *Chem. Phys. Lett.,* vol. 204, pp. 455-460, Mar 26 1993.

[7] A. S. Dimitrov, C. D. Dushkin, H. Yoshimura, and K. Nagayama, "Observations of Latex Particle 2-Dimensional-Crystal Nucleation in Wetting Films on Mercury, Glass, and Mica," *Langmuir,* vol. 10, pp. 432-440, Feb 1994.

[8] P. A. Kralchevsky, V. N. Paunov, N. D. Denkov, I. B. Ivanov, and K. Nagayama, "Energetical and Force Approaches to the Capillary Interactions between Particles Attached to a Liquid Fluid Interface," *J. Colloid Interface Sci.,* vol. 155, pp. 420-437, Feb 1993.

[9] P. Kralchevsky and K. Nagayama, *Particles at fluid interfaces and membranes: attachment of colloid particles and proteins to interfaces and formation of two-dimensional arrays* vol. 10: Elsevier, 2001.

[10] A. S. Dimitrov and K. Nagayama, "Continuous Convective Assembling of Fine Particles into Two-Dimensional Arrays on Solid Surfaces," *Langmuir,* vol. 12, pp. 1303-1311, 1996/01/01 1996.

[11] T. Ogi, L. B. Modesto-Lopez, F. Iskandar, and K. Okuyama, "Fabrication of a large area monolayer of silica particles on a sapphire substrate by a spin coating method," *Colloids and Surfaces A: Physicochemical and Engineering Aspects,* vol. 297, pp. 71-78, 4/5/ 2007.

[12] Y. K. Ee, R. A. Arif, N. Tansu, P. Kumnorkaew, and J. F. Gilchrist, "Enhancement of light extraction efficiency of InGaN quantum wells light emitting diodes using SiO_2/polystyrene microlens arrays," *Appl. Phys. Lett.,* vol. 91, Nov 2007.

[13] Y. K. Ee, P. Kumnorkaew, R. A. Arif, H. Tong, H. P. Zhao, J. F. Gilchrist*, et al.*, "Optimization of Light Extraction Efficiency of III-Nitride LEDs With Self-Assembled Colloidal-Based Microlenses," *Ieee J Sel Top Quant,* vol. 15, pp. 1218-1225, Jul-Aug 2009.

[14] P. Kumnorkaew, Y. K. Ee, N. Tansu, and J. F. Gilchrist, "Investigation of the Deposition of Microsphere Monolayers for Fabrication of Microlens Arrays," *Langmuir,* vol. 24, pp. 12150-12157, Nov 2008.

[15] X. H. Li, R. B. Song, Y. K. Ee, P. Kumnorkaew, J. F. Gilchrist, and N. Tansu, "Light Extraction Efficiency and Radiation Patterns of III-Nitride Light-Emitting Diodes With Colloidal Microlens Arrays With Various Aspect Ratios," *IEEE Photonics J.,* vol. 3, pp. 489-499, Jun 2011.

[16] X. H. Li, P. F. Zhu, G. Y. Liu, J. Zhang, R. B. Song, Y. K. Ee*, et al.*, "Light Extraction Efficiency Enhancement of III-Nitride Light-Emitting Diodes by Using 2-D Close-Packed TiO2 Microsphere Arrays," *J Disp Technol,* vol. 9, pp. 324-332, May 2013.

[17] H. C. Chang, K. Y. Lai, Y. A. Dai, H. H. Wang, C. A. Lin, and J. H. He, "Nanowire arrays with controlled structure profiles for maximizing optical collection efficiency," *Energy & Environmental Science,* vol. 4, pp. 2863-2869, Aug 2011.

[18] Y. K. Ee, P. Kumnorkaew, R. A. Arif, H. Tong, J. F. Gilchrist, and N. Tansu, "Light extraction efficiency enhancement of InGaN quantum wells light-emitting diodes with polydimethylsiloxane concave microstructures," *Opt. Express,* vol. 17, pp. 13747-13757, Aug 2009.

[19] W. Koo, W. Yun, P. Zhu, X. H. Li, N. Tansu, and F. So, "P ¡110: Light extraction of Phosphorescent OLEDs by Defective Hexagonal ¡Close ¡Packed Array," *SID Symposium Digest of Technical Papers,* vol. 43, pp. 1474-1476, 2012.

[20] W. H. Koo, W. Youn, P. Zhu, X.-H. Li, N. Tansu, and F. So, "Light Extraction of Organic Light Emitting Diodes by Defective Hexagonal-Close-Packed Array," *Adv. Funct. Mater.,* vol. 22, pp. 3453-3453, 2012.

[21] W. H. Koo, W. Youn, P. Zhu, X.-H. Li, N. Tansu, and F. So, "Light Extraction of Organic Light Emitting Diodes by Defective Hexagonal-Close-Packed Array," *Adv. Funct. Mater.,* vol. 22, pp. 3454-3459, AUG 21 2012 2012.

[22] K. K. Jang, P. Prabhakaran, D. Chandran, J.-J. Park, and K.-S. Lee, "Solution processable and photopatternable blue, green and red quantum dots suitable for full color displays devices," *Opt. Mater. Express,* vol. 2, pp. 519-525, 2012.

Chapter 5 Light Extraction Efficiency of GaN LED with TiO_2 Sphere Arrays

5.1 Importance of TiO_2 Microsphere Arrays for GaN LEDs

Our previous works showed that the deposition of hexagonal-close packed 500-nm or 1-μm SiO_2 microsphere or SiO_2/PS microlens arrays on GaN-based LED devices by rapid convective deposition (RCD) method has resulted in significant enhancement in light extraction efficiency of GaN-based LED devices [1-4]. Recent calculation results by employing finite-different time-domain (FDTD) method demonstrated that the advantages of using Anatase TiO_2 sphere arrays over SiO_2 sphere arrays to extract light from GaN-based LED devices [5, 6]. The RCD method is a robust method which can be used to deposit wafer-scale microsphere arrays with various packing density (sub monolayer, monolayer, and multilayer) and geometry (hexagonal-closed packed sphere arrays and square-close packed sphere arrays) [7, 8]. RCD method could easily lead to highly uniform monolayer deposition in wafer scales compared with other deposition methods, such as spin coating which results in uniformity within relatively small region (mm x mm) scale [9, 10].

Here, we present detailed experimental studies on the use of self-assembled 2-D anatase TiO_2 monolayer microsphere arrays to improve the light extraction efficiency of InGaN QW LEDs (see Figure 5-1). The refractive index of anatase TiO_2 in the visible spectrum range is 2.5 [11], thus the implementation of anatase TiO_2 microsphere arrays provides higher refractive index that can match with that of GaN. This results in larger light coupling from GaN to the TiO_2 microsphere arrays and improves LED light extraction efficiency compared with those of LEDs with SiO_2 microsphere arrays [5, 6]. Note that the current work focuses on the deposition studies of 2-D TiO_2 microsphere arrays on GaN LEDs, without the PS layers required to form the microlens arrays.

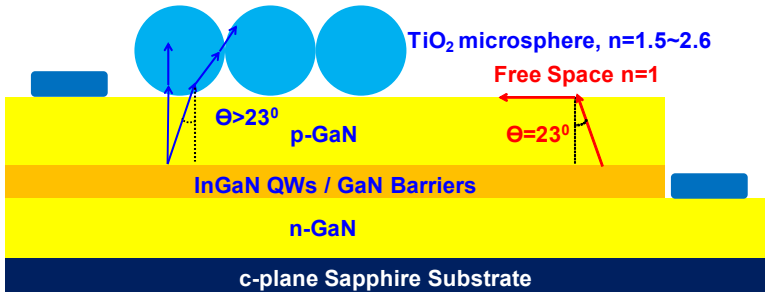

Figure 5-1. Schematic of InGaN QWs LEDs utilizing TiO_2 microsphere arrays on the top surface of LEDs.

5.2 Deposition of Microsphere Arrays on GaN LED

To obtain long-range and close-packed TiO_2 microsphere arrays, the rapid convective deposition (RCD) method was used for the deposition of TiO_2 microsphere arrays. Figure 5-2 shows schematic of experimental setup of RCD for the deposition of anatase TiO_2 microsphere arrays. Similarly, the RCD was also performed in the class-1000 clean room and the standard optical lithography was used to cover the n- and p-metal contacts of the LEDs by photoresist for lifting off TiO_2 microspheres afterwards. Prior to deposition, the TiO_2 microsphere water suspension was immersed in the ultrasonic bath for 1 hour and then were thoroughly shaken by the vortex for 1 minute. Previously, the RCD method was employed for the deposition of SiO_2 / PS microlens arrays, and hence the experimental setup of RCD for the TiO_2 microspheres is similar to that for the SiO_2 / PS microlens arrays. However, the deposition of the TiO_2 microsphere arrays was found to require more optimization than that of the SiO_2 / PS microlens arrays, which was attributed to the less mature synthesis process of TiO_2 microspheres, as compared to that of SiO_2 microspheres, leading to relatively poor monodispersity of the size of TiO_2 microspheres. The monodispersity of the microspheres is critical to achieve fully close-packed and defect-free microsphere arrays in our experiments, therefore the future development of TiO_2

microsphere synthesis can reduce difficulty in depositing TiO_2 microsphere arrays by RCD method.

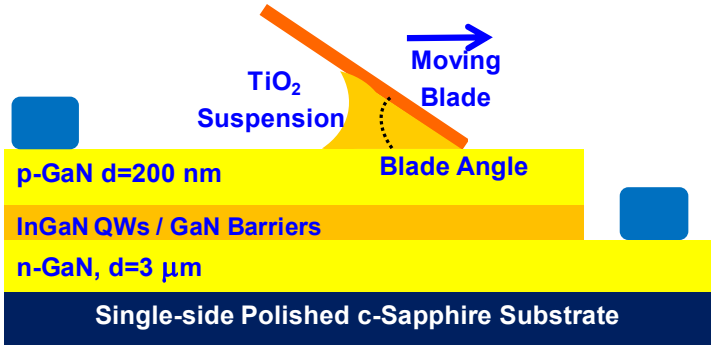

Figure 5-2. Schematic of the experimental setup of rapid convective deposition method for the deposition of TiO_2 microsphere arrays on InGaN QW LEDs.

As the synthesis of TiO_2 microspheres is less mature, the crystalline phase and the refractive index of the TiO_2 microspheres used in the RCD deposition were characterized by Raman spectroscopy measurement at room temperature. The details of the Raman spectroscopy measurement can be found in reference [11]. As shown in Figure 5-3, the TiO_2 microspheres shows strong Raman bands at 150 cm^{-1}, 400 cm^{-1}, 515 cm^{-1}, and 634 cm^{-1}, indicating TiO_2 microspheres consisted of crystals of anatase TiO_2 with index of 2.5 that matches with that of GaN [12].

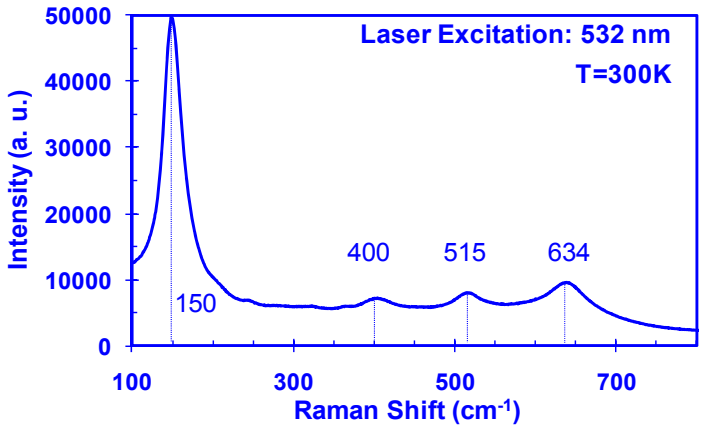

Figure 5-3. Raman spectrum (532 nm) of TiO_2 microsphere used in the RCD.

The surface morphologies of deposited TiO_2 microsphere arrays by RCD method are affected by the deposition temperature, humidity, and blade hydrophobicity, volume fraction of TiO_2 suspension, deposition speed, and blade angle. The RCD experiments were carried in the class-1000 clean room with invariable temperature (25^{O}C) and humidity (45%). The glass blades were covered by a layer of parafilm (Parafilm M Laboratory Wrapping Film) to ensure the hydrophobic of the surface. Therefore, the volume fraction of TiO_2 suspension, blade speed, and blade angle are the three most important factors for optimizing the deposition condition.

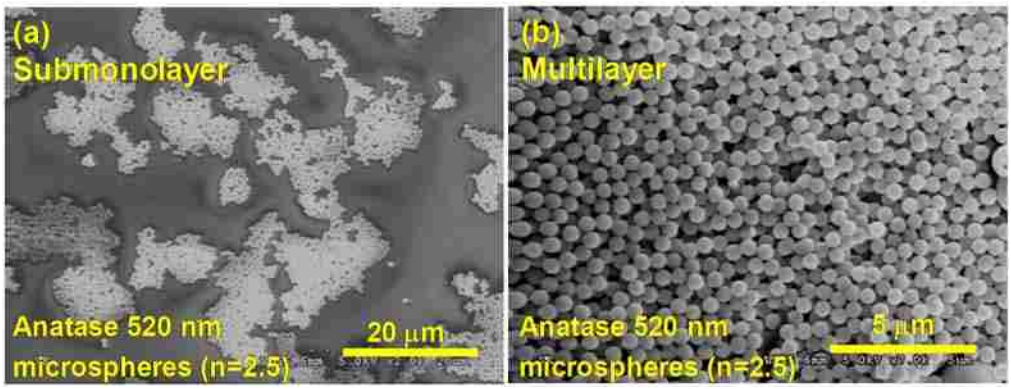

Figure 5-4. SEM images of TiO_2 microsphere deposited by RCD method on the emission surface of InGaN QW LEDs with unoptimized conditions leading to (a) submonolayer and (b) multilayer of TiO_2 microsphere arrays.

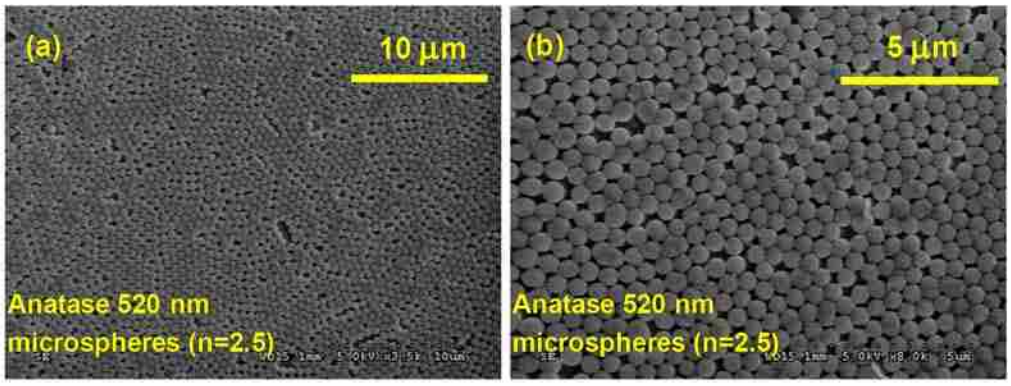

Figure 5-5. SEM images of 520-nm anatase TiO_2 microsphere deposited via the RCD method on the emission surface

In our RCD experiments, the blade angle was fixed at 55° while the blade speed and volume fraction were adjusted to obtain the optimized condition that results in close-packed monolayer TiO_2 microsphere arrays. The SEM measurements were carried out to investigate the surface morphology of TiO_2 microsphere arrays after the deposition. Figure 5-4 (a) and (b) show the SEM images of 520-nm anatase TiO_2 microsphere arrays deposited by the RCD method with unoptimized deposition conditions. As shown in Figure 5-4(a), the lower volume fraction or faster deposition speed in comparison with the optimized conditions led to the submonolayer morphology of TiO_2 microsphere arrays. Figure 5-4(b) shows that the higher volume fraction or slower deposition speed in comparison with the optimized conditions resulted in the multilayer morphology of TiO_2 microsphere arrays.

Figure 5-5(a) and (b) show the SEM images of 520-nm anatase TiO_2 microsphere arrays deposited by the RCD method with optimized conditions. The optimized deposition conditions for monolayer 2-D close-packed TiO_2 microsphere arrays were obtained as the following condition: volume fraction of 10%, blade speed of 12 μm/s, and blade angle of 55°. As shown in Figure 5-5(a) and (b), the post-deposited TiO_2 microspheres formed large-scale, monolayer and close-packed arrays by employing the optimized RCD condition. The point defects in the microsphere arrays is attributed to the poorer monodispersity of the TiO_2 microsphere diameter.

5.3 EL Measurement of LED Devices with TiO_2 Sphere Arrays

In order to provide comparison of the EL characteristics of planar LEDs and LEDs with anatase TiO_2 microsphere arrays deposited by RCD method, the InGaN QW LEDs employing 4 periods of InGaN QW with GaN barriers emitting at 490 nm were used. All LEDs structures studied here were grown on 3.0 μm n-GaN template on c-plane sapphire

substrates. The n-GaN is Si-doped with doping level of 5×10^{18} cm^{-3}. The p-GaN was grown utilizing 200 nm thick Mg-doped GaN with doping level of 3×10^{17} cm^{-3} at 970 °C, followed by annealing at 780 °C in the N_2 ambient. The LED devices were fabricated as top-emitting hexagonal devices with the device area of 7.5×10^{-4} cm^2, and Ti/Au as n-contact and Ni/Au as p-contact were evaporated followed by contact annealing. The LED devices were fabricated as top-emitting hexagonal devices with the device area of 7.5×10^{-4} cm^2. The on-wafer CW power measurements were performed at room temperature.

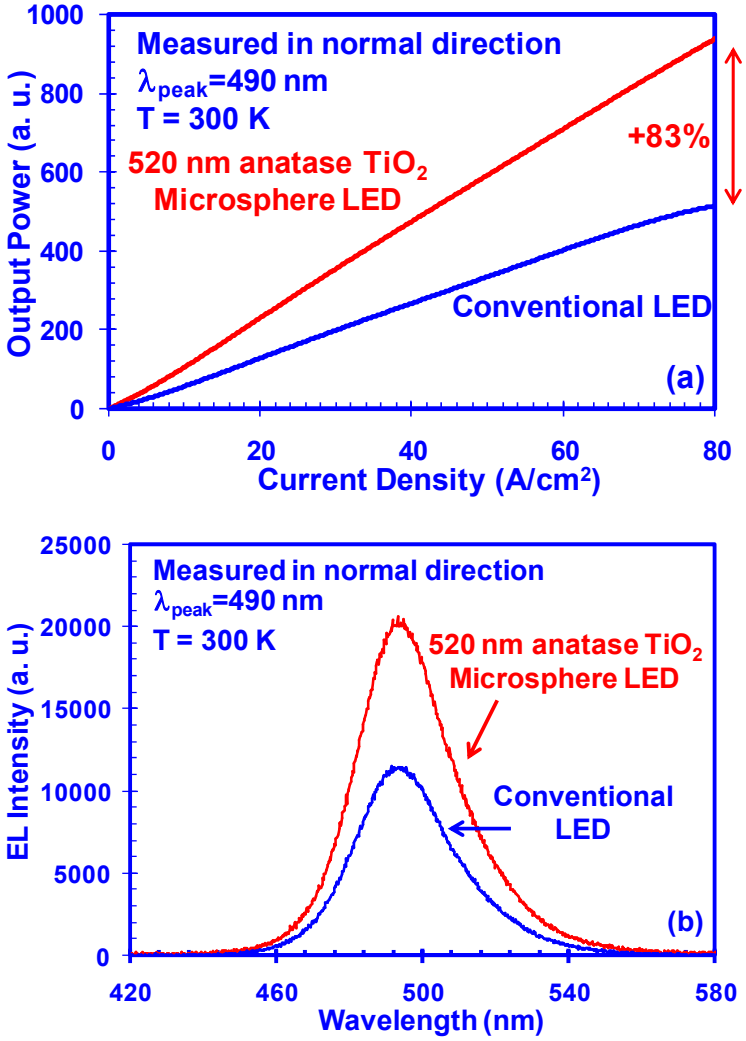

Figure 5-6. (a) Light output power vs current density and (b) EL spectra (J = 80 A/cm²) of InGaN QW LEDs emitting at 490 nm with and without 520-nm anatase TiO_2 microsphere arrays deposited via the RCD method.

Figure 5-6(a) shows the light output power as a function of current density for the 490-nm emitting InGaN QWs LEDs with and without 520-nm anatase TiO_2 microsphere arrays. As shown in Figure 5-6(a) and (b), the CW power-current and EL spectra measurements exhibit 1.83 times improvement in the output power for the LED device with TiO_2 microspheres arrays at the current density of 80 A/cm^2, as compared to that of LED without microspheres arrays. The significant increase in the output power is primarily attributed to significantly enlarged light escape cone between GaN (n=2.5) and anatase TiO_2 microspheres (n=2.5).

5.4 Far-field Radiation Pattern

To study the far-field emission patterns of LEDs with TiO_2 microsphere arrays, the output power measurement was carried at the current density of 80A/cm^2 on the 450-nm emitting InGaN QW LEDs with the device area of 6.75×10^{-4} cm^2. The far-field emission patterns of the LEDs with and without 520-nm anatase TiO_2 microsphere arrays deposited by the RCD method were measured.

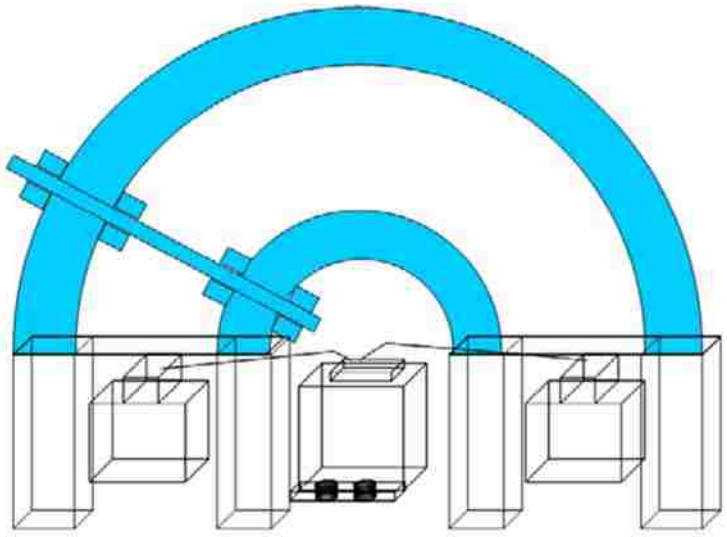

Figure 5-7. Schematic of LED far-field measurement set up employed in the radial far-field EL measurements

As shown in Figure 5-7, the far-field measurement setup consists of a semicircular structure on which the optical fiber can be rotated 180° in a single plane. The measured LEDs were placed in the center of the semicircular structure, hence the optical fiber kept equidistant away from the measured LED as the optical fiber rotated through 180° in the plane to collect the emission at varying angles [see Figure 5-7]. The distance between the optical fiber and measured LEDs was kept at 2.5 cm which was much larger than the dimension of the measured LEDs (161 μm), in order to ensure sufficient large distance for the far-field measurements [59]. In our current studies, the far-field radiation patterns of the LEDs were measured from emission angle from θ=0° up to θ=90°.

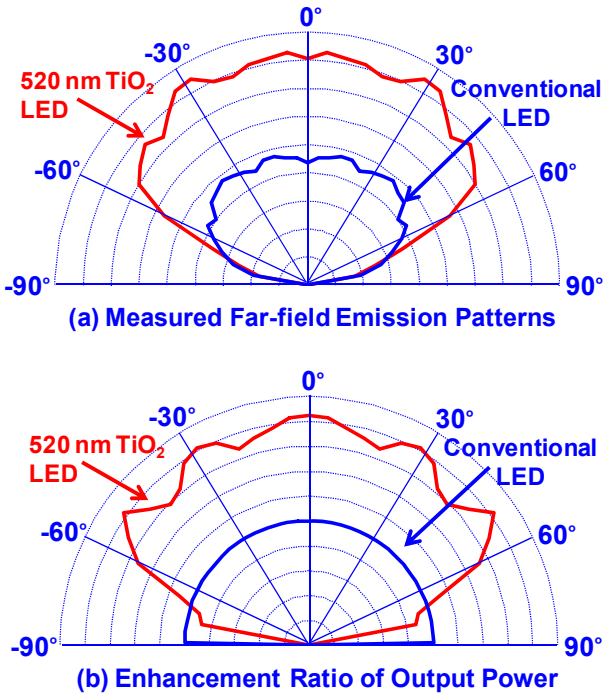

Figure 5-8. (a) Far-field emission patterns of the LEDs with and without and 520-nm anatase TiO_2 microsphere arrays deposited by the RCD method, and (b) enhancement ratio of output power as a function of far-field angle. The far-field radiation patterns of the LEDs were measured from emission angle from θ=0° up to θ=90°. Note that the results for θ=-90° up to θ=0° range, which are presented for completeness purpose, are identical with those of θ=0° up to θ=90° range.

As shown in Figure 5-8(a), the output power of the emission is radially plotted, with 0° as normal to the LED emitting surface. The Figure 5-8(a) shows that the far-field emission pattern of the LED with TiO_2 microsphere arrays exhibits overall stronger radiant intensity over that of the conventional LED. Hence TiO_2 microsphere arrays significantly increased the light extraction efficiency from widely enhanced light far-field pattern. From Figure 5-8(a), the measured far-field emission of the TiO_2 coated LEDs was much larger than that of the conventional LED. However, the enhancement of the far-field emission at varying angles is different. To illustrate this, the far-field emission of the TiO_2 coated LEDs was normalized to that of the conventional LED for obtaining the enhancement ratio of output power as a function of far-field angle, as shown in Figure 5-8(b).

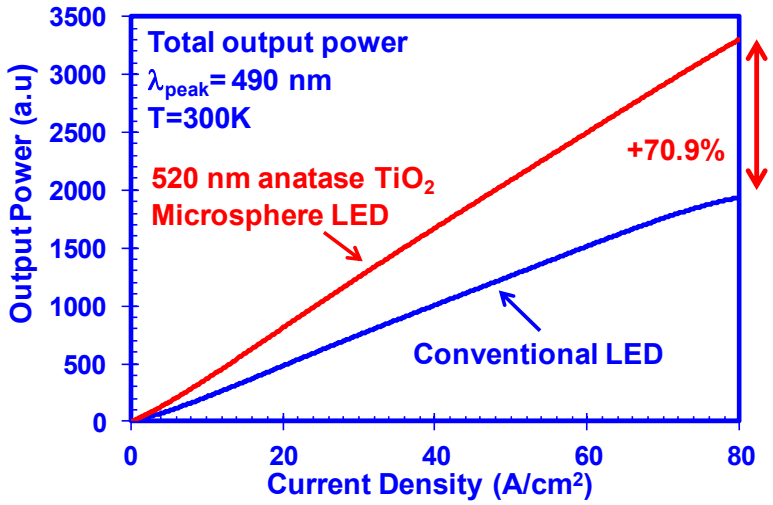

Figure 5-9. Comparison of integrated light output powers as a function of current density (J = 80 A/cm^2) of InGaN QW LEDs emitting at λ_{peak} ~ 490 nm employing 520-nm anatase TiO_2 microsphere arrays deposited via the RCD method, as compared to planar LEDs.

Figure 5-8(b) shows that the far-field intensity enhancement ratio of the TiO_2 coated LED is more significant at lower angles from 0° to 60° than that at higher angles from 60° to 90°. From Figure 5-8(b), three peaks of enhancement ratio at 0°, 30° and 50° are

observed, indicating that the output power enhancement brought by TiO_2 microsphere arrays is directionally dependent.

Based on Figure 5-8(a), the total output power of the LEDs with and without TiO_2 microsphere arrays was obtained by integrating the far-field output power over all the angles. The total output power of the LED with 520-nm anatase TiO_2 microsphere arrays exhibits ~71% enhancement [Figure 5-9], in comparison to that of the conventional LED. It is important to note that the enhancement of total output power is smaller than 83% enhancement of the output power measured in the normal direction [Figure 5-6]. The decrease in the enhancement is attributed to the non-uniform enhancement ratio especially the reduced enhancement ratio at higher angles from 60° to 90°, as shown in Figure 5-8(b).

In summary, the deposition of anatase TiO_2 sphere arrays was carried out and a monolayer of sphere arrays was obtained by tuning deposition speed, blade angle, and suspension concentration. EL measurement shows that much higher EL intensity was observed for the LED with anatase TiO_2 sphere arrays than that of planar LED, which resulted in 1.8 times enhancement in output power. The details of this work were performed in collaboration with other group members, specifically Xiaohang Li, and the work was published in reference 13.

References

[1] Y. K. Ee, R. A. Arif, N. Tansu, P. Kumnorkaew, and J. F. Gilchrist, "Enhancement of light extraction efficiency of InGaN quantum wells light emitting diodes using SiO_2/polystyrene microlens arrays," *Appl. Phys. Lett.,* vol. 91, Nov 2007.

[2] Y. K. Ee, P. Kumnorkaew, R. A. Arif, H. Tong, J. F. Gilchrist, and N. Tansu, "Light extraction efficiency enhancement of InGaN quantum wells light-emitting diodes with

polydimethylsiloxane concave microstructures," *Opt. Express,* vol. 17, pp. 13747-13757, Aug 2009.

[3] Y. K. Ee, P. Kumnorkaew, R. A. Arif, H. Tong, H. P. Zhao, J. F. Gilchrist*, et al.*, "Optimization of Light Extraction Efficiency of III-Nitride LEDs With Self-Assembled Colloidal-Based Microlenses," *Ieee J Sel Top Quant,* vol. 15, pp. 1218-1225, Jul-Aug 2009.

[4] H. C. Chang, K. Y. Lai, Y. A. Dai, H. H. Wang, C. A. Lin, and J. H. He, "Nanowire arrays with controlled structure profiles for maximizing optical collection efficiency," *Energy & Environmental Science,* vol. 4, pp. 2863-2869, Aug 2011.

[5] P. Zhu, J. Zhang, G. Liu, and N. Tansu, "FDTD Modeling of InGaN-Based Light-Emitting Diodes with Microsphere Arrays," in *Proc. of the IEEE Photonics Conference 2012*, Burlingame, CA, 2012.

[6] P. F. Zhu, G. Y. Liu, J. Zhang, and N. Tansu, "FDTD Analysis on Extraction Efficiency of GaN Light-Emitting Diodes With Microsphere Arrays," *J Disp Technol,* vol. 9, pp. 317-323, May 2013.

[7] P. Zhu, P. O. Weigel, G. Liu, J. Zhang, A. L. Weldon, T. Muanganphor*, et al.*, "Optimization of Deposition Conditions for Silica/Polystyrene Microlens and Nanolens Arrays for Light Extraction Enhancement in GaN Light-Emitting diodes," in *Proc. of the SPIE Photonics West 2013*, San Francisco, CA, 2013.

[8] P. Kumnorkaew, Y. K. Ee, N. Tansu, and J. F. Gilchrist, "Investigation of the Deposition of Microsphere Monolayers for Fabrication of Microlens Arrays," *Langmuir,* vol. 24, pp. 12150-12157, Nov 2008.

[9] H. K. Lee, Y. H. Ko, G. S. R. Raju, and J. S. Yu, "Light-extraction enhancement and directional emission control of GaN-based LEDs by self-assembled monolayer of silica spheres," *Opt. Express,* vol. 20, pp. 25058-25063, Oct 22 2012.

[10] T. Ogi, L. B. Modesto-Lopez, F. Iskandar, and K. Okuyama, "Fabrication of a large area monolayer of silica particles on a sapphire substrate by a spin coating method," *Colloids and Surfaces A: Physicochemical and Engineering Aspects,* vol. 297, pp. 71-78, 4/5/ 2007.

[11] Y. F. Gao, Y. Masuda, and K. Koumoto, "Micropatterning of TiO2 thin film in an aqueous peroxotitanate solution," *Chem Mater,* vol. 16, pp. 1062-1067, Mar 23 2004.

[12] E. I. Ross-Medgaarden, I. E. Wachs, W. V. Knowles, A. Burrows, C. J. Kiely, and M. S. Wong, "Tuning the Electronic and Molecular Structures of Catalytic Active Sites with Titania Nanoligands," *J Am Chem Soc,* vol. 131, pp. 680-687, Jan 21 2009.

Chapter 6 Overcome Fundamental Limit of Extraction Efficiency of LED

6.1 Introduction of Thin-Film Flip-Chip LED

The deposition of GaN was introduced by Murska and Tietjen at RCA Laboratories employing hydride vapor-phase epitaxy on a sapphire substrate in 1969 [1]. Since then, tremendous efforts has been devoted to the growth of wurtzite GaN and InGaN, control of conductivity of p-GaN and growth of LED structures [2-4]. These progress had been led to the invention of high-brightness blue LED in 1993 [5, 6].

However, one of major challenges for GaN-based LED is the poor electrical conductivity of p-GaN [7, 8]. This leads to a major problem for the current spreading underneath p-electrode, which results in nonhomogeneous light emission form the LED chip. This problem is solved by the deposition of semitransparent Ni/Au layer on the p-GaN [9, 10], which overcome the current spreading problem in p-GaN, however, the light extraction efficiency is reduced due to the absorption of Ni/Au layer. The performance of LED is a tradeoff between the current spreading and light extraction. Specifically, thicker Ni/Au can improve the current spreading of p-GaN, in the meantime, the light extraction efficiency will be significantly reduced; thinner Ni/Au layer can improve the light extraction efficiency, but the current spreading issue will exist. To eliminate the light absorption of the semitransparent metal, while keep good current spreading, the flip chip technology is implemented on LED devices [11]. In this approach, the thick Ni/Au metal is deposited on the p-GaN and the light is taken from the sapphire substrate. However, the refractive index of GaN is 2.5 and the refractive index of sapphire is 1.8, which are much larger than refractive index of free space. According to smell's law, the total reflection will be occurred both at the interface between GaN and sapphire and sapphire and free space, which leads to light being trapped in the GaN slab and thick sapphire substrate. To extract the guided

modes out of the devices, the laser-liftoff method is applied to the LED device to remove the sapphire substrate and followed by thinning down the n-GaN [12].

6.2 Microcavity Effect on Light Extraction Efficiency

The conventional LED structure is grown on the sapphire substrate by MOCVD method. The Thin-Film Flip-Chip LED is fabricated by laser-liftoff process to remove the sapphire substrate and followed by chemical-mechanical polishing (CMP) to thin down the n-GaN, which results in the TFFC LED structure with tunable n-GaN thickness [13]. The p-GaN thickness can be tuned in the MOCVD process. Thus, TFFC LED structure with various p-GaN and n-GaN thickness can be achieved by tuning growth time and CMP time.

The metal contact on the p-GaN side in the TFFC LED are able to reflect the light back to LED, which leads to the interference of light between the forward travelling light and the reflected light. Proper design of quantum well position will maximize the light extraction efficiency. In addition, a fraction of forward travelled electromagnetic wave will reflected back to the LED at the interface of GaN and free space, which will lead to interference too. Thus the thickness of cavity formed by LED will have significant effect on the light extraction efficiency, too [14-25].

6.2.1 Interferences between the up emitted light and down reflected light

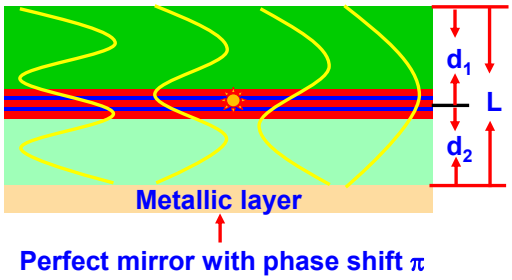

Figure 6-1. The effect of quantum well position on the light extraction efficiency.

Figure 6-1 is schematic diagram of TFFC LED structure. The distance between quantum well and metallic layer is labelled as d_2 and the total cavity thickness is L. The quantum well emits light in the isotropic media, thus the electromagnetic radiation have the same intensity (I_0) in all directions. The light which is traveling towards the metallic mirror will reflected back to the LED with phase shift of π and interferes with light which is traveling forward. According the interference theory, the total light intensity can be expressed as [26]

$$I_2(\mathrm{x,y,z}) = I_0 + I_1 + 2\sqrt{I_0 I_1}\cos\left[\Delta\phi\left(x,y,z\right)\right] = I_0 + I_1 + 2\sqrt{I_0 I_1}\cos\left[\left(\frac{\Delta d \cdot n_1}{\lambda}\right)\cdot 2\pi + \pi\right] \quad (6.1),$$

where the I_1 is the light intensity of reflected light, which is the same as the incident light intensity for the lossless mirror; n is the refractive index of material, which is ~2.5 in the visible region; Δ d is the optical path difference between the forward travelled light and the reflected light, which is $2d_2$ in the normal direction, thus total light output accounting for interference effect at normal direction can be expressed as

$$I_2(\mathrm{x,y,z}) = 2I_0 + 2I_0\cos\left[\left(\frac{2d_2 \cdot n_1}{\lambda}\right)\cdot 2\pi + \pi\right] \quad (6.2).$$

The enhancement of light intensity at particular position due to interference effect are plotted in Figure 6-2, here wavelength of 500 nm was chosen in this plotting. The maximum light intensity was achieved at $\left(\frac{2d_2 \cdot n_1}{\lambda}\right)\cdot 2\pi = \left(2m+1\right)\cdot\pi$, and minimum light intensity was achieved at $\left(\frac{2d_2 \cdot n_1}{\lambda}\right)\cdot 2\pi = \left(2m\right)\cdot\pi$. Thus, light output can be optimized by engineering quantum well position.

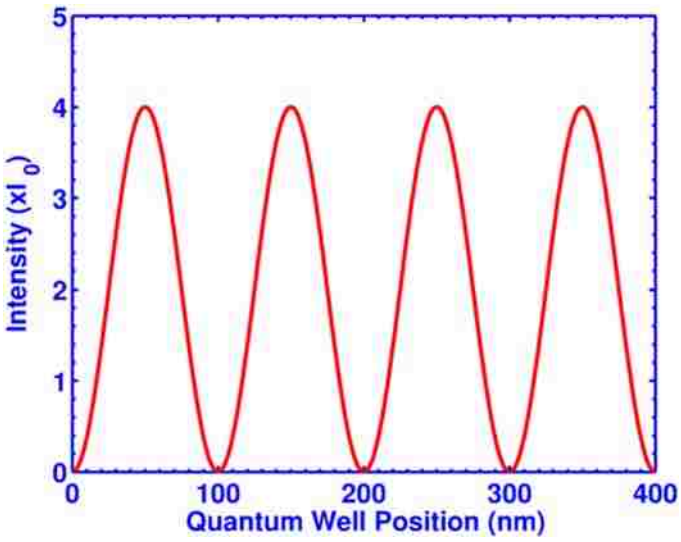

Figure 6-2. The light intensity variation due to interference effect as a function of quantum well position

6.2.2 Resonant Cavity Effect on the Light Extraction Efficiency

The light generated in the quantum well region bounds back and forth for many times in LED cavity and finally a fraction of light will be extracted out. The cavity thickness plays a significant role and the correct design of cavity thickness will significantly enhance the light extraction. When the electromagnetic waves with intensity of I_2 reaches the interface between the GaN with refractive index of $n_1$and free space with refractive index of n_2, some of electromagnetic wave will be reflected back to LED and reflected again by metallic mirror and interfere with forward traveling wave. The light reflected can be calculated as

$$I_3(\mathrm{x},\mathrm{y},\mathrm{z}) = I_2\left(\frac{n_1 - n_2}{n_1 + n_2}\right)^2 = I_2 r^2 \tag{6.3}$$

The total light intensity after interference will be

$$I_4(\mathrm{x},\mathrm{y},\mathrm{z}) = I_2 + I_3 + 2\sqrt{I_2 I_3}\cos\left[\left(\frac{2L\cdot n}{\lambda}\right)\cdot 2\pi + \pi\right] = (1+r)I_2 + 2rI_2\cos\left[\left(\frac{2L\cdot n}{\lambda}\right)\cdot 2\pi + \pi\right]$$

(6.4)

The light bounces back and forth for many times inside the LED. The final light intensity can be calculated as

$$I = I_n(\mathrm{x},\mathrm{y},\mathrm{z}) = (1+r)I_{n-2} + 2rI_{n-2}\cos\left[\left(\frac{2L\cdot n_1}{\lambda}\right)\cdot 2\pi + \pi\right] \tag{6.5}$$

From this equation, the final light intensity depends on the cavity thickness, the wavelength and refractive index of material. For a particular wavelength and particular material, there is optimized thickness, at which, the light intensity will be significantly enhanced.

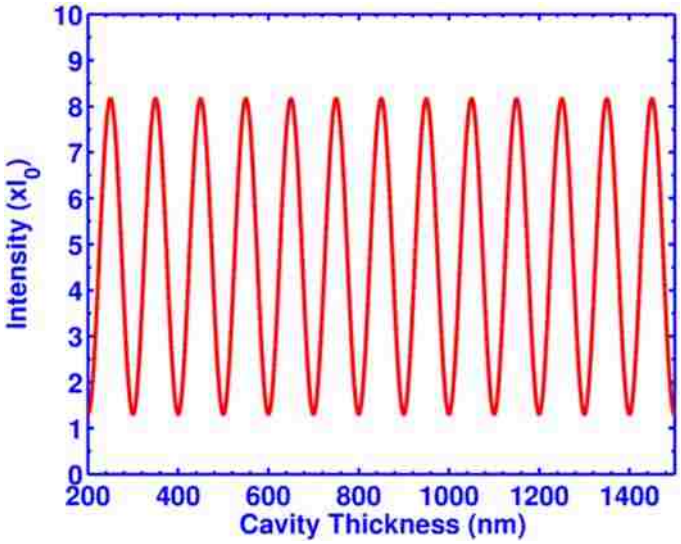

Figure 6-3. The light intensity enhancement due to interference as a function of cavity thickness for TFFC LED.

Figure 6-3 shows the light intensity enhancement for TFFC LED at wavelength of 500 nm. The maximum light output can be achieved at $\left(\frac{2L\cdot n_1}{\lambda}\right)\cdot 2\pi = (2m+1)\cdot\pi$ and minimum light output can be achieved at $\left(\frac{2L\cdot n_1}{\lambda}\right)\cdot 2\pi = (2m)\cdot\pi$. Thus, both quantum well position and cavity thickness play important role in the maximum light extraction of LED.

6.3 FDTD Calculation of Light Extraction Efficiency of Thin-Film Flip-Chip LED

The FDTD method [27, 28] was employed to calculate the light extraction efficiency of TFFC LED. The TFFC LED device structure analyzed in this study is shown in Figure 6-1. InGaN/GaN quantum well is sandwiched by p-GaN and n-GaN. The refractive index of GaN was set to 2.5. The metallic mirror was attached to the bottom of LED which is assumed to be a perfect mirror with 100% reflectance. The 3-D FDTD method requires a large amount of memory and computation time. It takes long time and a lot of resources to simulate such a big device. Therefore, in this calculation, we have taken the simulation domain to be 10 μm x 10 μm with perfect matched layer (PML) boundary conditions applied to the lateral boundaries and perfect electric conductor (PEC) boundary conditions to the bottom of LED. The grid size was set to be 10 nm to make sure the accurate results. The simulation time was set to be big enough to make sure the stabilized field output.

One dipole was chosen as light source within the quantum well region and positioned in the center region of quantum well. The emission wavelength used in this calculation was set as λ = 500 nm. The light extraction efficiency was calculated as the ratio of the optical output power extracted out from the top of LED to the total output power generated by dipole.

6.3.1 The Effect of Quantum Well Position on the Light Extraction Efficiency for Planar Thin-Film Flip-Chip LED with Cavity Thickness of 700 nm

As mentioned earlier, cavity thickness can be tuned by engineering the p-GaN thickness and n-GaN thickness. In this calculation, the cavity thickness was chosen as 700 nm and the quantum well position was tuned to investigate the effect of quantum well position on the light extraction efficiency of TFFC LED.

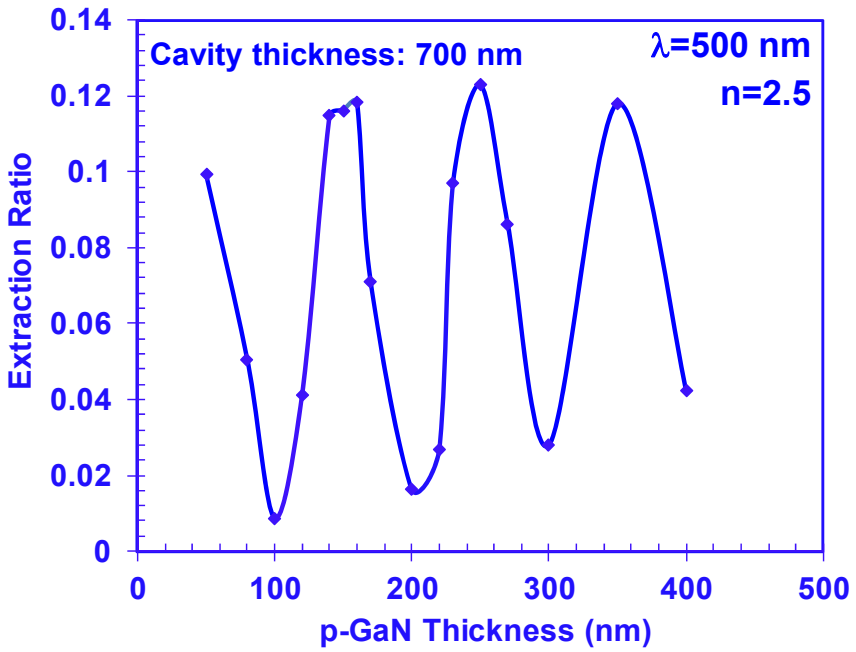

Figure 6-4. The quantum well position dependent light extraction efficiency of TFFC LED with cavity thickness of 700 nm.

Figure 6-4 shows the light extraction efficiency of TFFC LED at wavelength of 500 nm with cavity thickness of 700 nm. The extraction efficiency shows strong p-GaN thickness dependent. The higher efficiencies were achieved at p-GaN thickness of 50 nm, 150 nm, 250 nm, and 350 nm; the lower efficiencies were obtained at p-GaN thickness of 100 nm, 200 nm, and 300 nm. This finding shown here is consistent with the interference theory we mentioned earlier.

6.3.2 The Effect of Cavity Thickness on the Light Extraction Efficiency for the Planar Thin-Film Flip-Chip LED with p-GaN Thickness of 150 nm

To investigate resonant cavity effect on the light extraction efficiency, the light extraction of TFFC LED was also calculated for LED with various cavity thickness for the p-GaN thickness of 150 nm. p-GaN of 150 nm was chosen as it is one of optimized p-GaN thicknesses and physically implementable.

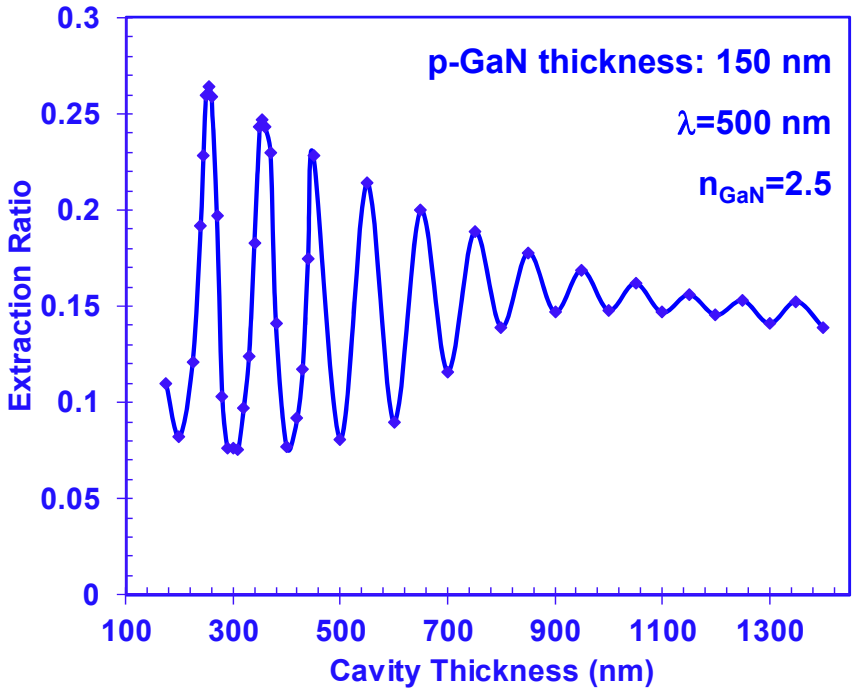

Figure 6-5. The light extraction efficiency of TFFC LED with various cavity thickness for the p-GaN thickness of 150 nm

The extraction efficiency is plotted as a function of cavity thickness for quantum well position of 150 nm where the maximum extraction efficiency was obtained in Figure 6-4. As shown in Figure 6-5, periodic modulation of the extraction efficiency with varying cavity thickness was observed, which is attributed to the interference effect of multiple reflection of light inside the LED. The extraction efficiency of ~27% was achieved for cavity thickness of 250 nm, which is more than 7 times enhancement than the conventional top-emitting LED devices. The modulation depth decreases as cavity thickness increases. At small cavity thickness, only a small number of the Fabry-Perot modes exist and the extraction efficiency is higher. Fabry-Perot modes increased with the increase in the cavity thickness, which led to averaging the many modes and the interference effect becomes weak.

6.3.3 Quantum Well Position Dependent Light Extraction Efficiency of Light Extraction Efficiency for the Cavity Thickness of 650 nm and 750 nm

From our previous calculation, the light extraction efficiency reach maximum at cavity thicknesses of 250 nm, 350 nm, 450 nm, 550 nm, 650 nm, and 750 nm. However, the maximum extraction efficiency decreases with the increase in the cavity thickness. We are especially interested in the thickness of 650 nm and 750 nm cavity as these thicknesses are experimentally implementable and has reasonable light extraction efficiency. Thus, we further optimized quantum well position for LED with cavity thickness of 650 nm and 750 nm to optimize light extraction efficiency.

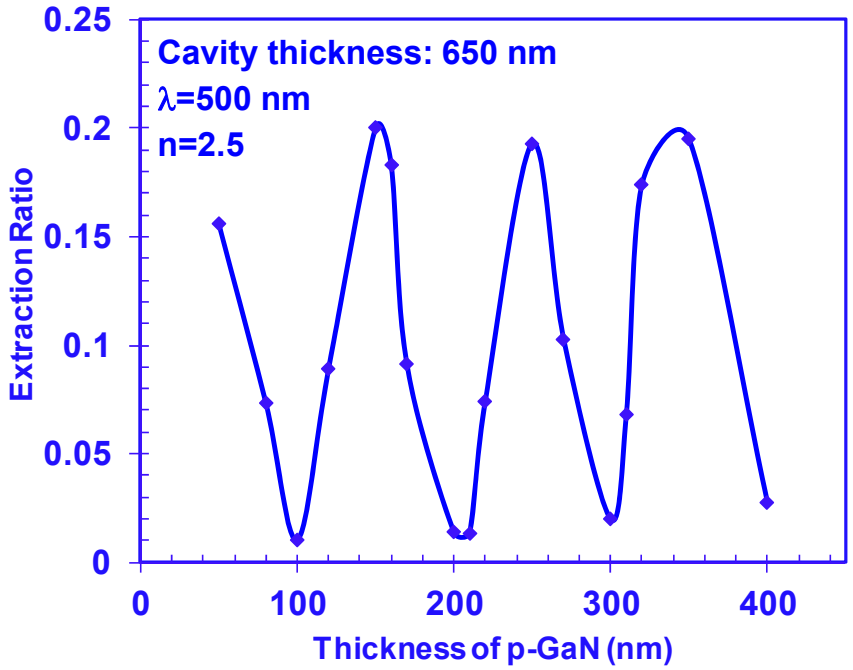

Figure 6-6. Quantum well position dependent light extraction efficiency of TFFC LED with cavity thickness of 650 nm

Figure 6-6 and Figure 6-7 show the light extraction efficiency as a function of quantum well position for TFFC LED with cavity thickness of 650 nm and 750 nm. The maximum light extraction efficiency of 20% and 19% was achieved at p-GaN thickness of 150 nm for LED with cavity thickness of 650 nm and 750 nm, respectively.

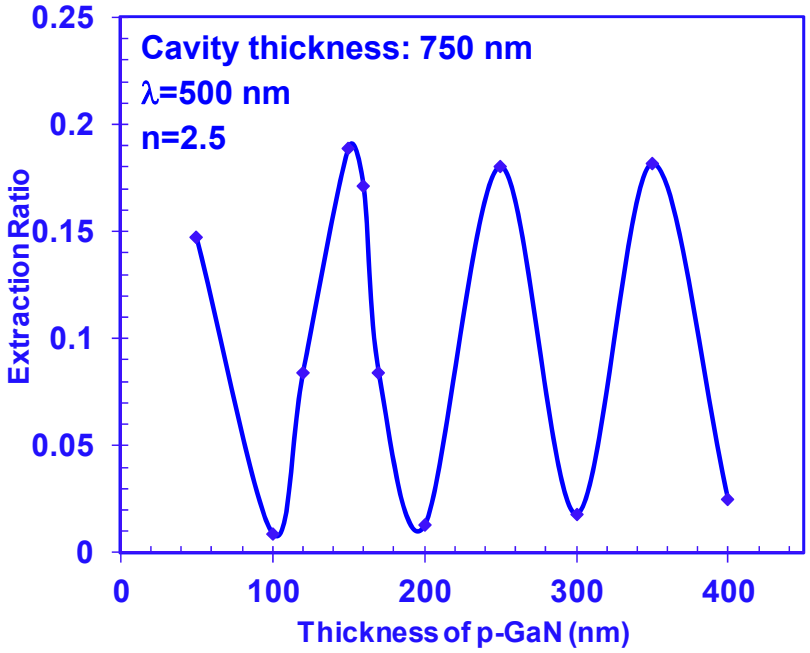

Figure 6-7. Quantum well position dependent light extraction efficiency of TFFC LED with cavity thickness of 750 nm

6.4 Thin-Film Flip-Chip LED with Microsphere Arrays

6.4.1 The Effect of Sphere Diameter on the Light Extraction Efficiency

Although, the light extraction efficiency of TFFC LED is much higher than that of conventional top-emitting LED, The widely adoption of GaN-based LED requires to further improve the quantum efficiency and cut down fabrication cost. Various methods has been employed to further enhance the light extraction efficiency of TFFC LED. Photonic crystal and surface roughness are two of effective approaches to enhance the light extraction of TFFC LED [29-34]. Light extraction efficiency of 65% has been achieved for the LED with surface roughness using photochemical etching. However, the electrical properties of LED could be degraded due to the photochemical etching process. In addition, it has little control over the light emission direction. The LED with photonic crystal showed high output and Light extraction efficiency of 72% has been achieved [29]. However, the high

fabrication cost of photonic crystals using electron beam lithography is a big obstacles. Other methods is relatively less effective to improve the light extraction efficiency.

Our goal is to employ the low-cost method to improve the performance of LED devices. The self-assembly microsphere or microlens arrays has been proven to be a very effective method to improve the light extraction efficiency of top-emitting LED devices as well as organic light-emitting diodes [28, 35-43]. However, the effect of microsphere or microlens array on the TFFC has not been investigated. In this work, the FDTD method is employed to investigate effect of microsphere arrays on the light extraction efficiency of TFFC. The comprehensive study was carried out to optimize the TFFC LED device structure with the goal of improving the device performance.

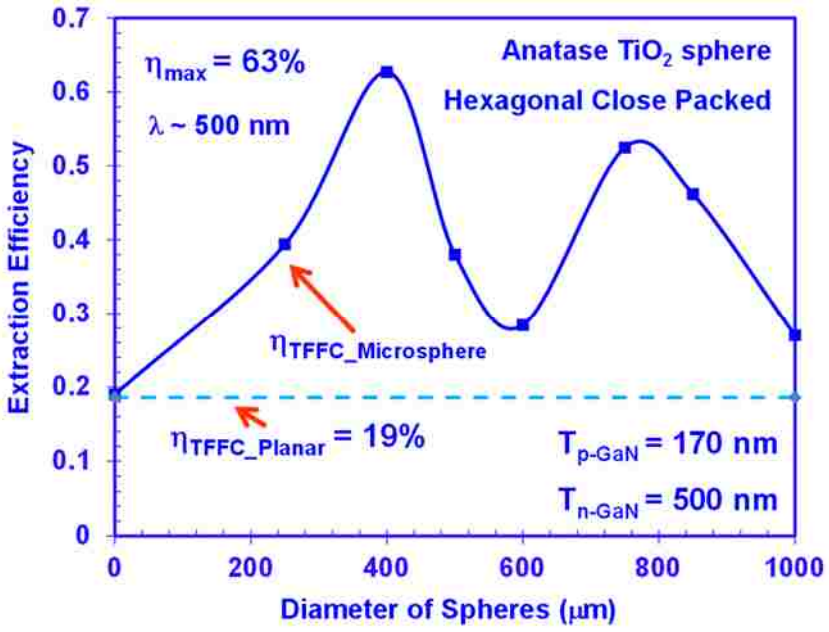

Figure 6-8. The light extraction efficiency of microsphere LED with microsphere arrays.

Monodisperse TiO_2 spheres can be synthesized by mixed-solvent method [44]. The diameter of spheres can be engineered by tuning concentration of ethanol, acetonitrile. In this work, the light extraction efficiencies of microsphere array TFFC LED with diameters of 250 nm, 400 nm, 500 nm, 600 nm, 750 nm, 850 nm and 1 μm were calculated and the

results are shown in figure 2. The light extraction is changing with the diameter of sphere. The extraction efficiency of 39%, 63%, 38%, 28%, 53%, 46% and 27% were achieved for LED with sphere diameter of 250 nm, 400 nm, 500 nm, 600 nm, 750 nm, 850 nm and 1 μm, respectively. Note that only 20% of light can be extracted out for the planar LED with same cavity thickness and quantum well position. The light extraction efficiency is significantly enhanced by deposition of TiO_2 spheres on the LED. This is attributed to the enlarged light escape cone due to the curvature formed between the sphere and free space. The light outside of escape cone initially cannot be extracted out, however, it can be extracted out after TiO_2 sphere deposition. Note that the diameter of sphere has significant effect on the light extraction efficiency of LED. LED with 400-nm sphere results in the extraction efficiency of 63%. Matter is composed of discrete electric charges such as electron and proton. When the light is incident on a particle, these charges are set in oscillation where the net effect is manifested in the emission of secondary radiation known as scattering. Light can be scattered and redirected in many directions. Particularly, when size of particles is comparable to the wavelength of the incident light, the Mie scattering happens. When the light collides with the TiO_2 sphere with size comparable to its wavelength, the light scatters strongly along the forward direction. This enhances the light extraction.

6.4.2 The effect of cavity thickness on the light extraction efficiency

The light extraction efficiency of TFFC LED with microsphere was further optimized by engineering the cavity thickness. p-GaN thickness was chosen as 170 nm, which is reasonable thickness for real LED fabrication. The Cavity thickness was tuned from 640 nm to 700 nm. Figure 3 shows the light extraction efficiency of TFFC LED with various cavity thickness. The extraction efficiencies of 46%, 59%, 74%, 62.7%, 59% and 50% were achieved for cavity thickness of 643 nm, 653 nm, 663 nm, 673 nm, 678 nm and 683

nm, respectively. The efficiency varies from 42% to 62.7%. The modulation of extraction efficiency with varying the cavity thickness is due to the interference of multiple reflection in the Fabry-Perot cavity structure. The extraction efficiency of 63% is achieved at cavity thickness of 673 nm, which is ~16 times enhancement than that of conventional top-emitting LED.

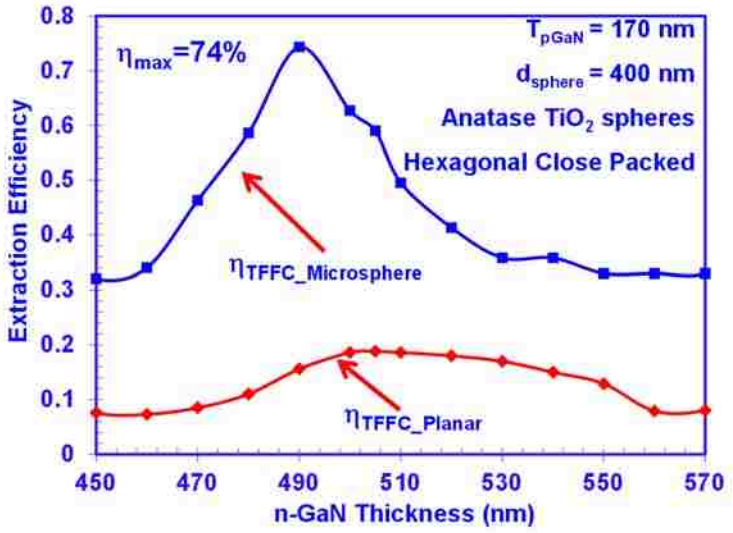

Figure 6-9. The cavity dependent of light extraction efficiency of TFFC LED with microsphere arrays.

6.4.3 The Effect of p-GaN Thickness on the Light Extraction Efficiency

The TFFC LED structure was further optimize by the tuning the quantum well position. The p-GaN thickness was varied from 140 nm to 190 nm. As shown in Figure 6-10, the extraction efficiency increases first and then decreases. The maximum extraction efficiency of 75% is achieved at p-GaN thickness of 160 nm. The light extraction efficiencies of planar TFFC LED with same p-GaN thickness and cavity thick are also plotted in Figure 6-10 for comparison purpose. The similar trend was observed, however, the efficiency is much lower than that of TFFC LED with microsphere arrays. The improved light extraction for TFFC LED is attributed to the cavity effect, and light-sphere interaction. The light which were trapped in the LED can be extracted out.

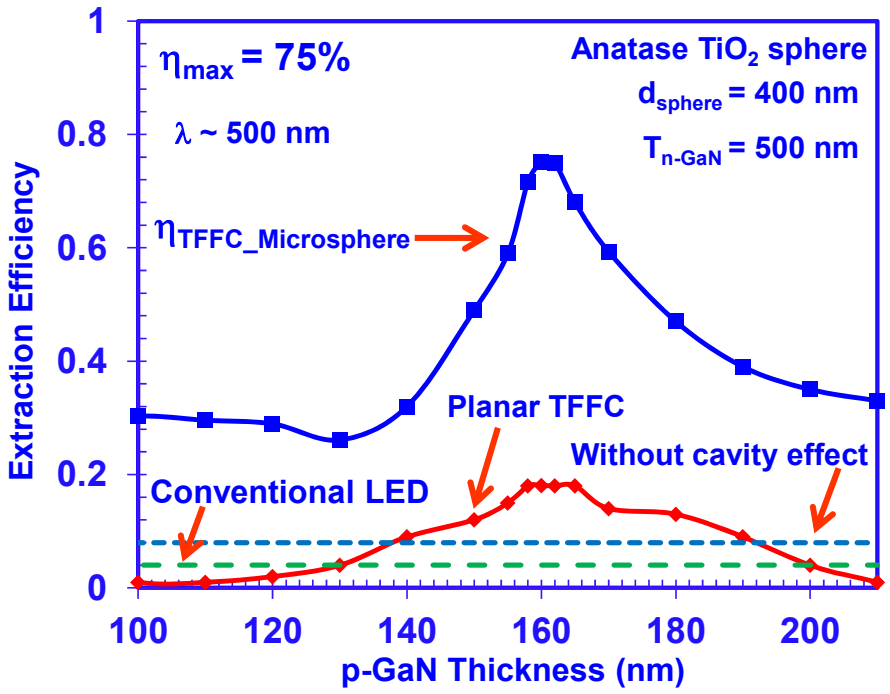

Figure 6-10. The p-GaN thickness dependent light extraction efficiency of TFFC with microsphere arrays.

In order to further investigate the cavity effect on the light extraction efficiency, the angular dependent light emission was calculated for the planar TFFC LEDs with various n-GaN thickness while the p-GaN thickness was kept as 170 nm. The far-field radiation pattern of conventional top-emitting LED (LED_con) was also plotted in Figure 6-11 (a) for comparison. The far-field radiation patterns were taken from θ=-90^o to θ=90^o. As shown in Figure 6-11 (a) and (b), the light intensity is radially plotted, with 0^o as normal to the LED emitting surface. The far-field radiation patterns of conventional LED shows Lambertian-like radiation patterns [see Figure 6-11(a)] due to large refractive index contrast between the GaN and free space [45]. However, far-field intensity of TFFC LED in different directions depends on the cavity thickness. The emission intensity increases in the normal direction with the increase in the cavity thickness [as shown in Figure 6-11(a)], which in turn results in the improved light extraction efficiency as shown in Figure 6-9. Further increase in the n-GaN thickness, the emission intensity started to increase in the larger

angular direction, while that of normal direction starts to decrease as shown in Figure 6-11 (b). The maximum light extraction efficiency is obtained when the n-GaN thickness increases to 500 nm.

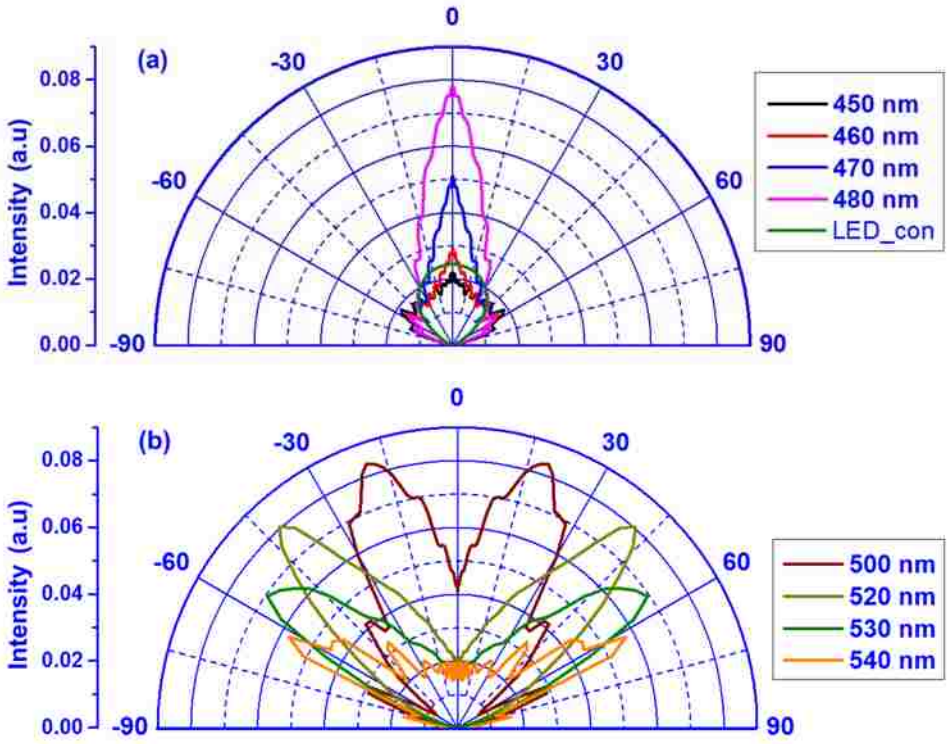

Figure 6-11. Far-field radiation patterns of planar TFFC LED with p-GaN thickness of 170 nm, the n-GaN thickness varied from 450 nm to 540 nm.

The light emitted from the quantum well is isotropic, the forward travelled light interfere with backward travelled light after total reflection by the metallic mirror which was attached to the p-GaN. Constructive interference will happen when optical length difference between the forward travelled light and backward traveled equal to integer of wavelength. The optical length difference depends on the cavity thickness and light emission direction. Cavity thickness is different for the different direction light in order for the constructive interference to happen. The total light intensity is the integration of light in all the directions above LED. The light emitted in the normal direction will have strongest interference effect, on the other hand, there are more light emitted in the oblique direction,

however, there suffer more reflection problem according to the Fresnel reflection. Thus the optimum light extraction efficiency was obtained at certain cavity thickness, at which the tradeoff between the reflection and emission was achieved.

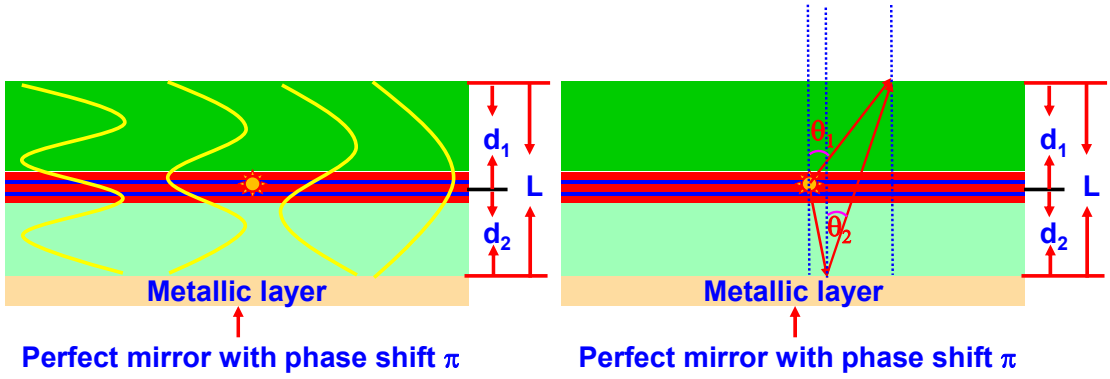

Figure 6-12. Schematics of interference between the forward travelled light and backward travelled light: (a) normal direction; (b) oblique direction.

The effect of quantum well positions on the light emission was also investigated by calculating the angular dependent emission intensity for the TFFC LEDs with various p-GaN thickness while the n-GaN thickness was kept as 500 nm for all the LEDs. Far-field radiation patterns of LEDs with various p-GaN thickness were plotted in two figures for better data presentation. The far-field emission intensity dramatically changes with the increase in the p-GaN thickness. The overall intensity is lower for the p-GaN thickness of 100 nm, 110 nm, 120 nm, 130 nm and 140 nm, which results in the light extraction efficiency as shown in Figure 6-10. The intensity in the normal direction increases with the increase in the p-GaN thickness and it reaches the maximum when the p-GaN thickness increased to 150 nm. Further increase the p-GaN thickness, the emission intensity in the normal direction started to decrease, while significant enhancement in the intensity emission at the larger angular direction was observe which resulted in optimum light extraction efficiency at the p-GaN thickness of 160 nm as shown in Figure 6-10. The emission intensity further decreases when the p-GaN thickness increases to 170 nm, while

only small increase in the larger angular direction is observed. This leads to the decrease in the light extraction efficiency.

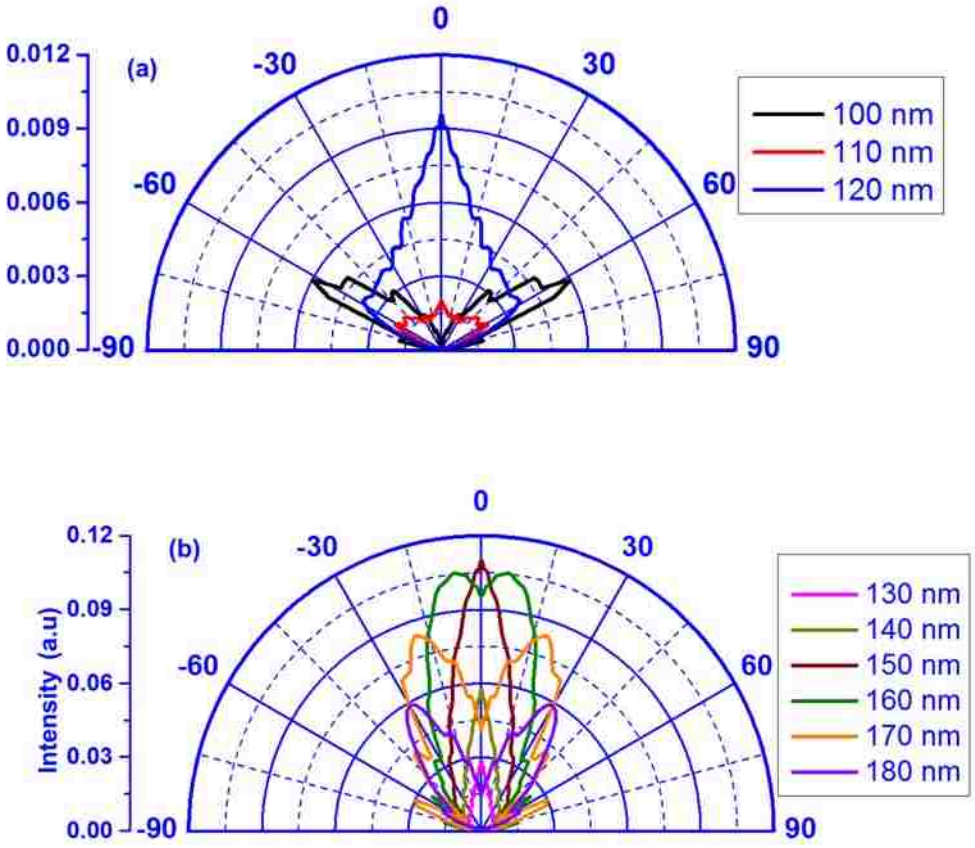

Figure 6-13. Far-field radiation patterns of planar TFFC LEDs with various p-GaN thickness. The n-GaN thickness was kept as 500 nm.

In summary, the quantum well position and cavity thickness have significant effect on the light emission from LED. The optimum light extraction efficiency will achieved by tuning the p-GaN thickness and cavity thickness.

6.4.4 The Effect of Packing Density on the Light Extraction Efficiency

The fabrication of microsphere arrays on top of LED was performed by rapid convective deposition method (RCD). RCD is a self-assembly process of the negative charged particles under the capillary force based on the following equation[46]:

$$v_c = \frac{K\phi}{h(1-\varepsilon)(1-\phi)} \tag{6.6}$$

Here, the v_c is the thin film growth rate; K depends on the evaporation rate, which is determined by the temperature and humidity; h is the height of thin film; is porosity of the colloidal crystal, in other words, 1-ϕ is the packing fraction of colloidal crystal, which is 0.605 for hexagonal close packed sphere arrays and 0.52 for the square close packed spheres arrays; ε is the volume fraction of suspension. The monolayer was obtained when the substrate withdraw speed was equal to film growth rate. The submonolayer was obtained when substrate withdraw speed was higher than crystal growth rate. The multilayer was obtained when substrate withdraw speed was lower than crystal growth rate. Microsphere arrays with various packing density and packing geometry: submonolayer [Figure 6-14 (c)], hexagonal close-packed monolayer [Figure 6-14 (a)], multilayer [Figure 6-14 (d)], and the square close-packed monolayer [Figure 6-14 (b)] were obtained by tuning the deposition speed (v_d).

In order to investigate effect of packing density of microsphere arrays on the light extraction efficiency of microsphere LED, the light extraction efficiency of microsphere (n = 2.5) array LEDs with submonolayer, monolayer, multilayer hexagonal packed shape were calculated. Figure 6-15 shows the light extraction efficiency of microsphere array LEDs with various $R_{d/p}$. Here, $R_{d/p}$ is defined as the ratio of diameter to the lattice period. For example, the hexagonal close-packed monolayer sphere array has an $R_{d/p}$ of 1. For the $R_{d/p}$ smaller than 1, it is submonolayer, and for the $R_{d/p}$ larger than 1, it is multilayer. The ratios of the light extraction efficiencies of the LEDs with microsphere arrays to those of planar LED are shown in Figure 6-15. Light extraction efficiency increased with the increase in $R_{d/p}$ and light extraction efficiency of 75% is achieved when monolayer of

microsphere is deposited on the LED. The extraction efficiency starts to decrease with further increasing the $R_{d/p}$.

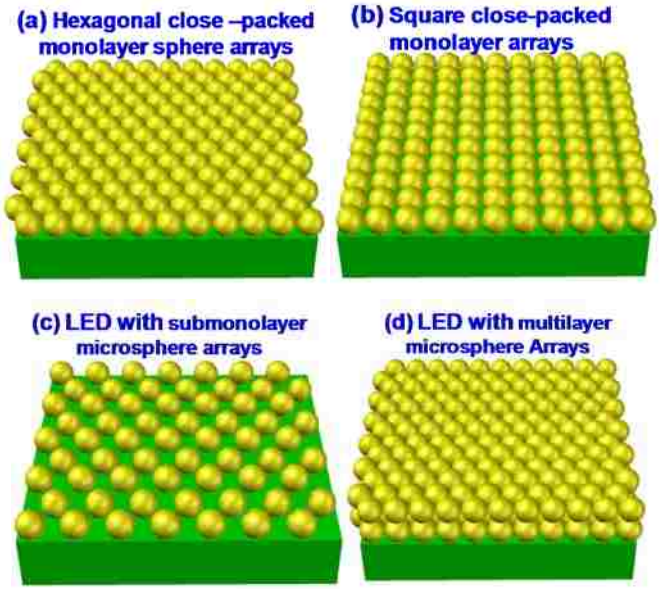

Figure 6-14. Schematic of microsphere LEDs with hexagonal close-packed sphere arrays (a), with square close-packed sphere arrays (b), with submonolayer sphere arrays (c), and with multilayer microsphere arrays (d).

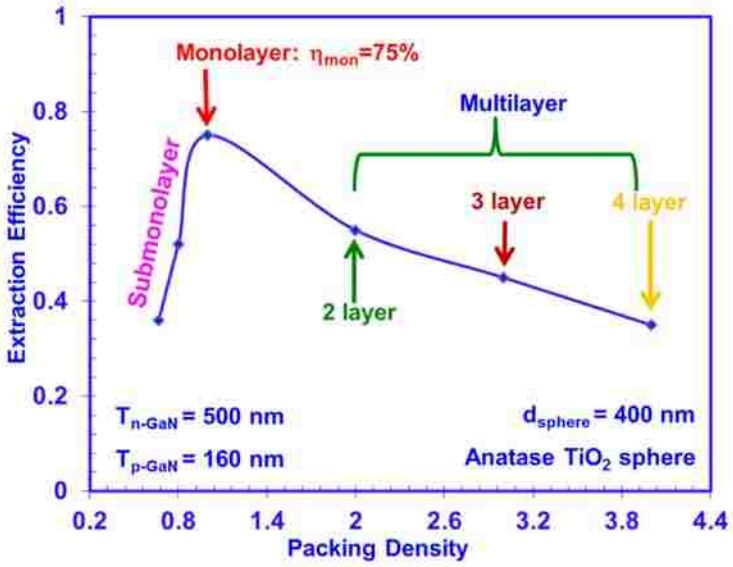

Figure 6-15. Extraction efficiency of microsphere TFFC LED with various packing density.

The comparison for the far-field radiation patterns for the planar LED, LEDs with submonolayer sphere arrays, LEDs with monolayer sphere arrays, and LEDs with multilayer sphere arrays is presented in Figure 6-16. The Far-field radiation pattern for planar LED [as shown in Figure 6-17 (e). exhibits Lambertian radiation patterns with only angular dependent, while symmetrically azimuthal distribution. The far-field intensity is much weaker in all angular direction compared to the microsphere LEDs due to the small light escape cone and only a small fraction of light can be extracted out from the LED device. The inner and outer radiation rings are attributed to the direct emission from the InGaN QWs and reflected emission by PEC reflectors, respectively. The LEDs with microsphere arrays exhibits both angularly and azimuthally dependent as shown in figure 3(a)-3(f). The significantly higher intensity is observed for far-field radiation patterns for microsphere array LEDs for both the normal and large angular distribution, which in turn results in the improved light extraction efficiency for these LEDs. The far-field intensity of LEDs with microsphere arrays exhibits hexagonal symmetry due to hexagonal packed nature of sphere arrays. However, the light distributions along angular direction and azimuthal direction for the LEDs with submonolayer sphere arrays, monolayer arrays and multilayer arrays are very different. For the LED with monolayer microsphere arrays, most of light were extracted out in the larger angular direction, which resulted in the enhanced light extraction efficiency, while only a small amount of light were extracted out in the smaller angular direction. For the case of LED with submonolayer sphere arrays, the light is spread over larger surface, and it can be extracted out in relatively larger angular range, however the overall intensity is lower than that of LED with monolayer sphere arrays. The same phenomenon is observed for the LED with multilayer sphere arrays, but the light intensity is much lower than that of LED with monolayer of sphere arrays. This leads to the relatively lower light extraction ratio compared to the LED devices with monolayer sphere arrays. Note that the comparison of light extraction efficiency ratio for microsphere

array LEDs and planar LED were carried out by taking the total output power integrated over the whole solid angle.

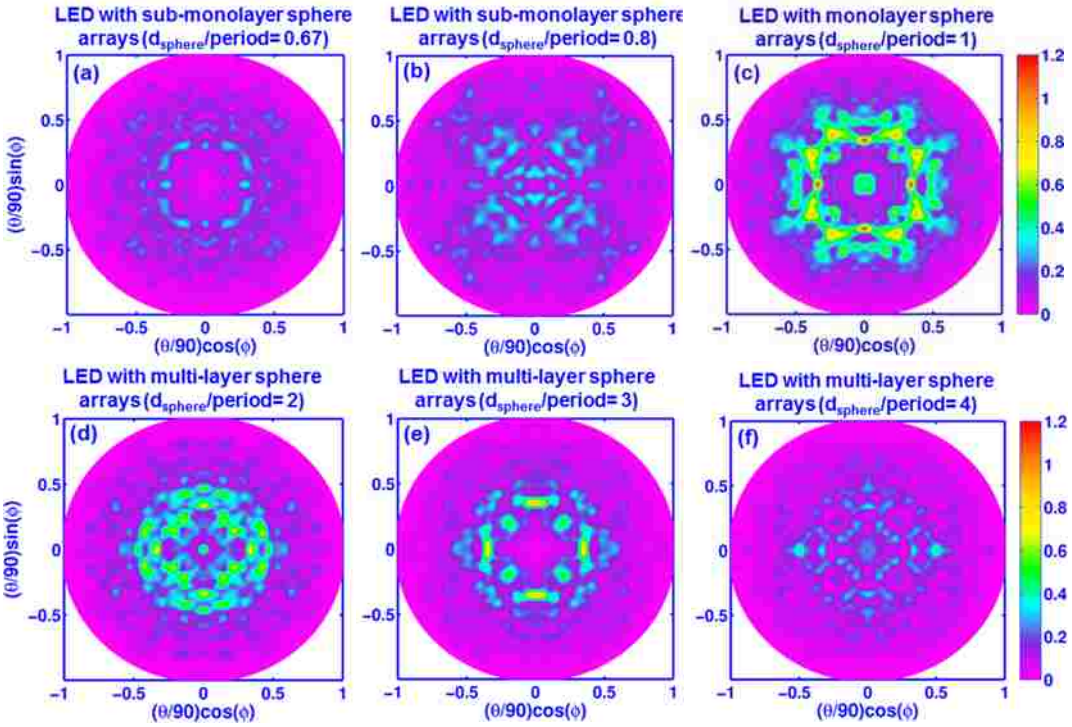

Figure 6-16. Far-field radiation pattern of microsphere TFFC LED with submonolayer, monolayer, and multilayer sphere arrays: (a) with packing density of 0.67; (b) with packing density of 0.8; (c) with packing density of 1; (d) with packing density of 2; (e) with packing density of 3 and (f) with packing density of 4.

6.4.5 The Effect of Packing Geometry on the Light Extraction Efficiency

In addition to hexagonal close packed lattice structure [see figure 5 (c)], we also investigated the square close packed lattice structure [see Figure 6-17 (d)]. As we mentioned in the third part of this manuscript earlier, the packing fraction for square close packed structure is 0.52 and the square close packed monolayer are obtained when substrate withdraw speed was equal to the crystal growth speed under the condition of 1-ε equal to 0.52. The overall light extraction of LED with square close packed monolayer sphere arrays is lower than that of LED with hexagonal close-packed monolayer structure.

The light extraction efficiency for LED with square close-packed is 47%, which is lower that of LED with hexagonal close packed sphere arrays. We recall that packing fraction for hexagonal close packed sphere arrays is 0.6 while it is 0.52 for the square close packed sphere arrays, which leads to the relatively lower light extraction efficiency for the square close packed sphere arrays. Another thing we should notice is that there are 4 nearest neighbors for the square close packed sphere arrays and 6 nearest neighbors for hexagonal close packed sphere arrays. The difference in the scattering center leads to different light extraction efficiency.

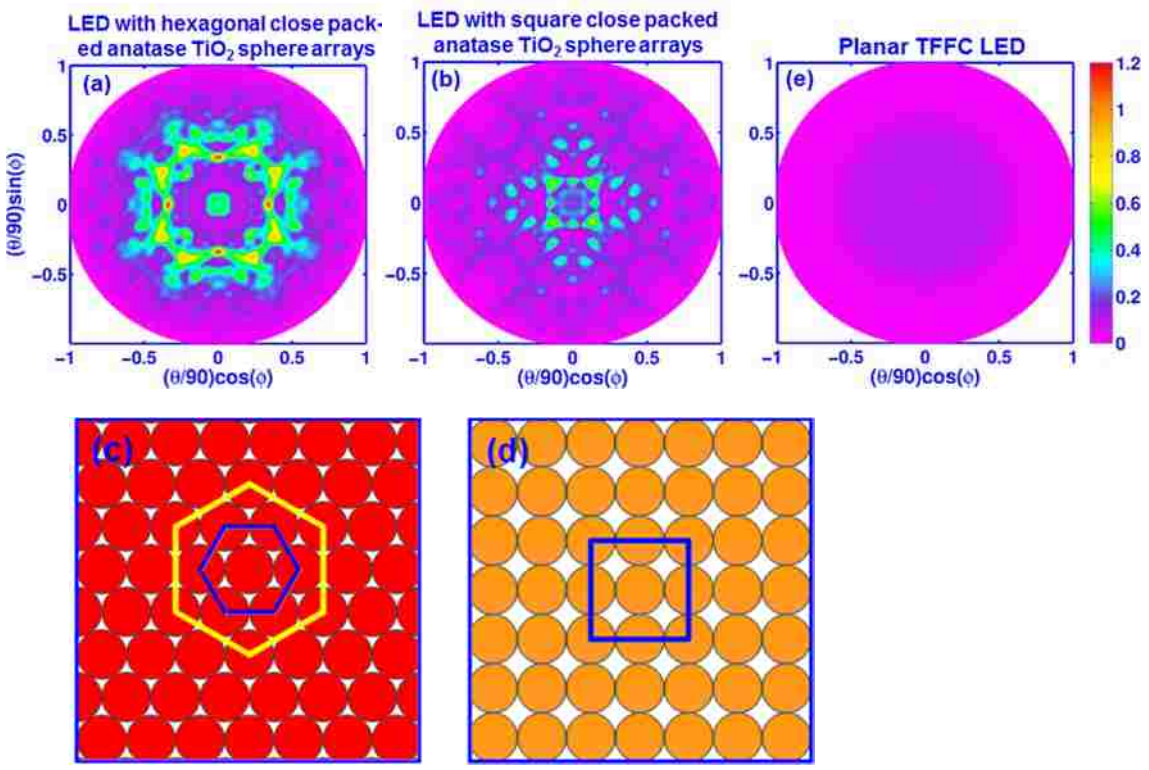

Figure 6-17. Far-field radiation pattern of microsphere TFFC LED with different packing geometry: a) with hexagonal close-packed geometry, b) with square close packed geometry, (e) planar LED.

In addition to difference of light extraction efficiency, the far-field radiation patterns are also different. Far field radiation patterns [see Figure 6-17 (a) and (b)] show that significant enhancement of light extraction efficiency in larger angular direction is observed

for the LED with hexagonal close-packed monolayer sphere arrays. The enhancement of light extraction efficiency of LED with square close-packed sphere arrays is observed both in the large angular direction and normal direction. However, Far-field intensity exhibit different symmetry, which is hexagonal shaped pattern for the microsphere LED with hexagonal close-packed structure, while it has square-shaped radiation pattern for the microsphere array LED with square close-packed symmetry due to different microsphere arrangement. The sphere array arrangement has significant effect on the far-field radiation pattern due to the scattering effect of light. The RCD method is an easy to be implemented method. It provides low cost ways to fabricate microsphere arrays on the TFFC LED, which leads to the tremendous improvement in light extraction efficiency. This method is applicable for the large scale roll-to-roll printing method.

The Finite-Difference Time-Domain method was employed to calculate the light extraction efficiency of thin-film flip-chip LEDs with TiO_2 based microsphere arrays. Specifically, the light extraction efficiency of TiO_2 microsphere array LED with different diameter to lattice ratio: submonolayer, monolayer, and multilayer, and different packing geometry: square close-packed and hexagonal close-packed geometry, are compared. The optimized packing density and packing geometry is hexagonal close-packed monolayer of TiO_2 sphere arrays. The use of hexagonal close-packed monolayer of TiO_2 microsphere arrays is expected to result in 3.6 times enhancement of light extraction efficiency compared to that of planar LED.

6.5 Thin-Film Flip-Chip LED with Microlens Arrays

6.5.1 The Effect of PS Thickness on the Light Extraction Efficiency

The use of hexagonal-close packed anatase TiO_2 sphere arrays has resulted in significant enhancement in light extraction efficiency for TFFC LED. This is attributed to the enlarged escape cone due to curvature formed between the sphere and free space.

However, limitation of using microsphere is that the chance for the light from GaN couple into the sphere is relatively low. Thus the coupling efficiency should be improved in order to further enhance the light extraction efficiency.

The microlens arrays which some portion of spheres is embedded in the PS layer can improve the light coupling efficiency. Our previous work regarding the SiO_2/PS microlens array LEDs have proved that microlens arrays have advantages over microsphere arrays regarding enhancement of light extraction efficiency [41]. 2.7 times enhancement in the light extraction efficiency has been achieved for the LED with microlens arrays, which is much higher than that of LED with microsphere arrays [41].

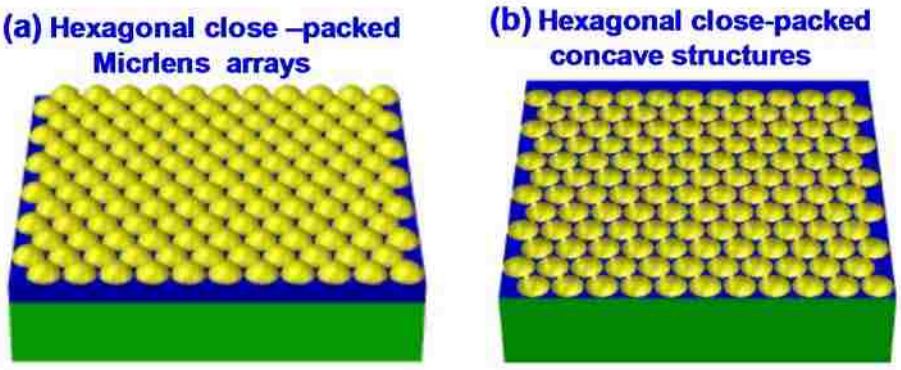

Figure 6-18. (a) Schematics of LED devices with hexagonal close-packed microlens arrays. (b) Schematics of LED device with concave structures.

The work on the SiO_2/PS microlens arrays showed that the aspect ratios of microlens have significant effect on the light extraction ratio as well as the light emission distribution in the far-field region. In order to optimize the light extraction efficiency of LED with microlens arrays regarding TiO_2 microsphere, FDTD calculation were conducted to investigate the effect of microlens aspect ratio on the light extraction efficiency of the thin-film flip-chip LED. The TiO_2 microlens arrays [see Figure 6-18 (a)] can be obtained by melting the TiO_2/PS binary sphere arrays. First, TiO_2/PS binary sphere arrays are deposited on the top of GaN LED devices. Then, these binary sphere arrays are melted

at 140°C. The thickness of the PS layer can be adjusted by tuning the annealing time. The thickness of PS layer can be tuned from 0 to the diameter of sphere by adjusting the annealing time. The PS fills the Gap between the TiO_2 spheres. In this calculation, the diameter of microsphere is 0.40 μm, while tuning the thickness of PS layer which is corresponding to aspect ratio from 0 to 1. Here, the aspect ratio is defined as the thickness of PS layer to the diameter of microsphere.

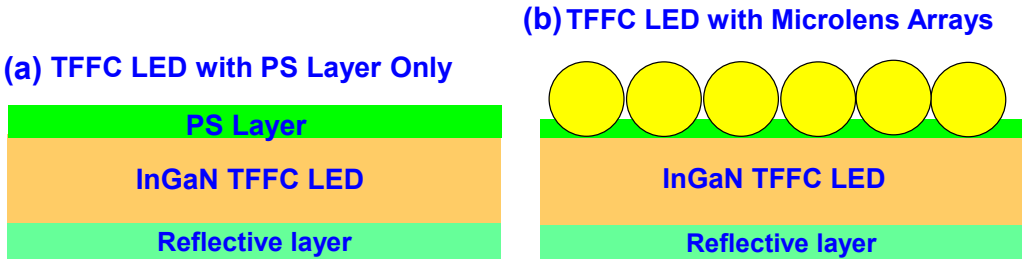

Figure 6-19. Schematics of Thin-Film Flip-Chip LED with Planar PS layer (a) and LED with microlens arrays (b).

The light extraction efficiencies of microlens array LEDs with various aspect ratio are shown in Figure 6-20. The light extraction efficiency increases with the increase in the aspect ratio, and the maximum light extraction efficiency is obtained at PS thickness of 75 nm. Further increase the PS thickness, the extraction efficiency starts to decrease. For the case of the PS thickness is smaller than the 75 nm, less photon are coupled into the microlens arrays for light extraction. Therefore, the maximum effective photon escape cone is achieved, when the optimum PS thickness is used, as it allows for the optimum amount of photons to be coupled into the microspheres.

As comparison, the light extraction efficiency of TFFC LED with planar PS layer was also calculated and plotted in the same figure. As shown in Figure 6-20, the same trend is observed as in the case of LED with microlens arrays. The extraction efficiency varies with PS thickness. However, the overall extraction efficiency is much lower than that of LED with microlens arrays. The PS layer was deposited on the top LED, which can be

served as anti-reflecting coating to reduce the Fresnel reflection. In the planar PS antireflection coating film, the Fresnel reflection will be reduced. The extraction efficiency depends on the thickness of PS as shown in Figure 6-20. The constructive interference can be achieved by tuning the thickness of PS layer, which led to the enhancement in the light extraction efficiency.

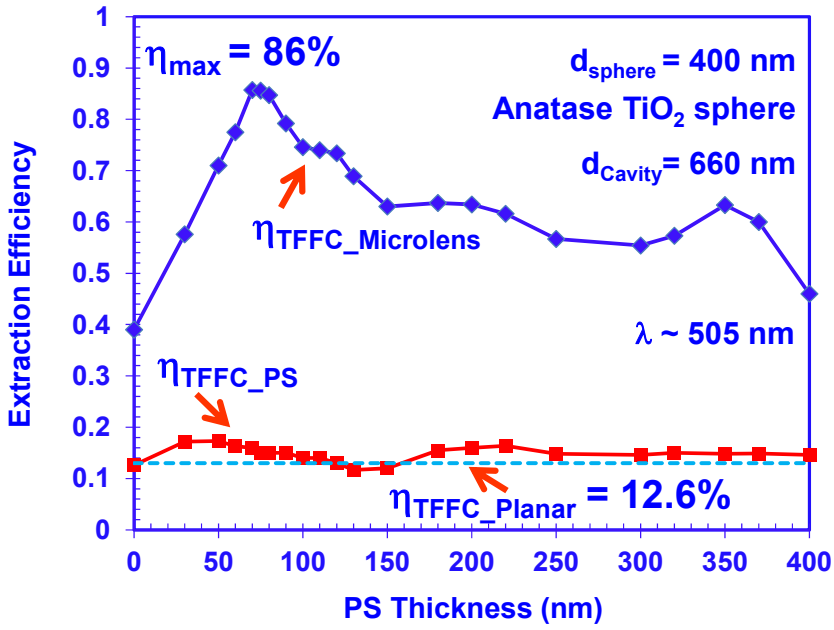

Figure 6-20. The light extraction efficiency of Thin-Film Flip-Chip LED with microlens arrays compared with LED with planar PS layer, the planar Thin-Film Flip-Chip as references.

To further understand the effect of planar PS layer on the light extraction efficiency. The angular dependent light emission from TFFC LED with PS layers is plotted at a particular azimuthal direction of ϕ =0 (as shown in Figure 6-21). The PS thickness varies from 30 nm to 150 nm. Angular dependent light emission of the planar LED without PS layer is also plotted for comparison purpose. Strong emission in the normal direction is observed for the planar LED due to the strong constructive interference effect in the normal direction. The light emission in the normal direction starts to decrease and that of larger angular direction starts to increase with the increase in the PS thickness. This is attributed

to the increased constructive interference of light in the larger angular direction with increase in PS thickness. The optimum light extraction efficiency is obtained at PS thickness of 30 nm, at which the tradeoff between the constructive interference and reflection was achieved. Further increase the PS thickness, the light intensity increased more, however, the light extraction efficiency started to decrease due to the increased Fresnel reflection. The light intensity in larger angular direction starts to decrease and that of normal direction starts to increase when the PS thickness increased to 100 nm, which in turn results in the decrease in the light extraction. Light emission in the normal direction dramatically increases at PS thickness of 150 nm, and the light extraction efficiency starts to increase.

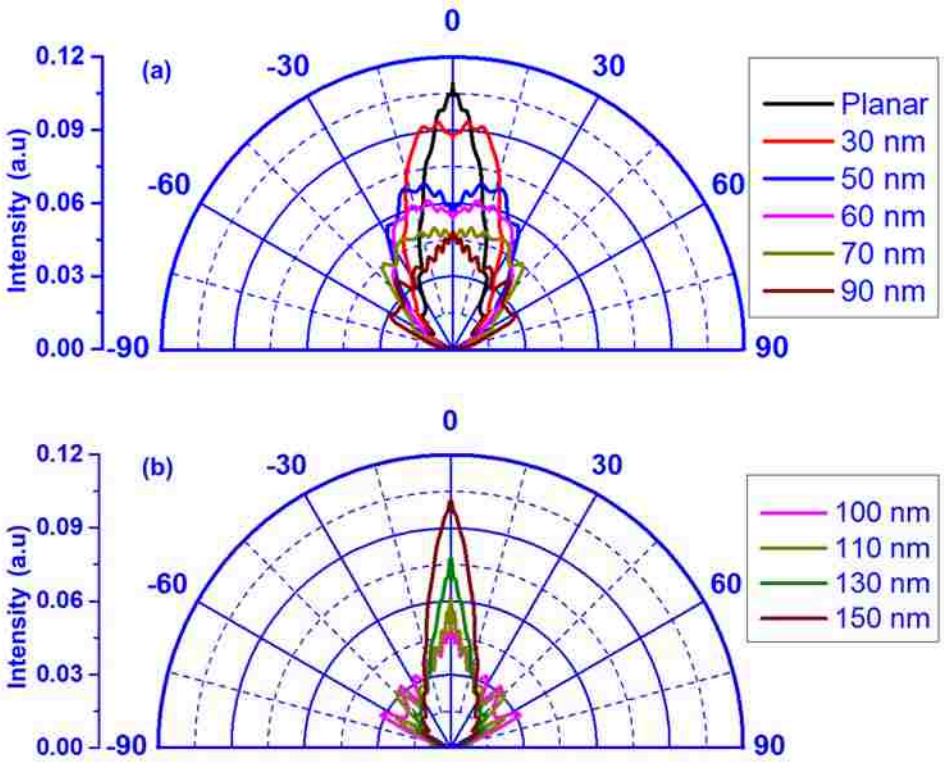

Figure 6-21. Far-field radiation patterns of planar TFFC LED with various PS thickness.

In summary, the light extraction efficiency of TFFC LED with microsphere arrays and microlens arrays was investigated. Light extraction efficiency of 86% has been achieved

by tuning the quantum well position, cavity thickness, sphere refractive index, sphere diameter. The use of microlens arrays method on TFFC LEDs is expected to overcome the limitation presented in state-of-the-art TFFC LEDs by improving the extraction from 65% to 86%.

References

[1] H. P. Maruska and J. J. Tietjen, "Preparation and Properties of Vapor-Deposited Single-Crystalline Gan," *Appl. Phys. Lett.,* vol. 15, pp. 327-&, 1969.

[2] S. Nakamura, Y. Harada, and M. Seno, "Novel Metalorganic Chemical Vapor-Deposition System for Gan Growth," *Appl Phys Lett,* vol. 58, pp. 2021-2023, May 6 1991.

[3] S. Nakamura, T. Mukai, M. Senoh, and N. Iwasa, "Thermal Annealing Effects on P-Type Mg-Doped Gan Films," *Jpn J Appl Phys 2,* vol. 31, pp. L139-L142, Feb 15 1992.

[4] S. Nakamura, S. J. Pearton, and G. Fasol, *The blue laser diode: the complete story*: Springer Verlag, 2000.

[5] S. Nakamura, T. Mukai, and M. Senoh, "High-Brightness Ingan/Algan Double-Heterostructure Blue-Green-Light-Emitting Diodes," *J Appl Phys,* vol. 76, pp. 8189-8191, Dec 15 1994.

[6] S. Nakamura, T. Mukai, and M. Senoh, "Candela-Class High-Brightness Ingan/Algan Double-Heterostructure Blue-Light-Emitting Diodes," *Appl Phys Lett,* vol. 64, pp. 1687-1689, Mar 28 1994.

[7] D. A. Steigerwald, J. C. Bhat, D. Collins, R. M. Fletcher, M. O. Holcomb, M. J. Ludowise*, et al.*, "Illumination with solid state lighting technology," *Ieee J Sel Top Quant,* vol. 8, pp. 310-320, Mar-Apr 2002.

[8] H. Kim, S. J. Park, and H. Hwang, "Effects of current spreading on the performance of GaN-based light-emitting diodes," *IEEE Trans. Electron Devices,* vol. 48, pp. 1065-1069, Jun 2001.

[9] X. A. Cao, E. B. Stokes, P. Sandvik, N. Taskar, J. Kretchmer, and D. Walker, "Optimization of current spreading metal layer for GaN/InGaN-based light emitting diodes," *Solid-State Electronics,* vol. 46, pp. 1235-1239, Aug 2002.

[10] D. L. Hibbard, S. P. Jung, C. Wang, D. Ullery, Y. S. Zhao, H. P. Lee*, et al.*, "Low resistance high reflectance contacts to p-GaN using oxidized Ni/Au and Al or Ag," *Appl Phys Lett,* vol. 83, pp. 311-313, Jul 14 2003.

[11] J. J. Wierer, D. A. Steigerwald, M. R. Krames, J. J. O'Shea, M. J. Ludowise, G. Christenson*, et al.*, "High-power AlGaInN flip-chip light-emitting diodes," *Appl. Phys. Lett.,* vol. 78, p. 3379, 2001.

[12] O. B. Shchekin, J. E. Epler, T. A. Trottier, T. Margalith, D. A. Steigerwald, M. O. Holcomb*, et al.*, "High performance thin-film flip-chip InGaN-GaN light-emitting diodes," *Appl. Phys. Lett.,* vol. 89, Aug 14 2006.

[13] L. Chun-Feng, K. Hao-Chung, C. Chia-Hsin, Y. Peichen, and W.-Y. Yeh, "Structural Effects on Highly Directional Far-Field Emission Patterns of GaN-Based Micro-Cavity Light-Emitting Diodes With Photonic Crystals," *Lightwave Technology, Journal of,* vol. 28, pp. 2881-2889, 2010.

[14] A. Kastler, "Atomes à l'Intérieur d'un Interféromètre Perot-Fabry," *Appl. Opt.,* vol. 1, pp. 17-24, 1962.

[15] W. Lukosz, "Theory of Optical-Environment-Dependent Spontaneous-Emission Rates for Emitters in Thin-Layers," *Physical Review B,* vol. 22, pp. 3030-3038, 1980.

[16] G. B. Friedmann and H. S. Sandhu, "Phase changes on reflection from a metallic surface," *Am. J. Phys.,* vol. 56, pp. 270-273, 1988.

[17] D. G. Deppe and C. Lei, "Spontaneous Emission and Optical Gain in a Fabry-Perot Microcavity," *Appl. Phys. Lett.,* vol. 60, pp. 527-529, Feb 3 1992.

[18] H. De Neve, J. Blondelle, P. Van Daele, P. Demeester, R. Baets, and G. Borghs, "Recycling of guided mode light emission in planar microcavity light emitting diodes," *Appl. Phys. Lett.,* vol. 70, pp. 799-801, 1997.

[19] H. Benisty, H. De Neve, and C. Weisbuch, "Impact of planar microcavity effects on light extraction - Part II: Selected exact simulations and role of photon recycling," *IEEE J. Quantum Electron.,* vol. 34, pp. 1632-1643, Sep 1998.

[20] H. Benisty, H. De Neve, and C. Weisbuch, "Impact of planar microcavity effects on light extraction - Part I: Basic concepts and analytical trends," *IEEE J. Quantum Electron.,* vol. 34, pp. 1612-1631, Sep 1998.

[21] D. Delbeke, R. Bockstaele, P. Bienstman, R. Baets, and H. Benisty, "High-efficiency semiconductor resonant-cavity light-emitting diodes: a review," *Selected Topics in Quantum Electronics, IEEE Journal of,* vol. 8, pp. 189-206, 2002.

[22] Y. C. Shen, J. J. Wierer, M. R. Krames, M. J. Ludowise, M. S. Misra, F. Ahmed*, et al.*, "Optical cavity effects in InGaN/GaN quantum-well-heterostructure flip-chip light-emitting diodes," *Appl. Phys. Lett.,* vol. 82, pp. 2221-2223, Apr 7 2003.

[23] K. J. Vahala, "Optical microcavities," *Nature,* vol. 424, pp. 839-846, Aug 14 2003.

[24] H. Y. Ryu, "Modification of the Light Extraction Efficiency in Micro-cavity Vertical InGaN Light-emitting Diode Structures," *J Korean Phys Soc,* vol. 55, pp. 1267-1271, Sep 2009.

[25] K. S. Daskalakis, P. S. Eldridge, G. Christmann, E. Trichas, R. Murray, E. Iliopoulos*, et al.*, "All-dielectric GaN microcavity: Strong coupling and lasing at room temperature," *Appl. Phys. Lett.,* vol. 102, Mar 11 2013.

[26] M. Bass, C. DeCusatis, J. Enoch, V. Lakshminarayanan, G. Li, C. Macdonald*, et al.*, *Handbook of Optics, Volume I: Geometrical and Physical Optics, Polarized Light, Components and Instruments* vol. I: McGraw-Hill, Inc., USA, 2010.

[27] P. F. Zhu, G. Y. Liu, J. Zhang, and N. Tansu, "FDTD Analysis on Extraction Efficiency of GaN Light-Emitting Diodes With Microsphere Arrays," *J Disp Technol,* vol. 9, pp. 317-323, May 2013.

[28] P. Zhu, J. Zhang, G. Liu, and N. Tansu, "FDTD Modeling of InGaN-Based Light-Emitting Diodes with Microsphere Arrays," in *Proc. of the IEEE Photonics Conference 2012*, Burlingame, CA, 2012.

[29] J. J. Wierer, A. David, and M. M. Megens, "III-nitride photonic-crystal light-emitting diodes with high extraction efficiency," *Nat Photonics,* vol. 3, pp. 163-169, Mar 2009.

[30] A. David, H. Benisty, and C. Weisbuch, "Photonic crystal light-emitting sources," *Rep. Prog. Phys.,* vol. 75, Dec 2012.

[31] E. Matioli, B. Fleury, E. Rangel, T. Melo, E. Hu, J. Speck*, et al.*, "High Extraction Efficiency GaN-Based Photonic-Crystal Light-Emitting Diodes: Comparison of Extraction Lengths between Surface and Embedded Photonic Crystals," *Appl. Phys. Express,* vol. 3, 2010.

[32] C. Wiesmann, K. Bergenek, N. Linder, and U. T. Schwarz, "Photonic crystal LEDs - designing light extraction," *Laser Photonics Rev.,* vol. 3, pp. 262-286, May 2009.

[33] C. C. Kao, H. C. Kuo, K. F. Yeh, J. T. Chu, W. L. Peng, H. W. Huang*, et al.*, "Light-output enhancement of nano-roughened GaN laser lift-off light-emitting diodes formed by ICP dry etching," *IEEE Photonics Technol. Lett.,* vol. 19, pp. 849-851, May-Jun 2007.

[34] M. R. Krames, O. B. Shchekin, R. Mueller-Mach, G. O. Mueller, Z. Ling, G. Harbers*, et al.*, "Status and Future of High-Power Light-Emitting Diodes for Solid-State Lighting," *Display Technology, Journal of,* vol. 3, pp. 160-175, 2007.

[35] Y. K. Ee, R. A. Arif, N. Tansu, P. Kumnorkaew, and J. F. Gilchrist, "Enhancement of light extraction efficiency of InGaN quantum wells light emitting diodes using SiO_2/polystyrene microlens arrays," *Appl. Phys. Lett.,* vol. 91, Nov 2007.

[36] Y. K. Ee, P. Kumnorkaew, R. A. Arif, H. Tong, J. F. Gilchrist, and N. Tansu, "Light extraction efficiency enhancement of InGaN quantum wells light-emitting diodes with polydimethylsiloxane concave microstructures," *Opt. Express,* vol. 17, pp. 13747-13757, Aug 2009.

[37] Y. K. Ee, P. Kumnorkaew, R. A. Arif, H. Tong, H. P. Zhao, J. F. Gilchrist*, et al.*, "Optimization of Light Extraction Efficiency of III-Nitride LEDs With Self-Assembled Colloidal-Based Microlenses," *Ieee J Sel Top Quant,* vol. 15, pp. 1218-1225, Jul-Aug 2009.

[38] W. Koo, W. Yun, P. Zhu, X. H. Li, N. Tansu, and F. So, "P ¡110: Light extraction of Phosphorescent OLEDs by Defective Hexagonal ¡Close ¡Packed Array," *SID Symposium Digest of Technical Papers,* vol. 43, pp. 1474-1476, 2012.

[39] K. K. Jang, P. Prabhakaran, D. Chandran, J.-J. Park, and K.-S. Lee, "Solution processable and photopatternable blue, green and red quantum dots suitable for full color displays devices," *Opt. Mater. Express,* vol. 2, pp. 519-525, 2012.

[40] P. Kumnorkaew, Y. K. Ee, N. Tansu, and J. F. Gilchrist, "Investigation of the Deposition of Microsphere Monolayers for Fabrication of Microlens Arrays," *Langmuir,* vol. 24, pp. 12150-12157, Nov 2008.

[41] H. C. Chang, K. Y. Lai, Y. A. Dai, H. H. Wang, C. A. Lin, and J. H. He, "Nanowire arrays with controlled structure profiles for maximizing optical collection efficiency," *Energy & Environmental Science,* vol. 4, pp. 2863-2869, Aug 2011.

[42] X. H. Li, P. F. Zhu, G. Y. Liu, J. Zhang, R. B. Song, Y. K. Ee*, et al.*, "Light Extraction Efficiency Enhancement of III-Nitride Light-Emitting Diodes by Using 2-D Close-Packed TiO2 Microsphere Arrays," *J Disp Technol,* vol. 9, pp. 324-332, May 2013.

[43] P. Zhu, G. Liu, J. Zhang, and N. Tansu, "FDTD Analysis on Extraction Efficiency of GaN Light-Emitting Diodes With Microsphere Arrays," *J. Display Technol.,* vol. 9, pp. 317-323, 2013.

[44] P. Zhu, H. Zhu, W. QIN, C. K. Tan, and N. Tansu, "Eu3+-doped TiO2 Nanospheres for GaN-based White Light-Emitting Diodes," in *Proc. of the SPIE Optics + Photonics 2014*, San Diego, CA, 2014.

[45] E. F. Schubert, T. Gessmann, and J. K. Kim, *Light emitting diodes*: Wiley Online Library, 2005.

[46] B. G. Prevo and O. D. Velev, "Controlled, Rapid Deposition of Structured Coatings from Micro- and Nanoparticle Suspensions," *Langmuir,* vol. 20, pp. 2099-2107, 2004/03/01 2004.

Chapter 7 Light Extraction Efficiency of Organic Light-emitting Diode

7.1 Introduction to Organic Light-emitting Diode

Organic light-emitting diodes (OLEDs) are one of promising candidates for the next-generation light sources due to advantages of a wide viewing angle, low operating voltage, fast response time and flexibility [1]. There have been great interests and advances in the OLEDs in recent years. However, to successfully replace conventional light sources, the quantum efficiency needs to be further improved. The quantum efficiency of OLEDs is determined by the internal quantum efficiency and light extraction efficiency. Although the internal quantum efficiency of OLED devices has already been increased to close to 100% [2], light extraction efficiency of conventional bottom-emitting OLED devices is low due to total internal reflection at ITO (n~1.8)/ glass (n~1.5) and glass/air interfaces [3, 4]. Only ~20% of light generated in the organic layer can be extracted out from the device.

Previously, the self-assembly microsphere or microlens arrays was deposited on the top of GaN LED, which resulted in the significant enhancement in light extraction efficiency [5-13]. The concave structure fabricated by imprinting method using microlens arrays as template was also implemented on GaN LED to improve light extraction [14]. However, it is more challenging to extract the light emitted in the organic active region to free space due to the complicated structure of OLED devices. The refractive index differences between transparent electrode (n=1.7-2) and glass substrate (n=1.5), the glass substrate and the free space (n=1), led to the light was trapped in the organic layer and substrate. Some of the substrate wave guiding modes can be extracted out by modifying glass/air interface, such as introducing microstructures or nanostructures [15-17]. However, the ITO/organic wave guiding modes remain unchanged due to thick glass substrate.

Various approaches have been employed to enhance the light extraction efficiency of OLED devices. One of the approaches is to employ substrate with higher refractive index and the ITO/organic-wave guiding modes can be effectively coupled into the substrate due to the matching of the refractive indices [18]. In this case, the refractive index matched material, such as microsphere or microlens arrays can be deposited on the substrate to help extract the substrate modes out [19]. However, high refractive index materials are too expensive for use in the large area panels. An alternative way is to fabricate photonic crystals between the glass substrate and ITO Layer to extract the ITO/organic layer guiding modes out [20-23]. However, the fabrication process is complicated and expensive.

Recently, the micro-spherically textured structures which can effectively extract the organic mode attracted tremendous attention [24]. The use of micro-spherical structure increased surface area which reduced resistivity of device and enhanced the extraction of organic mode. However, the microsphere arrays was formed by spin-coting method, which is not homogenous due to radius dependent velocity. In addition, fabrication of micro-spherical structure is complicated.

Therefore, other lower cost approaches and easy to implemented solutions are still needed. Previously, we employed rapid convective deposition (RCD) method to fabricate microsphere arrays or microlens arrays on the GaN LEDs, and light extraction efficiency is significantly enhanced [6-8, 14, 25] due to the increased light escape cone and reduced Fresnel reflection. The advantage of RCD method is simple, inexpensive, and scalable[26]. While other methods, such as spin coating, suffer non-uniformity in large area due to the radius dependent centrifuge force which results in the coexist of multilayer, monolayer, and submonolayer [27]. Furthermore, the self-assembly microslens arrays was also used

as imprinting template to form the concave structures on GaN-based LED, which resulted in significant enhancement in the light extraction efficiency [14].

In this work, the microsphere arrays which was deposited by rapid convective method was used as imprinting template to fabricate the OLED with corrugated structures and the output power was measured and compared to that of conventional LED.

7.2 Fabrication OLED Device with Corrugated Structures

The schematics of device fabrication process was shown in Figure 7-1.

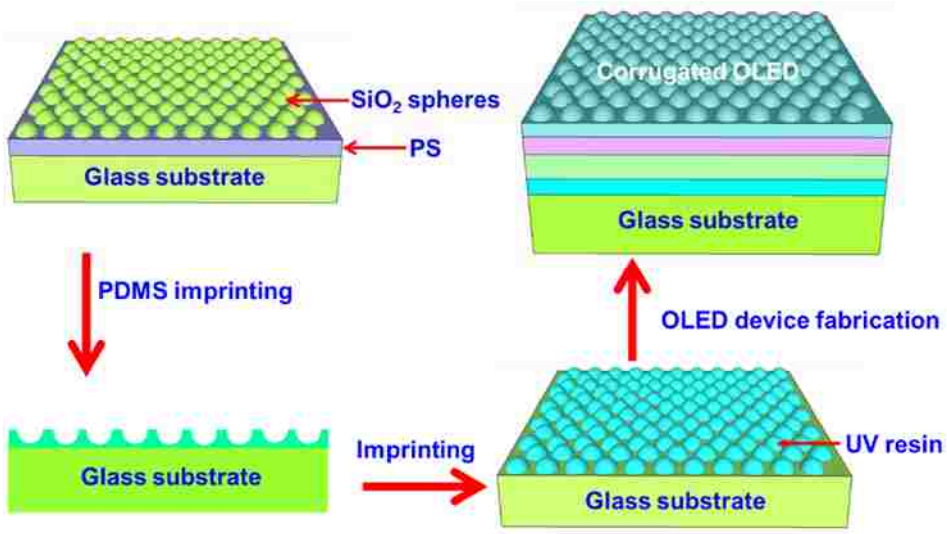

Figure 7-1. Schematics of device fabrication process of LED with corrugated structures

The hexagonal-close packed microlens arrays was prepared by the rapid convective deposition method. Binary suspension of 14% Silica and 4% polystyrene was prepared by dispersing 1.0-μm or 0.5-μm silica microspheres and 100-nm/75-nm polystyrene nanospheres into distilled water. The obtained suspension was injected between blade and substrate and then the substrate was translated by a linear motor. The microsphere arrays were obtained under the tradeoff between the electrostatic force and capillary force. A typical SEM images of 500-nm SiO_2 sphere embed in the 75-nm PS sphere is shown in

Figure 7-2 (a). The microlens arrays was obtained by thermal annealing process and the 500-nm SiO_2 hexagonal-close packed sphere arrays was embedded in the planar PS to form the lens structure as shown in Figure 7-2(b). The aspect ratio of the lens was tuned by controlling thermal annealing time to adjust the PS thickness. The detailed experimental results can be found in reference [8].

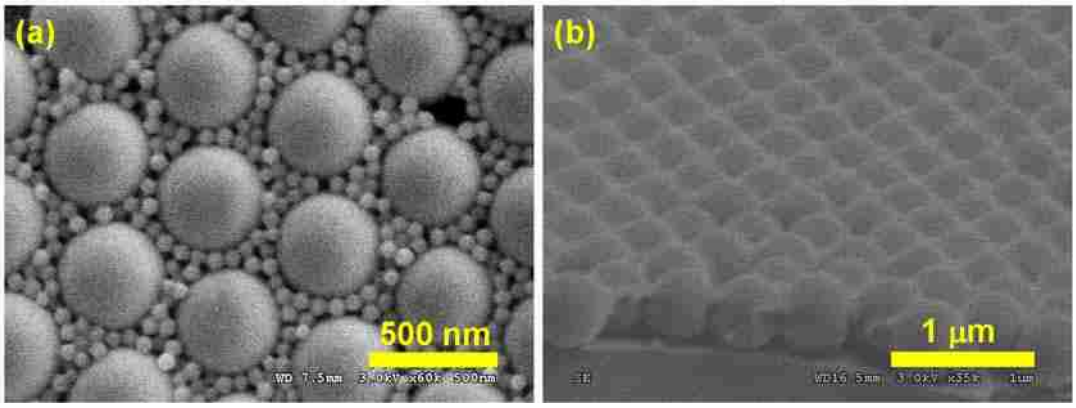

Figure 7-2. (a) SEM image of 500-nm SiO_2 sphere arrays embedded in 75-nm PS spheres before heat treatment. (b) SEM images of SiO_2 sphere arrays embedded in PS layer after heat treatment.

In general, the diffraction efficiency of the grating increases with the depth of grating, however, too high depth will cause the device failure due to the high leakage current paths. Thus, over here, the grating depth of 75 nm and 185 nm was selected for 500-nm grating and 1-µm grating, respectively. To form the OLED with corrugated structures, the polydimethylsiloxane (PDMS) concave structure was made by using SiO_2/PS microlens arrays as template. Subsequently, the PDMS concave structure was stamped onto the UV-curable resin coated glass substrate. Finally, the corrugated resin layer having HCP close-packed structures were used for grating. Note that the microlens arrays was deposited by RCD method, which is a self-assembly process. The non-uniformity of microsphere will cause the locally HCP structure but lack of longer ordering.

During the fabrication of OLED devices, the following layers were deposited on the corrugated and flat resin layers coated glass substrate: a 120-nm ITO, a 50-nm NPB N,N'-bis(naphthalene-1-yl)-N,N'-bis-(phenyl)benzidine), a 60-nm-thick Alq_3 (tris-(8-hydroxyquinoline)-aluminum), a 1.0-nm-thick lithium fluoride (LiF), and a 100-nm-thick aluminum (Al). The schematic device structure is shown in Figure 7-3.

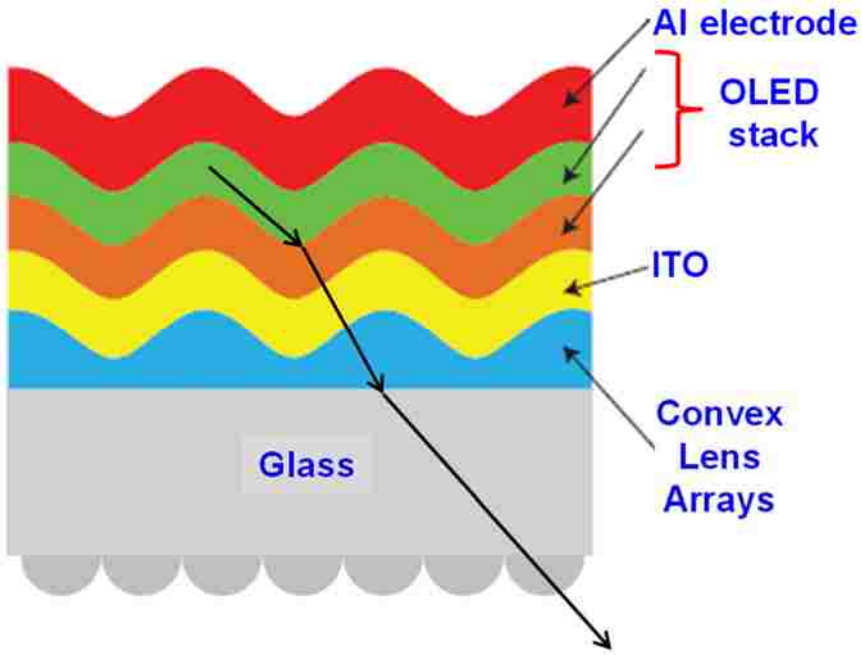

Figure 7-3. Schematics of organic light-emitting diode with corrugated structures.

7.3 Output Power Enhancement of OLED with Corrugated Structures

The typical current densities (mA/cm^2) and luminances (cd/m^2) for the devices with and without 1.0 μm grating are plotted as a function of applied voltage in (a). The 1.0 μm grating device shows a higher current density and a higher luminance at a constant voltage compared with to that of the reference device. The leakage current of the grating device below turn-on voltage showed little difference with that of the reference device on a log-log scale, indicating smooth surface of the corrugated structure for the grating device.

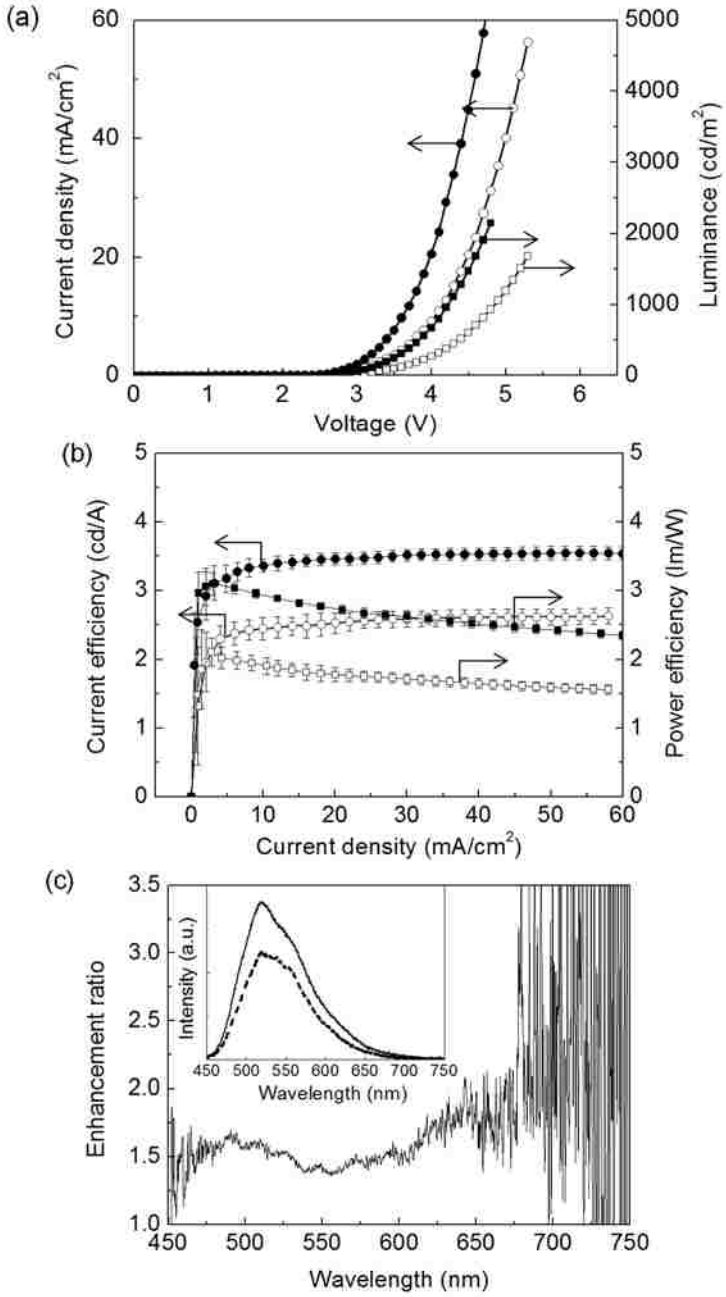

Figure 7-4. (a) Current density (mA/cm^2) and luminance (cd/m^2) and (b) Current efficiency (cd/A) and power efficiency (lm/W) for the 1.0 μm grating (filled symbols) and reference (open symbols) devices. (c) Enhancement ratio of EL intensity, plotted by

dividing the spectrum of the grating device by that of the reference devices. Inset: EL spectra of the grating (—) and reference (– –) devices.

Much higher current density in the grating device is attributed to increased surface area due to the grating and enhanced electric field resulted from non-uniformity of the organic layer thicknesses in a corrugated structure. Despite of the increased current density, the higher enhancement of the luminance in the grating device represents the extraction of the waveguide modes. The current (cd/A) and power efficiencies (lm/W) at a current density of 40 mA/cm^2 are 2.6 cd/A and 1.64 lm/W for the reference device and 3.5 cd/A and 2.5 lm/W for the grating device ((b)). The grating device shows 35% and 50% enhancements in the current and power efficiencies compared to the reference devices. The higher enhancement in the power efficiency than the current efficiency is due to the lower operating voltage in the grating devices, as shown in (a). The electroluminescence (EL) spectra of the grating and reference devices at normal direction show that there is no spectral change due to the 1.0-μm grating (inset of (c)). Dividing the EL intensity of the grating device by that of the reference device, the enhancement ratio for the emission wavelengths is obtained and the results are shown in (c). The enhancement ratio is fairly uniform across the EL spectrum with slightly higher intensities at around 500 and 650~700 nm.

Figure 7-5(a) shows the current densities and luminances for the 0.5-μm grating device and the reference device. Similar to the 1.0-μm grating device, the 0.5-μm grating device exhibits a higher current density and higher luminance than those of the reference device. However, the enhancement of the current density in the 0.5-μm grating device is lower than that in the 1.0 μm grating device because of the lower surface area ratio of the 0.5-μm grating (~7%) than the 1.0 μm grating (~12%). The current and power efficiencies at a current density of 40 mA/cm^2 in Figure 5(b) are 2.57 cd/A and 1.58 lm/W for the

reference devices, and 4.38 cd/A and 2.95 lm/W for the grating devices, respectively. Enhancements of ~70% and ~90% were achieved for the current and power efficiencies due to the 0.5 μm grating. The larger enhancement of the 0.5 μm grating device, compared to the 1.0 μm grating device, is associated with the larger grating vector of the 0.5-μm grating. The EL spectra of the grating and reference devices at normal direction again show a broad enhancement over all emission wavelengths (inset of Figure 7-5(c)). The enhancement ratio in Figure 7-5(c) represents two strong intensities at around 470 and 700 nm. Noted that the enhancements at both ends of the spectrum are slightly larger compared to the 1.0 grating device.

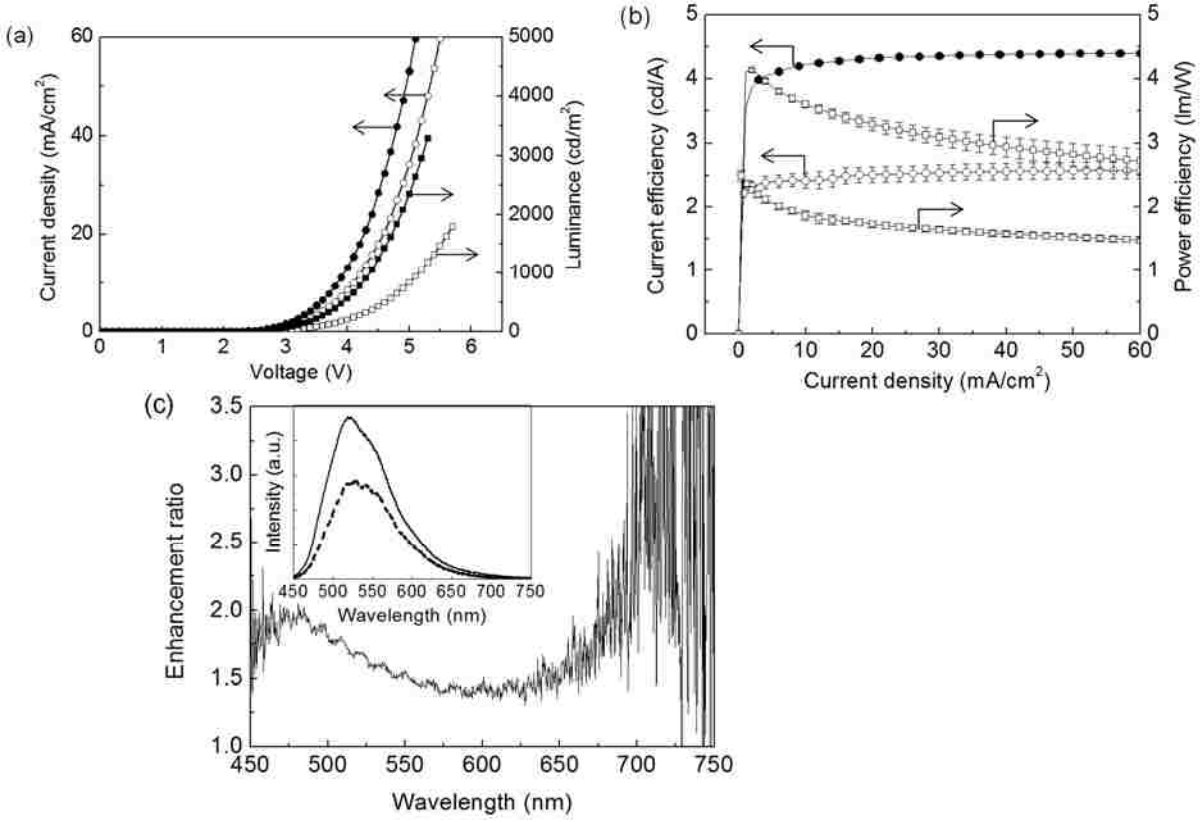

Figure 7-5. (a) Current density (mA/cm^2) and luminance (cd/m^2) and (b) Current efficiency (cd/A) and power efficiency (lm/W) for the 0.5 μm grating (filled symbols) and reference (open symbols) devices. (c) Enhancement ratio of EL intensity. Inset: EL spectra of the grating (—) and reference (– –) devices.

A defective silica sphere array pattern having locally HCP structure but lack of long ordering was fabricated by rapid convective deposition. The defective silica array pattern was incorporated into the devices as grating to extract the *ITO/organic* modes and additionally the *substrate* mode via a thin glass substrate. The results showed that the 1.0-μm grating devices showed the 35% and 50% enhancements in the current and power efficiencies by transferring the *ITO/organic* modes to the *substrate* mode and then scattering the *substrate* mode. The 0.5-μm grating devices were able to effectively extract the *ITO/organic* modes, thereby improved the current and power efficiency by 70% and 90%, respectively, without spectral changes and directionality. With the low-cost and large-area processing, the defective HCP silica array pattern can supply a practical solution for light extraction in the field of OLED applications.

7.4 FDTD Calculation of Light Extraction Efficiency of Organic LED

Recently, our works have demonstrated the use of corrugated structures led to improvement in power efficiency in OLED [9]. These grating structures were obtained by employing 500-nm and 1-μm SiO_2/PS microlens arrays as template. However, this is not optimized device structure. It necessary to further investigate other grating dimensions to achieve maximum light extraction efficiency in OLED.

In this work, we present the numerical simulation studies based on finite-difference time-domain (FDTD) method for analyzing the light extraction efficiency of OLEDs with corrugated structures. Specifically, the light extraction characteristics of OLEDs with corrugated structures will be compared with those of planar OLEDs. The grating period and depth were optimized to achieve optimum light extraction.

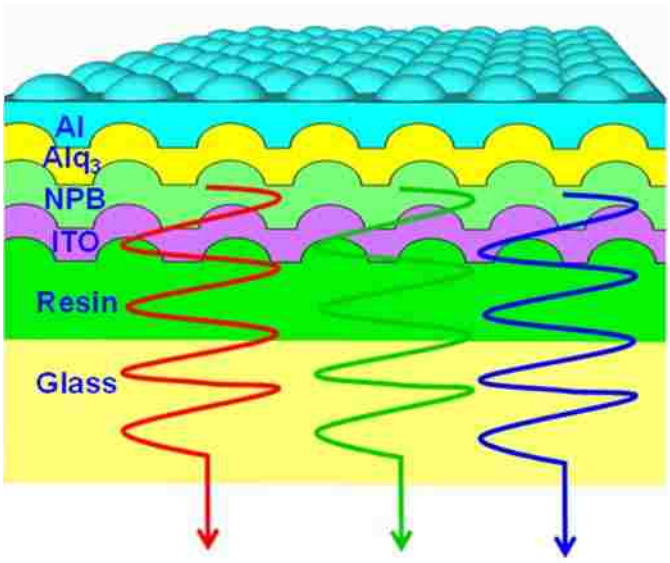

Figure 7-6. The schematic device structure of OLED with corrugated structures.

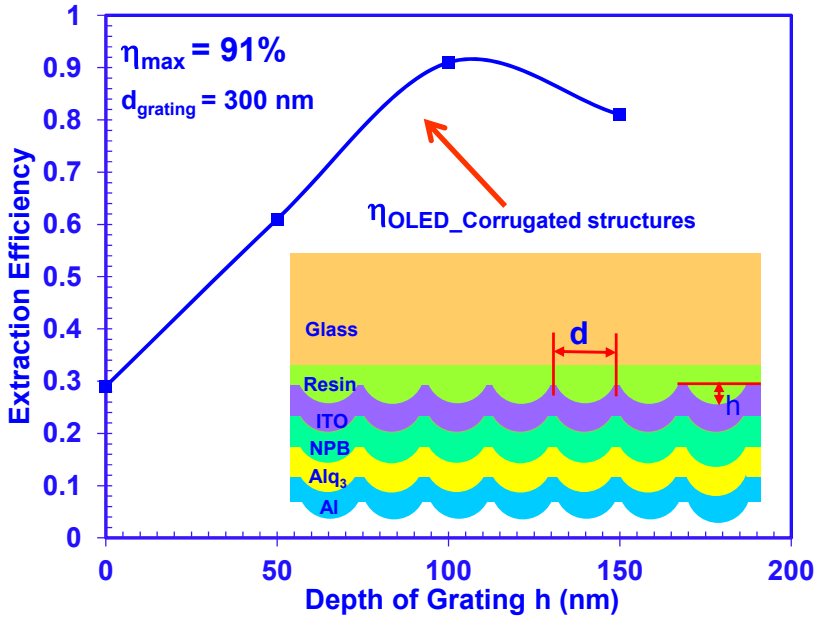

Figure 7-7. The light extraction efficiency of corrugated OLED with grating period of 300 nm as a function of grating depth.

The OLED device structure analyzed in this study is shown in Figure 7-3 and the fabrication process are shown in Figure 7-6. The device was fabricated by imprinting method employing the microlens arrays as template. The deposition of SiO_2/PS binary

sphere arrays were carried out by using rapid convective deposition (RCD) method and the microlens arrays with various aspect ratio was obtained by thermal annealing process. The structure consists of glass substrate, ITO, NPB, Alq3, and Aluminum as cathode. In order to calculate the light extraction efficiency of OLEDs with corrugated structures, the OLED devices are considered as three-dimensional structure solved by vectorial method. The simulation for optimizing the dimension of microstructures were carried out by using FDTD method with perfect electric conductor (PEC) boundary conditions employed for the bottom and sides of the OLEDs. The light extraction efficiency of OLEDs with corrugated structures were obtained by integrating the light output power at the far-field region with the power of the light source at active region.

The light extraction efficiency of OLED with corrugated structures was computed for OLED employing 400-nm and 300-nm SiO_2/PS microlens arrays with various aspect ratio as template. The use of microlens arrays as imprinting template to fabricate OLED resulted in significant enhancement in light extraction efficiency. The light extraction efficiency depends on both the sphere diameter and aspect ratio of microlens arrays. Specifically, the use of 400-nm SiO_2/PS microlens arrays as template resulted in light extraction efficiency of 59%. The use of 300-nm SiO_2/PS microlens arrays resulted in the light extraction efficiency of 91%. Both the diameter of sphere and aspect ratio of microlens have significant effect on the light extraction. The optimized device structure is OLED employing 300-nm SiO_2/PS microlens arrays with depth of 100 nm from the top as shown in Figure 7-7.

In summary, the effects of grating dimensions and grating depth on the light extraction efficiency of OLEDs employing SiO_2/PS microlens arrays as template were investigated. The use 300-nm SiO_2/PS microlens arrays as template is expected to lead to optimized

light extraction efficiency in microsphere LEDs, and the optimization of grating dimension is important for engineering the far-field radiation pattern in OLED.

References

[1] T. Sekitani, H. Nakajima, H. Maeda, T. Fukushima, T. Aida, K. Hata*, et al.*, "Stretchable active-matrix organic light-emitting diode display using printable elastic conductors," *Nat Mater,* vol. 8, pp. 494-499, 06//print 2009.

[2] M. A. Baldo, D. F. O'Brien, Y. You, A. Shoustikov, S. Sibley, M. E. Thompson*, et al.*, "Highly efficient phosphorescent emission from organic electroluminescent devices," *Nature,* vol. 395, pp. 151-154, 09/10/print 1998.

[3] K. Hong and J. L. Lee, "Review paper: Recent developments in light extraction technologies of organic light emitting diodes," *Electron. Mater. Lett.,* vol. 7, pp. 77-91, Jun 2011.

[4] N. Thejo Kalyani and S. J. Dhoble, "Organic light emitting diodes: Energy saving lighting technology—A review," *Renewable and Sustainable Energy Reviews,* vol. 16, pp. 2696-2723, 6// 2012.

[5] P. Kumnorkaew, Y. K. Ee, N. Tansu, and J. F. Gilchrist, "Investigation of the Deposition of Microsphere Monolayers for Fabrication of Microlens Arrays," *Langmuir,* vol. 24, pp. 12150-12157, Nov 2008.

[6] Y. K. Ee, R. A. Arif, N. Tansu, P. Kumnorkaew, and J. F. Gilchrist, "Enhancement of light extraction efficiency of InGaN quantum wells light emitting diodes using SiO_2/polystyrene microlens arrays," *Appl. Phys. Lett.,* vol. 91, Nov 2007.

[7] Y. K. Ee, P. Kumnorkaew, R. A. Arif, H. Tong, H. P. Zhao, J. F. Gilchrist*, et al.*, "Optimization of Light Extraction Efficiency of III-Nitride LEDs With Self-Assembled Colloidal-Based Microlenses," *Ieee J Sel Top Quant,* vol. 15, pp. 1218-1225, Jul-Aug 2009.

[8] H. C. Chang, K. Y. Lai, Y. A. Dai, H. H. Wang, C. A. Lin, and J. H. He, "Nanowire arrays with controlled structure profiles for maximizing optical collection efficiency," *Energy & Environmental Science,* vol. 4, pp. 2863-2869, Aug 2011.

[9] X. H. Li, P. F. Zhu, G. Y. Liu, J. Zhang, R. B. Song, Y. K. Ee*, et al.*, "Light Extraction Efficiency Enhancement of III-Nitride Light-Emitting Diodes by Using 2-D Close-Packed TiO2 Microsphere Arrays," *J Disp Technol,* vol. 9, pp. 324-332, May 2013.

[10] P. Zhu, C. K. Tan, and N. Tansu, "Extraction Efficiency Enhancement of Thin-Film Flip-Chip GaN Light-Emitting Diodes with Self-Assembled Microsphere Arrays," in *Proc. of the International Conference on White LEDs and Solid State Lighting (WLED 5) Conference*, Jeju, Korea, 2014.

[11] P. ZHU, C. K. Tan, and N. Tansu, "Comparison of Extraction Efficiency for Thin-Film Flip-Chip InGaN Light-Emitting Diodes with Microsphere and Microconcave Array Structures," in *Proc. of the SPIE Optics + Photonics 2014*, San Diego, CA, 2014.

[12] P. Zhu, J. Zhang, G. Liu, and N. Tansu, "FDTD Modeling of InGaN-Based Light-Emitting Diodes with Microsphere Arrays," in *Proc. of the IEEE Photonics Conference 2012*, Burlingame, CA, 2012.

[13] P. F. Zhu, G. Y. Liu, J. Zhang, and N. Tansu, "FDTD Analysis on Extraction Efficiency of GaN Light-Emitting Diodes With Microsphere Arrays," *J Disp Technol,* vol. 9, pp. 317-323, May 2013.

[14] Y. K. Ee, P. Kumnorkaew, R. A. Arif, H. Tong, J. F. Gilchrist, and N. Tansu, "Light extraction efficiency enhancement of InGaN quantum wells light-emitting diodes with polydimethylsiloxane concave microstructures," *Opt. Express,* vol. 17, pp. 13747-13757, Aug 2009.

[15] F. Galeotti, W. Mróz, G. Scavia, and C. Botta, "Microlens arrays for light extraction enhancement in organic light-emitting diodes: A facile approach," *Organic Electronics,* 2012.

[16] W. J. Hyun, S. H. Im, O. O. Park, and B. D. Chin, "Corrugated structure through a spin-coating process for enhanced light extraction from organic light-emitting diodes," *Org. Electron.,* vol. 13, pp. 579-585, 2012.

[17] S.-H. Eom, E. Wrzesniewski, and J. Xue, "Close-packed hemispherical microlens arrays for light extraction enhancement in organic light-emitting devices," *Org. Electron.,* vol. 12, pp. 472-476, 3// 2011.

[18] S. Reineke, F. Lindner, G. Schwartz, N. Seidler, K. Walzer, B. Lussem*, et al.*, "White organic light-emitting diodes with fluorescent tube efficiency," *Nature,* vol. 459, pp. 234-8, May 14 2009.

[19] T. D. Schmidt, B. J. Scholz, C. Mayr, and W. Brutting, "Efficiency Analysis of Organic Light-Emitting Diodes Based on Optical Simulations," *Ieee J Sel Top Quant,* vol. 19, Sep-Oct 2013.

[20] Y. R. Do, Y.-C. Kim, Y.-W. Song, and Y.-H. Lee, "Enhanced light extraction efficiency from organic light emitting diodes by insertion of a two-dimensional photonic crystal structure," *J. Appl. Phys.,* vol. 96, p. 7629, 2004.

[21] Y.-J. Lee, S.-H. Kim, J. Huh, G.-H. Kim, Y.-H. Lee, S.-H. Cho*, et al.*, "A high-extraction-efficiency nanopatterned organic light-emitting diode," *Appl. Phys. Lett.,* vol. 82, p. 3779, 2003.

[22] A. M. Adawi, R. Kullock, J. L. Turner, C. Vasilev, D. G. Lidzey, A. Tahraoui*, et al.*, "Improving the light extraction efficiency of polymeric light emitting diodes using two-dimensional photonic crystals," *Org. Electron.,* vol. 7, pp. 222-228, 8// 2006.

[23] Q. Yue, W. Li, F. Kong, and K. Li, "Enhancing the Out-Coupling Efficiency of Organic Light-Emitting Diodes Using Two-Dimensional Periodic Nanostructures," *Advances in Materials Science and Engineering,* vol. 2012, pp. 1-9, 2012.

[24] T. Bocksrocker, J. Hoffmann, C. Eschenbaum, A. Pargner, J. Preinfalk, F. Maier-Flaig*, et al.*, "Micro-spherically textured organic light emitting diodes: A simple way towards highly increased light extraction," *Org. Electron.,* vol. 14, pp. 396-401, Jan 2013.

[25] J. F. Gilchrist, P. Kumnorkaew, Y. K. Ee, and N. Tansu, "Investigation of the Deposition of Microsphere Monolayers for Fabrication of Microlens Arrays," *Langmuir,* vol. 24, pp. 12150-12157, Nov 4 2008.

[26] B. G. Prevo, Y. Hwang, and O. D. Velev, "Convective Assembly of Antireflective Silica Coatings with Controlled Thickness and Refractive Index," *Chem. Mater.,* vol. 17, pp. 3642-3651, 2005/07/01 2005.

[27] T. Ogi, L. B. Modesto-Lopez, F. Iskandar, and K. Okuyama, "Fabrication of a large area monolayer of silica particles on a sapphire substrate by a spin coating method," *Colloids and Surfaces A: Physicochemical and Engineering Aspects,* vol. 297, pp. 71-78, 4/5/ 2007.

Chapter 8 Eu^{3+}- doped TiO_2 Nanospheres for White LED

8.1 The Important of TiO_2 Spheres to Solve Light Extraction Issue

GaN-based light-emitting diodes (LEDs) are rapidly emerging as the best choice for future lighting and display technology due to their potential superior efficiency. High-efficiency LEDs have been realized due to the breakthroughs in GaN-based material growth leading to substantial improvement in its internal quantum efficiency, and in the implementation of high light extraction efficiency structures [1, 2]. However, the light extraction efficiency is still low due to large refractive index contrast between GaN (~2.5 in the visible region) and free space which led to most of light trapped in the LED devices and only 4% of light is extracted out for conventional LED.

A number of approaches have been employed to improve the light extraction efficiency, such as LEDs grown over patterned substrate as well as shaped, flip-chip, thin-film and thin-film rough-surface LEDs [3, 4]. Surface roughening is among the most widely used approaches, and relies on randomizing the light reflected at the interfaces destroying the light propagation in straight paths and leading to multiple attempts to escape the LED devices within the critical angle [5]. Although surface roughening offers high extraction efficiency in LEDs, it provides little control on the direction of the light emission in the device, and result in Lambertian radiation patterns. The photonic crystal led to improved performance [6]; however, light emission directionality remains largely restricted to the emission angles close to the surface normal. Also, the fabrication of photonic crystal is complicated and expensive.

In our previous work, the rapid convective method was employed to deposit 500-nm and 1-μm SiO_2 microsphere arrays on the top of LED to improve the light extraction efficiency. This method is low cost, easy to be implement, and can be scaled up to wafer

scale deposition [7-11]. Previously, SiO_2 was selected as the microspheres in our experiment owning to the ease to obtain monodispersed SiO_2 spheres with various diameters from several nanometers to hundreds of micrometers. The enhancement of light extraction efficiency of LED devices with SiO_2 sphere arrays is consistent with our Ray-tracing and FDTD calculation results [11], and the results from FDTD calculation are much more close to the experimental results, which indicated that FDTD calculation is more accurate than ray-tracing calculation.

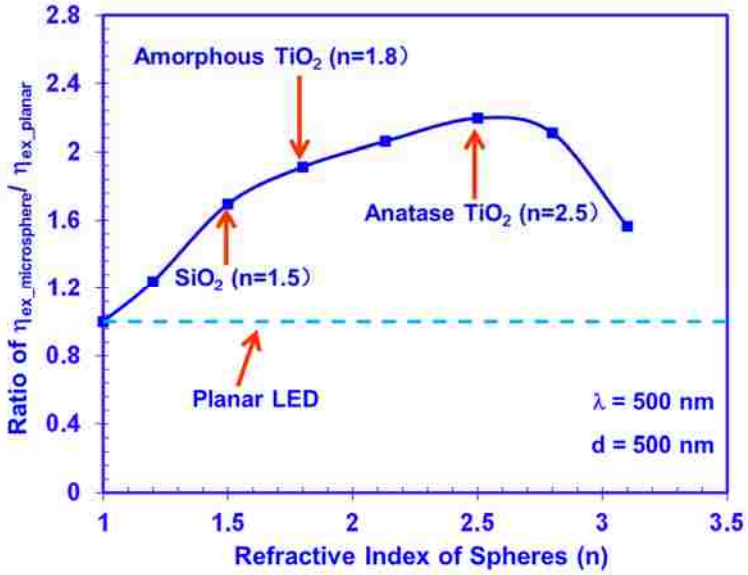

Figure 8-1. The enhancement of light extraction of LED with microsphere arrays as a function of refractive index.

The refractive index of SiO_2 is 1.5 which is lower than that of GaN (2.5 in the visible region). According to the Snell' law, only the incident light within 37° incident range can have chance to go into the SiO_2 spheres and later on, being extracted out. Obviously, the SiO_2 is not the best material choice for the microsphere arrays, and we carried out light extraction calculation of LEDs with higher refractive index material spheres employing FDTD method. The results (see Figure 8-1) showed that light extraction efficiency of LED with amorphous, anatase and rutile TiO_2 sphere arrays are higher than that of LED with SiO_2 sphere arrays. Specifically, 2.1 times enhancement is obtained for LED employing

amorphous TiO_2 (n~1.8) sphere arrays, 2.4 times enhancement is achieved for the LED employing anatase TiO_2 (n~2.4) sphere arrays (see Figure 8-2) and 2.3 times enhancement is obtained for the LED with rutile TiO_2 (n~2.9) sphere arrays. The best material choice for the microsphere arrays is antase TiO_2 with refractive index of 2.5 which is matched with that of GaN.

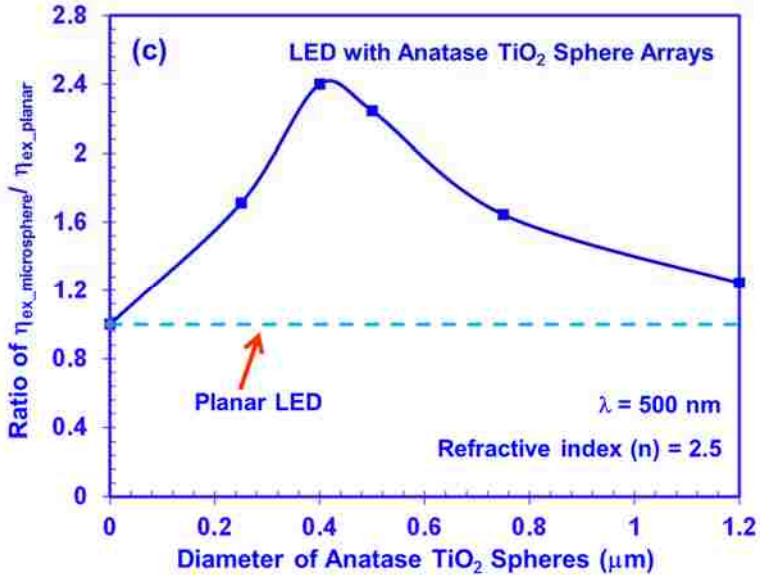

Figure 8-2. Effect of diameter of Anatase TiO_2 sphere on the light extraction efficiency.

The deposition experiments were also carried out for amorphous TiO_2 and anatase TiO_2 microspheres arrays in our previous experiments, and resulted in 1.8 times enhancement in power efficiency, which is lower than that from our FDTD calculation (2.1 times enhancement for LED with amorphous TiO_2 sphere arrays and 2.4 times enhancement for LED with anatase TiO_2 sphere arrays). [12] The discrepancy between the experimental results and calculation results is due to nonhomogenous deposition of TiO_2 spheres, which is caused by the large size variation of TiO_2 spheres in our previous experiment. [12] The nonhomogeneous deposition results in co-exist of the monolayer, submonolayer and multilayer. According to our calculation, hexagonal-close-packed monolayer sphere arrays is highly desirable for the light extraction efficiency purpose and

the highest efficiency is obtained by employing hexagonal-closed packed monolayer sphere arrays. [13] Therefore, the measured light extraction efficiency of LED with TiO_2 sphere arrays is lower than that from FDTD calculation.

However, the TiO_2 spheres with high quality are not commercially available and the growth condition is quiet critical. Obtaining monodisperse homogenous spheres is quiet challenging due to the high hydrolysis rate nature of titanium tetrabutoxide. This led to the non-uniformity of deposition of TiO_2 microsphere arrays on the LED and the decrease in light extraction efficiency for LED with TiO_2 sphere arrays compared to the simulation results.[14] Therefore, further investigation of TiO_2 growth condition is needed in order to further enhance the light extraction efficiency of GaN LED.

8.2 Phosphor Materials for White LED

White-light sources based on InGaN LEDs have a promising future in general illumination with advantages over conventional light sources (e.g., incandescent, fluorescence and high intensity discharge lamps), as they are energy-saving, compact, and environmentally friendly. There are three approaches to generate white light: 1) Blue LED pumped yellow phosphors or green and red phosphors, 2) UV LED pumped blue and yellow phosphors or blue, green and red phosphors, and 3) multi-chip approach that combines blue, green, and red LEDs. The first two approaches based on phosphor-converted LEDs with advantage of low cost, high efficiency and color stability over a wide range of temperatures. White light based on the blue LEDs is commonly used as a simple long-life white-light source due to its efficiency and stability compared to the UV LED chip. Among them, the most popular approach for commercial white LEDs is made by coating an InGaN blue LED with a yellow-emitting phosphors, which has led to its wide use in the various outdoor lighting applications. The first as well as the most widely used yellow phosphor is Ce^{3+}-doped $Y_3Al_5O_{12}$ (YAG: Ce) owing to its many favorable properties such

as strong absorption of blue light (~420-480 nm), broad emission band in the visible region (500-700 nm), fast luminescence decay time (<100 ns), high external quantum efficiency (~75% under blue LED excitation), remarkable chemical and thermal stability and easy to synthesize. Due to these advantages, white LEDs made of the blue LED and YAG: Ce phosphors are currently the mainstream in the LED market and are being widely used in not only point light sources, but also wide-illumination equipment, back-lighting of liquid-crystal TVs and high-power automotive headlights. Despite their wide applications and high luminous efficacy (>100 lm W^{-1}), the disadvantage for white LEDs using only YAG: Ce is that they are limited to high correlated color temperature (CCT; usually ~6000 K) and low color rending index (CRI: usually < 75), due to the lack of sufficient red spectral component. The resulting cool, bluish-white light makes such devices undesirable for indoor use. For indoor lighting, the white light should be warm (CCT<4000 K) with sufficient color rendition (CRI>80). On the other hand, the white LED based on the multichip approach can provide high color rendition, high stability of chromacity, however, the low efficiency of green LED, and the high fabrication cost hinder the further applications. To obtain warm-white LEDs for general illumination, two strategies have generally been adopted to modify the phosphors. One strategy is based on a single-phosphor, multi-emitting centers-conversion model, in which additional red-emitting centers are introduced into the YAG: Ce lattice to compensate the red spectral deficiency of YAG: Ce. The other strategy is based on a multiphosphors-conversion model in which either a red-emitting material is blended with YAG: Ce powder, or a variety of blue, green, yellow and red emitting phosphor are mixed together. Both the multi-emitting-centers model and multi-phosphor model can produce warm-white light with sufficiently high CRI values (80-98); The development of the new green and red phosphors that are efficiently excited by blue LED encourage the use of these phosphors to produce the white LED with high color rendering index and high color temperature.

In the pc-wLEDs, phosphor materials play an important role in the quality of LEDs, such as luminous efficacy, color rendering index, color temperature, lifetime, and etc. Thus, to realize the high efficiency and reliable LED, it is of great importance to choose appropriate phosphors. There are several considerations in choosing phosphor:

8.2.1 The Excitation Spectrum

The excitation spectrum is determined by monitoring emission spectrum at the wavelength of maximum intensity while the phosphor is excited through a group of consecutive wavelengths. To convert the emitted light of LED more efficiently, the excitation spectrum should be broad enough to cover the emission spectrum. This requires the phosphor to absorb strongly the light of LEDs, and to have flat excitation spectrum near the maximum emission wavelength of LEDs.

8.2.2 The Emission Spectrum

The emission spectrum records emission intensity as a function of wavelength of phosphor when it is excited by a certain wavelength of light. The emission spectrum of a phosphor is required to be useful and broad sufficiently to realize the high color rendering white light, when it is combined with the LED chip. On the other hand, the emission spectrum should be as narrow as possible.

8.2.3 The Quantum Efficiency

The quantum efficiency of phosphor is determined by internal quantum efficiency and external quantum efficiency. The internal quantum efficiency is the ratio of emitted photons to the number of absorbed photons. The external quantum efficiency is the ratio of number of emitted photons to the number of absorbed photons. Higher luminous efficiency of white LED require high quantum efficiency of phosphor.

8.2.4 The Stability of Phosphor

The stability of a phosphor require the shape of luminescence spectra, luminescence intensity, and quantum efficiency do not change over entire operating temperature range and lifespan of wLED. The thermal quenching of LED phosphor should be as small as possible for enabling high temperature operation.

8.2.5 The Particle Size and Morphology of Phosphor Particles

The particle size and morphology of phosphor particles affects the quantum efficiency of phosphor as well as luminous efficiency of w-LED. Generally, to reduce the light scattering and quantum efficiency, the particle size should be as uniform as possible, and the distribution is as narrow as possible. Spherical particles is highly desired for enabling uniform deposition process.

8.2.6 The Production Cost of Phosphor

The production cost of the phosphor should be as low as possible. The phosphor is required to be synthesized cost-effectively for large scale production.

8.3 The importance of Eu^{3+}-doped TiO_2 spheres as red phosphor in GaN White LED

TiO_2 is promising phosphor host material due to its low cost, high transparency in the visible light region, and good thermal, chemical, and mechanical properties. Phosphors with special shape, in particular, small and ideally spherical particles are highly desired in luminescent devices because they offer the possibility of improved luminescent performance, definition, and screen packing. The idea morphology of phosphor particles is spherical shape, narrow size distribution, and nonagglomeration. Owning to the advantages of TiO_2, Eu-doped TiO_2 is becoming promising red phosphor as it is transparent in the visible region. Therefore, In addition to the light extraction efficiency

applications, TiO_2 spheres doped with Eu^{3+} can serve as red phosphor for GaN blue LED based white LED applications.

However, preparation of monodispersed TiO_2 particles with spherical shape is very difficult because of the fast hydrolysis rate of Titania precursor at room temperature [7]. Xia and Pale showed that the hydrolysis rate of precursors could be slowed by forming a coordination complex with ethylene glycol [8, 9]. Recently, mixed-solvent method has been developed into an effective method to obtain monodisperse spherical particles, such as CeO_2, CdS [10, 11]. Adjusting the ratio of mixed solvents affects not only the hydrolysis rate but also the diffusion rate of the precursors, both of which have great effect on the morphology of the particles.

Synthesis of TiO_2 Spheres has been a challenging task for many years. In this work, the growth conditions of the TiO_2 spheres were also investigated. The effects of ammonia, the ratio of acetonitrile to acetone in the mixed solvents and the concentration of titanium tetrabutoxide (TBOT) on the morphology were investigated. The phase transformation condition was investigated, from amorphous TiO_2, to anatase TiO_2, and to rutile TiO_2. The Eu-doped TiO_2 spheres were also synthesized by mixed-solvent method. The strong red emission peaking at 610 nm was observed under excitation of 464 nm and 397 nm. Especially, for the Eu-doped anatase TiO_2 spheres. This leads to the potential applications for Eu-doped TiO_2 in high efficiency white light emitting diode. Introduction to GaN-based White LED

White light-emitting diode are attracting considerable attention from both academic and industrial communities, as they are generally accepted as the next generation energy saving and green solid-state lighting devices. The word record of 130 lm/W at 1A drive current for white LEDs with the color temperature of the 4700 K was announced by Nichia [15], and Cree also claimed a R&D record of 254 lm/W at a drive current of 350 mA. Such

performance greatly surpass that of fluorescence tubes (~80-100 lm/W), and far exceed that of incandescent (~17 lm/W) and halogen (~25 lm/W) lamps. Due to the tremendous progress in optical qualities, white LED are now penetrating the light market very rapidly, which are steadily replacing incandescent lamps and fluorescent tubes for general lighting, cold cathode fluorescent lamps for automotive headlights. The use of white LEDs will significantly save huge electrical energy, and reduce carbon emissions.

There are three approaches to generate white light: 1) Blue LED pumped yellow phosphors or green and red phosphors, 2) UV LED pumped blue and yellow phosphors or blue, green and red phosphors, and 3) Multi-chip approach that combines blue, green, and red LEDs [16]. The white LED based on the multichip approach provide high color rendition, high stability of chromacity. However, the low efficiency of green LED, and the high fabrication cost hindered the further applications [17, 18]. While phosphor-converted LEDs can overcome these disadvantages [16, 19, 20]. Thus, it is important to further explorer new phosphor materials as well as improve the performance of current phosphors. The work presented in this section was performed in collaboration with Prof. W. Qin (Jilin University).

In this work, we employ the low-cost mixed solvent method to synthesize the Eu^{3+}-doped TiO_2 nanospheres, which can effectively absorb the blue light emitted from the GaN blue chip and emit red color. It will be a very promising red phosphor which can be served as red phosphor for GaN-based white LED.

8.4 Synthesis of TiO_2 Spheres by Mixed-Solvent Method

Ethanol (GR) and ammonia (AR) were obtained from Beijing Chemical Corporation (Beijing, China). Titanium tetrabutoxide (TBOT) (AR) and acetonitrile (GR) were from

Tianjin Guangfu Chemical Corporation (Tianjin, China). All the reactants were used without further purification.

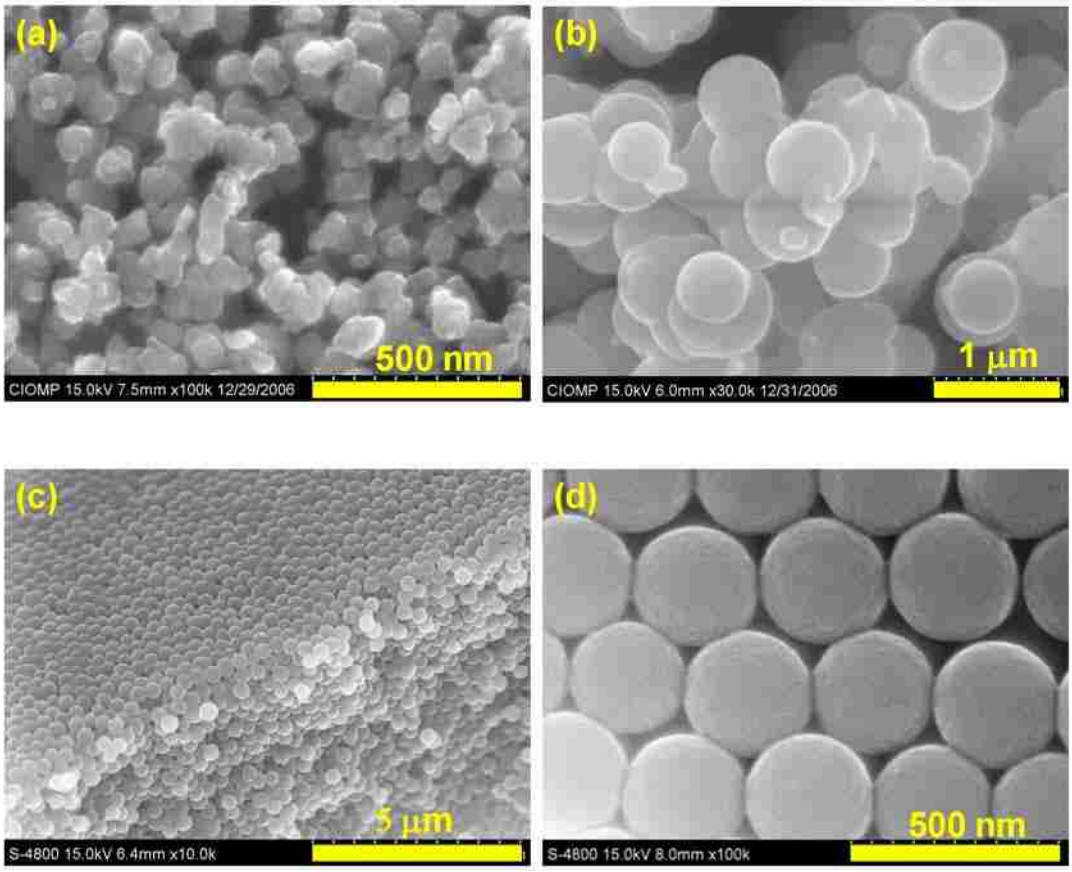

Figure 8-3. SEM images of TiO_2 particles synthesized under the different conditions: (a). without ammonia and acetonitrile, (b). with ammonia but without acetonitrile, (c). with ammonia and acetonitrile (the insert is an enlarged image).

In order to investigate the effect of ammonia on the morphology of TiO_2, the TiO_2 particles were prepared in the Ethanol solvent with and without ammonia, respectively. Also, to investigate the effect of acetonitrile on the formation of TiO_2 particles, we adjusted the ratio of acetonitrile to Ethanol. As a typical synthesis, two identical solutions were prepared by mixing acetonitrile and Ethanol with different ratio. The mixed solution was

stirred for 30 min. Next, an amount of ammonia and TBOT were added to the two solutions respectively. After substantial stirring, the two solutions were mixed and stirred for 2 h. The obtained products were centrifuged, washed 4 times with absolute ethanol, and dried at 80°C for 12 h. The Eu^{3+}-doped TiO_2 was prepared as following: Two identical solutions were prepared by mixing acetonitrile and Ethanol. The mixed solution was stirred for 30 min. Then an amount of ammonia was added to one of two identical solutions. $Eu(NO_3)_3$ and TBOT with different ratio were added to the other solution. After substantial stirring for half an hour, these two solutions were mixed and stirred for 2 h. The obtained products were centrifuged, washed for 4 time with absolute ethanol, and dried at 80^{o}C for 12 h. The as-prepared TiO_2 particles were annealed at 350^{o}C, 500^{o}C, 650^{o}C, and 850^{o}C for 2 h, respectively.

The structure of TiO_2 particles were analyzed by X-ray diffraction (XRD) (Rigaku D/max-2000 X-ray powder diffractometer) using Cu Kα radiation (λ=1.54178Å). The overall images and sizes of the particles were characterized by field emission scanning electron microscopy (SEM, S-4800).

Figure 8-3 (a) and (b) shows the SEM images of TiO_2 particles prepared in the ethanol, without and with ammonia, respectively. Except for the ammonia, the concentrations of other chemicals in each reaction are the same. It shows that spherical TiO_2 particles were formed with addition of ammonia [see Figure 8-3(b)]. However, when the ammonia is substituted by distilled water, irregular particles were obtained [see Figure 8-3 (a)]. This indicated that $NH_3 \cdot H_2O$ played a very important role in forming the spherical particles. In the solution, the ammonia was decomposed into ammonium (NH_4^+) and hydroxide (OH^-). The NH_4^+ overcame repulsive barrier and draw the negatively charged $\equiv TiO^-$ together. The formation mechanism of TiO_2 spheres can be seen in Figure 2. The NH_4^+ is absorbed by the negatively charged $\equiv TiO^-$ and the cores are formed. When $\equiv TiO^-$ migrates to the

core, the condensation process occurs. Therefore, the ammonia as a catalyst contributes to the formation of spherical TiO_2 particles.

$$NH_3 + H_2O \leftrightarrow NH_4^+ + OH^- \tag{8.1}$$

$$(C_4H_9OH)_3 Ti OH + NH_3 \leftrightarrow (C_4H_9OH)_3 TiO^- + NH_4^+ \tag{8.2}$$

$$(C_4H_9O)_3 TiOC_4H_9 + OH^- \leftrightarrow (C_4H_9O)_3 TiOH + C_4H_9O^- \tag{8.3}$$

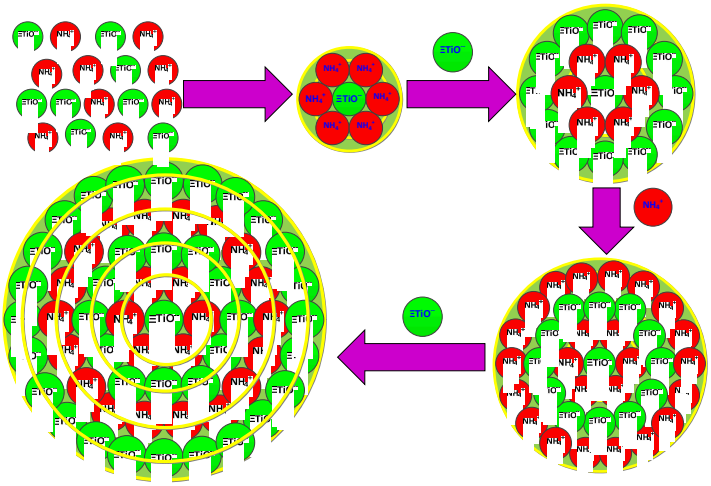

Figure 8-4. Schematics of sphere formation process in the ethanol and acetonitrile.

However, although the spherical particles is formed under the catalysis of ammonia, the particles tend to stick together due to the high solubility of TBOT and its hydrolysates. The hydrolysis of TBOT molecules will result in the coexistence of TBOT and its hydrolysates in the solution. TBOT and its hydrolysates have high solubility in Ethanol, which means that there are relatively strong interactions between the solute and the solvent molecules; however, it is not the case for acetonitrile as the solvent because of the low solubility of TBOT in it. As a result, when a certain amount of acetonitrile is added to the Ethanol solution, the interactions between solutes (TBOT and its hydrolysates) and solvents (ethanol and acetonitrile) became weaker. Therefore, the TBOT can easily diffuse

onto the surface of hydrolysates and then hydrolyze and condense under the catalysis of NH_4^+ to form monodisperse spherical TiO_2 particles. By adjusting the ratio of acetonitrile to acetone, an appropriate diffusion for TBOT and their partial hydrolysates can be obtained. Our results show that monodisperse TiO_2 spheres can be obtained when the ratio of acetonitrile to acetone is 3:1, as shown in Figure 8-3 (c) and (d).

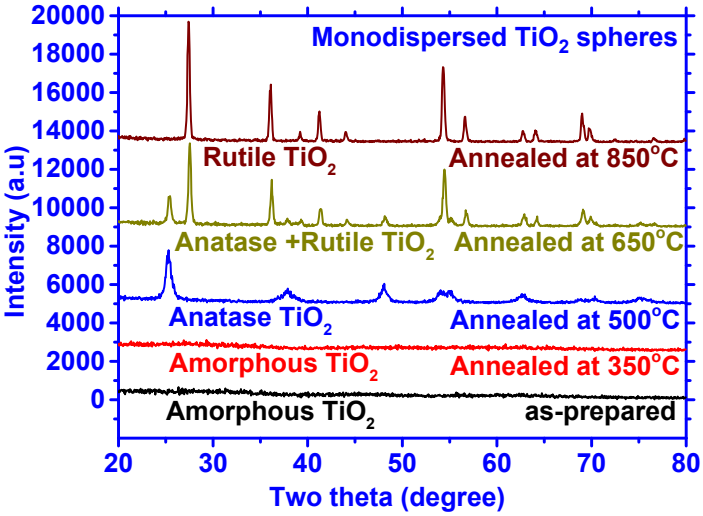

Figure 8-5. XRD patterns of TiO_2 at different annealing temperatures.

When the ratio of acetonitrile to acetone is constant at 3:1, the size of TiO_2 particles depends on the concentration of TBOT in the mixed solvent. This is because at such a ratio almost all TBOT molecules in the mixed solvent can easily diffuse to form spherical TiO_2 particles. The particle size is determined by hydrolysis rate and condensation rate. Hydrolysis rate increases with water concentration, however, decreased with TBOT concentration [12]. The particle size decreased with decreasing TBOT concentration. Therefore, the particle size can be adjusted by controlling the concentration of TBOT. In addition, the reaction temperature has great effect on the particle size. High reaction temperature should promote hydrolysis of TBOT and then increase the number of titania nuclei. As a result, the size decreased with increasing reaction temperature [13].

Figure 8-5 presents the XRD patterns for the sample with a 300-nm in diameter before and after annealed at various temperatures (350^{o}C, 500^{o}C, 650^{o}C, 850^{o}C) for 2 h. The as-prepared sample did not show any diffraction peaks, indicating that the as-synthesized TiO_2 is amorphous. When the sample is annealed at 350^{o}C, there were also no peaks, until the temperature increased to 500^{o}C, several diffraction peaks appeared and all of them is attributed to the anatase phase of TiO_2 (JCPDS 21-1272). No other phase such as rutile or brookite could be found. However, all the diffraction peaks for the sample annealed at 800^{o}C correspond to the rutile phase of TiO_2 (JCPDS 21-1276). From the XRD patterns, the phase transition from anatase to rutile seems to occur at 650^{o}C, as diffraction peaks of both anatase and rutile phase were detected at this annealing temperature.

8.5 Optical Properties of Eu^{3+}-doped TiO_2 Nanospheres

8.5.1 The energy transfer between the TiO_2 and Eu^{3+}

The photoluminescence excitation spectrum corresponding to the 611 nm emission of Eu^{3+} doped TiO_2 was shown in Figure 8-6.The spectra exhibit several sharp peaks owing to the Eu^{3+} f→f transition and a broad excitation band with a maximum at 270 nm. Tsuboi et al.[21, 22] observed two broad excitation bands in Eu^{3+} doped TiO_2 nanoparticles: one is at around 320 nm, the other is at 270 nm. The 320 nm excitation band is the same as the absorption band observed in non-doped TiO_2. Therefore, the 320 nm band was assigned as band-to-band transition in the host lattice while the 270 nm band corresponds to the charge transfer (CT) band from the 2p orbital of O^{2-} ligands to the 4f orbital of Eu^{3+} ion. Zeng and coworkers[23] also measured the excitation of Eu^{3+}-doped TiO_2 nanotube and conclude that the peak at 275 nm is attributed to the charge transfer between Eu^{3+} and O^{2-} and the excitation peak at 312 nm is attributed to the energy transfer from the TiO_2

nanotube matrix to Eu^{3+} ions. In our experiment, only the 270 nm band was observed. There are two possibilities: it is either CT band or it is absorption band of TiO_2.

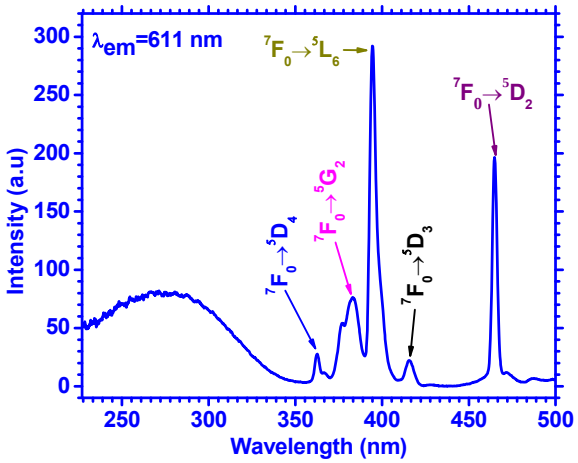

Figure 8-6. The excitation spectrum of Eu-doped amorphous TiO_2 spheres monitoring 610 nm emission.

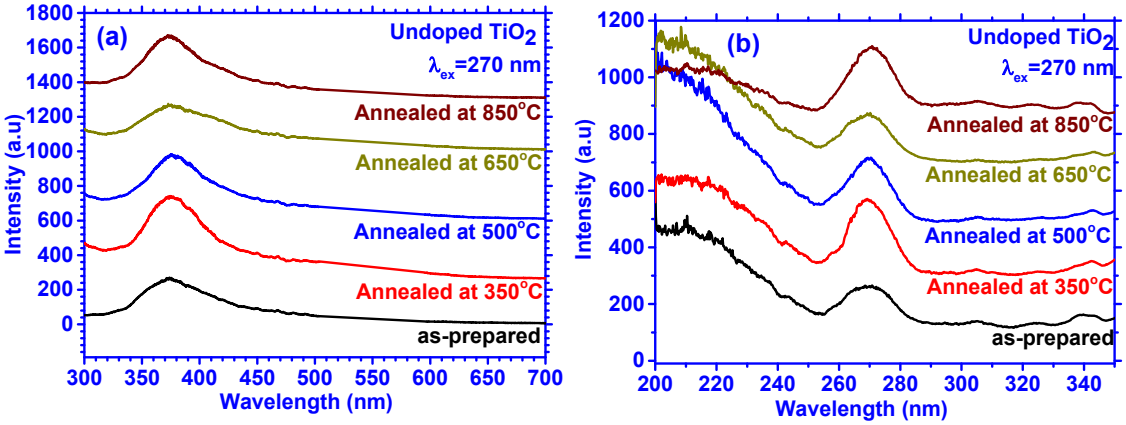

Figure 8-7. (a) The emission spectra of TiO_2 spheres under 270 nm excitation. (b) The excitation spectra monitoring 380 nm emission.

In order to clarify this 270 nm broad band absorption, The excitation and PL of pure TiO_2 spheres annealed at 350°C, 500°C, 650°C, 850°C were measured. The PL spectrum under 270 nm excitation exhibits a broad ultraviolet emission band centered at 380 nm with full width at half maximum (FWHM) of about 69 nm [see Figure 8-7 (a)], which is attributed to electron transition from the conduction band to the valence band. There is no obvious peak shift. On the photoluminescence excitation spectra, monitored 380 nm

emission, a broad excitation band with maximum at 270 nm was observed [see Figure 8-7 (b)], which is due to the excitation from the valence band to the conduction band of TiO_2. Therefore, the 270 nm broad band in Eu^{3+}-doped TiO_2 is attributed to the absorption of TiO_2. When the TiO_2 is excited by UV light, the excitation energy absorbed by TiO_2 promotes the electrons from the valence band (VB) to conduction band (CB). The electrons are then trapped by the defect states through the nonradiative decay process. The recombination of the electrons in the defect states with the holes in the VB result in the TiO_2 UV emission. Compared with the reported band gap of TiO_2 crystals [24-26]. The band gap of TiO_2 synthesized in this work is larger. The band gap obtained in this work is consistent with the results got from Pan and coworkers[27]. However, the FWHM is larger than one they got, which is probably caused by the different crystal phase: it is anatase phase for their case, while the XRD patterns show that the TiO_2 particles we got are amorphous. The band gap in the amorphous material will be poorly defined due to its lack of ordered crystal structure, and will be larger than for the crystalline titania polymorphs[28]. Thus, the 270 nm broad band absorption most possibly originates from the TiO_2.This result suggested that Eu^{3+} emission is associated with an energy transfer process from the TiO_2 to the Eu^{3+}.

More information about the energy transfer between TiO_2 and Eu^{3+} can be obtained by investigation of the emission spectra of TiO_2 doped with various concentration of Eu^{3+}. The photoluminescence spectrum 270 nm excitation for the samples with Eu^{3+} concentration of 0, 1%, 10%, and 15%, respectively, are shown in Figure 8-8 (a). To do comparison, the spectrum is normalized by 380 nm emission. The pure TiO_2 exhibits only the broad UV emission band due to the emission from the pure TiO_2 sphere, but upon Eu^{3+} addition, five emission bands centered at 576, 590, 611, 649, and 697 nm, respectively,

was observed, corresponding to the Eu^{3+} transition from $^5D_0$ to ^7F_J (J=0, 1, 2, 3, 4), respectively [29].

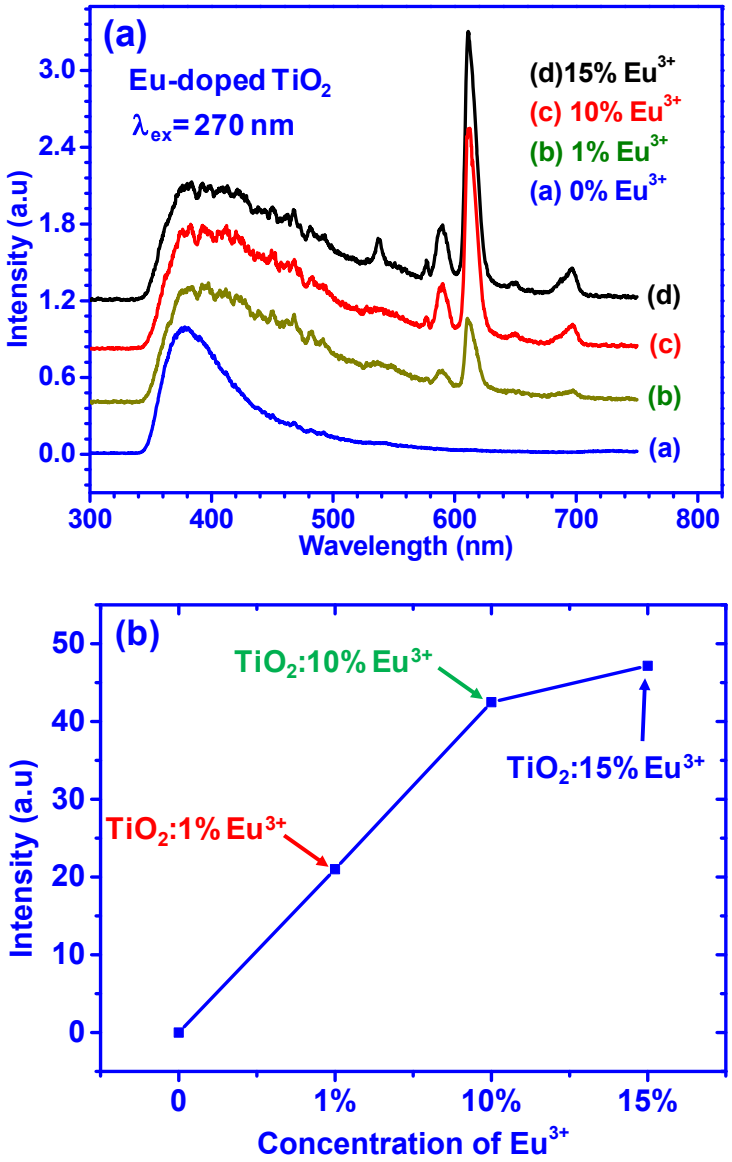

Figure 8-8. The emission (normalized by 380 nm emission) spectra of Eu^{3+}-doped TiO_2 spheres with various Eu^{3+} concentrations under 270 nm excitation. (b) Integrated intensity of emission centered at 610 nm for Eu^{3+}-doped TiO_2 spheres with various concentration.

These bands show strong inhomogeneous broadening because the ionic radius of Eu^{3+} (0.098 nm) is much larger than that of Ti^{4+} (0.068 nm) [30] and Eu^{3+} is distributed in

the amorphous titania region. The emission ratio of Eu^{3+} to TiO_2 increases [see Figure 8-8(b)] with the increase in the Eu^{3+} concentration. The band-to-band transition of TiO_2 peaking at 380 nm is higher than that of Eu^{3+} centered at 610 nm at relatively lower Eu^{3+} concentration. The emission of Eu^{3+} became higher than the emission of TiO_2 with the increase in the Eu^{3+} concentration. This finding indicates that the increase in the Eu^{3+} emission in the sacrifice of TiO_2 emission. This further proved that there is energy transfer process between the TiO_2 and Eu^{3+}. The ratio of TiO_2 emission (peaking at 380 nm) intensity to that of Eu^{3+} (peaking at 611 nm) decreased with increasing the Eu^{3+} concentration. This is consistent with the conclusion obtained by Zeng et al [31] that the $^5D_0$ emission of Eu^{3+} increased with the increase in Eu^{3+} content in Eu^{3+}-doped TiO_2 particles. Tachikawa et al[32] use time-resolved photoluminescence to prove the energy transfer between the TiO_2 host and Eu^{3+} ions.

8.5.2 Emission spectrum of Eu^{3+}-doped TiO_2 under blue light excitation

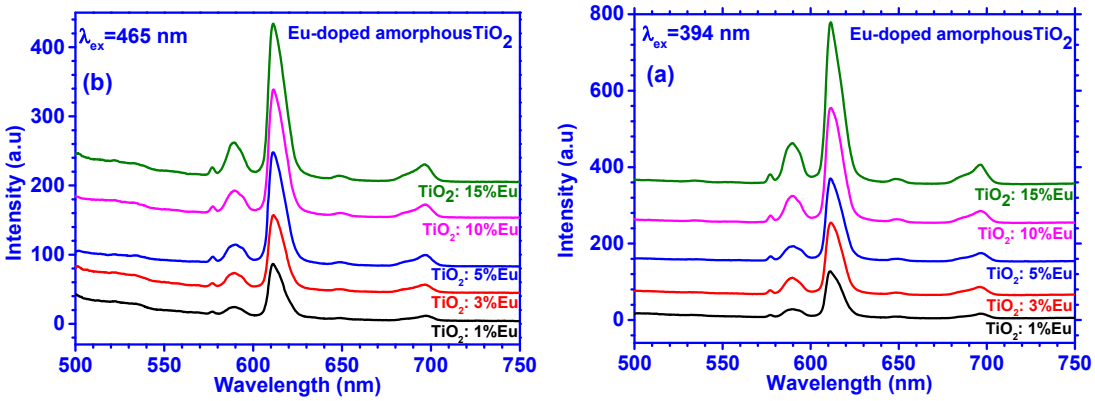

Figure 8-9. (a) The emission spectra of Eu^{3+}-doped TiO_2 spheres with various Eu^{3+} concentrations under 394 nm excitation. (b) The emission spectra of Eu^{3+}-doped TiO_2 spheres with various Eu^{3+} concentrations under 465 nm excitation.

In addition to 270 nm broadband absorption, there are two stronger absorption peaks in the longer wavelength: one is centered at 397 nm; the other is centered at 464 nm. The

intensity of these two peaks increase with the increase in the Eu^{3+} concentration as expected. However, the increase rate became slower for the higher Eu^{3+} concentration, which is attributed to the strong interaction between the Eu^{3+} ions. These two absorption peaks located at the blue regime, which is indicate that Eu^{3+}-doped TiO_2 can be excited by the GaN blue LED and emit red light. Thus, the emission spectrum was also investigated for TiO_2 with various Eu^{3+} concentrations under the excitation of 394 nm and 464 nm. The intensity for emission under the excitation of 394 nm increased with the increase in Eu^{3+} concentration. This is attributed to the increased luminescent center in the TiO_2 matrix. The emission spectra were also measured under the excitation of 464 nm. The same trend was observed for the Eu^{3+}-doped TiO_2 under the excitation of 464 nm.

8.5.3 The phase transformation and luminescence properties of Eu^{3+}-doped TiO_2 nanospheres

As mentioned earlier, the anatase TiO_2 spheres can be obtained by annealing amorphous TiO_2 spheres. The more important thing is that light extraction efficiency of LED devices with anatase TiO_2 sphere is higher than that with amorphous TiO_2 spheres. This leads us to further investigate the optical properties of Eu^{3+}-doped TiO_2 at various annealing temperatures. Figure 8 (b) shows the excitation spectrum of 10% Eu^{3+}-doped TiO_2 sphere at various annealing temperatures. Both 394 nm and 464 nm absorption peaks exist for the as-prepared sample and the samples at lower annealing temperatures. However, only absorption band centered at 464 nm still exist for the samples at higher annealing temperatures, and the absorption band centered at 394 nm disappeared. Specifically, the intensity of absorption centered at 394 nm decreases with increasing annealing temperature and completely disappeared when the annealing temperature increased to 750^{o}C. The intensity of the absorption centered at 464 nm initially increased with annealing temperature, the maximum intensity is obtained at annealing temperature of 500^{o}C, which corresponds to the anatase TiO_2. Further increase the temperature, the

intensity started to decrease. This also reflected from the emission spectra. The emission spectra of 10% Eu^{3+}-doped TiO_2 at various annealing temperatures are shown in Figure 8-10 (a). The emission intensity peaking at 610 nm increased with the increase in the annealing temperature, the maximum intensity was obtained when Eu^{3+}-doped TiO_2 was annealed at 500°C.

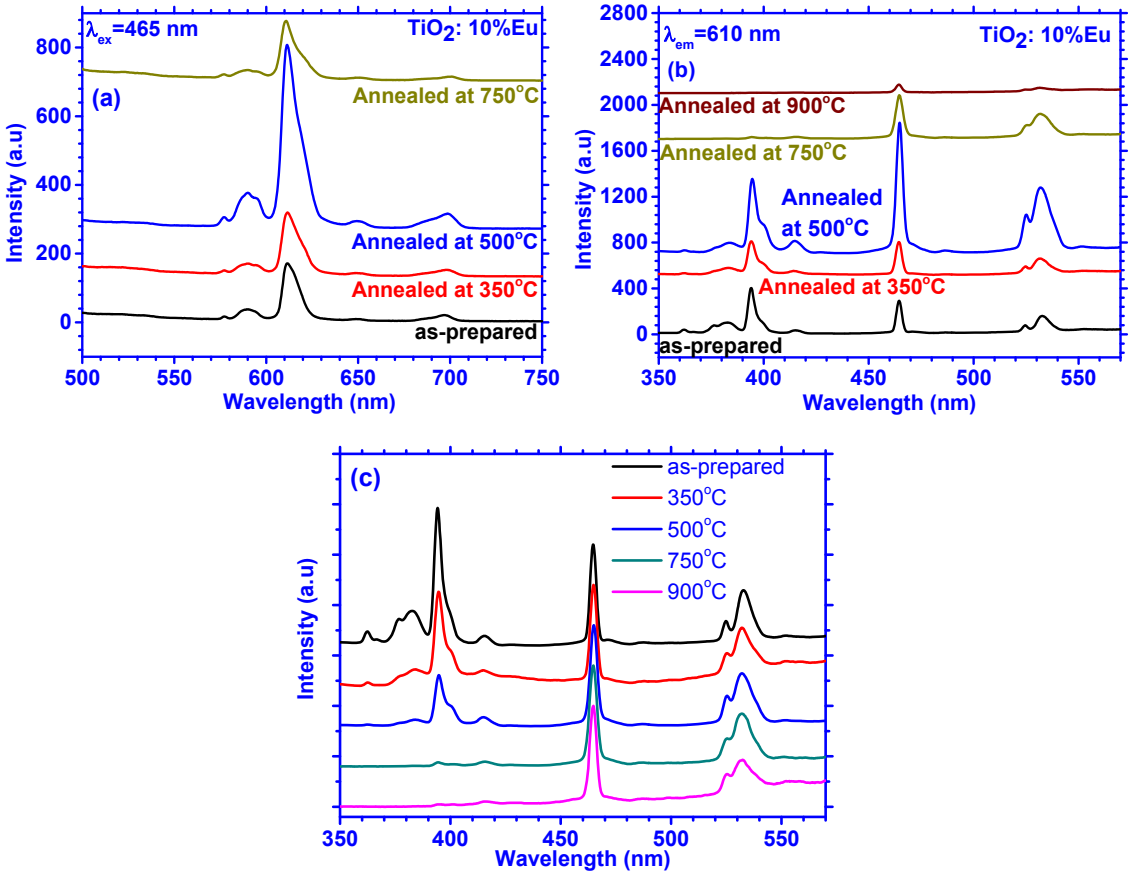

Figure 8-10. (a) The emission spectra of 10% Eu-doped TiO_2 spheres annealed at various temperatures under 464 nm excitation. (b) The excitation spectra of 10% Eu-doped TiO_2 spheres annealed at different temperature monitoring 610 nm emission. (c) The normalized excitation spectra Eu^{3+}-doped TiO_2 spheres annealed at different temperature monitoring 610 nm emission.

Further increase in the temperature, the emission intensity peaking at 610 nm started to decrease, and when the increase the annealing temperature to 900°C, the emission

centered at 610 nm almost disappear. Therefore, the Eu^{3+}-doped TiO_2 annealed at 500°C, which corresponds to the anatase TiO_2, have highest emission intensity under excitation of 464 nm. To make the comparison more obvious, the normalized excitation spectra (normalized by 464 nm excitation) was also plotted in the Figure 8-10 (c). This result shows its potential for usage in white LED application.

Eu^{3+} ions are used in spectroscopy to determine the environment around the Eu^{3+} ion in the host as compared to other Ln^{3+} ions, since its electric dipole transition is hypersensitive to its local symmetry. The excitation spectrum change with the annealing temperature, which indicate the environment of Eu^{3+} changed with annealing temperature.

In summary, the light extraction efficiency can be improved by implementing the amorphous, anatase, or rutile TiO_2 spheres on the top of LED. This led to enhanced light extraction efficiency. However, the TiO_2 spheres with small size distribution and large size range are not commercially available. This led to the difficulty to implement the TiO_2 sphere arrays on the top of LED and reduced light extraction efficiency compared to the simulation results. The monodisperse TiO_2 spheres were prepared by mixed-solvent method; ammonia plays an important role in forming the spherical TiO_2 particles. The ratio of acetonitrile to acetone is the key factor to form monodisperse TiO_2 particles. In the presence of ammonia, we obtained monodisperse spherical TiO_2 particles when the ratio of acetonitrile to acetone is 3:1. The size of TiO_2 particles can be adjusted by changing the precursor's concentration and reaction temperature. We have also demonstrated that these spherical TiO_2 particles could be converted from amorphous to anatanse and then to rutile by annealed at elevated temperatures. The optical properties of Eu^{3+}-doped TiO_2 was investigated, we found that there are some strong absorption in blue region and emit red light. Especially for the anatase TiO_2. This leads to potential applications for the Eu^{3+}-doped TiO_2 in high efficiency LED devices.

References

[1] H. P. Zhao, G. Y. Liu, J. Zhang, J. D. Poplawsky, V. Dierolf, and N. Tansu, "Approaches for high internal quantum efficiency green InGaN light-emitting diodes with large overlap quantum wells," *Opt. Express,* vol. 19, pp. A991-A1007, Jul 4 2011.

[2] H. P. Zhao, G. Y. Liu, and N. Tansu, "Analysis of InGaN-delta-InN quantum wells for light-emitting diodes," *Appl Phys Lett,* vol. 97, Sep 27 2010.

[3] Y. K. Ee, J. M. Biser, W. J. Cao, H. M. Chan, R. P. Vinci, and N. Tansu, "Metalorganic Vapor Phase Epitaxy of III-Nitride Light-Emitting Diodes on Nanopatterned AGOG Sapphire Substrate by Abbreviated Growth Mode," *Ieee J Sel Top Quant,* vol. 15, pp. 1066-1072, Jul-Aug 2009.

[4] P. Zhao and H. P. Zhao, "Analysis of light extraction efficiency enhancement for thin-film-flip-chip InGaN quantum wells light-emitting diodes with GaN micro-domes," *Opt. Express,* vol. 20, pp. A765-A776, Sep 2012.

[5] T. Fujii, Y. Gao, R. Sharma, E. L. Hu, S. P. DenBaars, and S. Nakamura, "Increase in the extraction efficiency of GaN-based light-emitting diodes via surface roughening," *Appl. Phys. Lett.,* vol. 84, pp. 855-857, Feb 2004.

[6] J. J. Wierer, A. David, and M. M. Megens, "III-nitride photonic-crystal light-emitting diodes with high extraction efficiency," *Nat Photonics,* vol. 3, pp. 163-169, Mar 2009.

[7] Y. K. Ee, R. A. Arif, N. Tansu, P. Kumnorkaew, and J. F. Gilchrist, "Enhancement of light extraction efficiency of InGaN quantum wells light emitting diodes using SiO_2/polystyrene microlens arrays," *Appl. Phys. Lett.,* vol. 91, Nov 2007.

[8] Y. K. Ee, P. Kumnorkaew, R. A. Arif, H. Tong, J. F. Gilchrist, and N. Tansu, "Light extraction efficiency enhancement of InGaN quantum wells light-emitting diodes with polydimethylsiloxane concave microstructures," *Opt. Express,* vol. 17, pp. 13747-13757, Aug 2009.

[9] Y. K. Ee, P. Kumnorkaew, R. A. Arif, H. Tong, H. P. Zhao, J. F. Gilchrist*, et al.*, "Optimization of Light Extraction Efficiency of III-Nitride LEDs With Self-Assembled Colloidal-Based Microlenses," *Ieee J Sel Top Quant,* vol. 15, pp. 1218-1225, Jul-Aug 2009.

[10] H. C. Chang, K. Y. Lai, Y. A. Dai, H. H. Wang, C. A. Lin, and J. H. He, "Nanowire arrays with controlled structure profiles for maximizing optical collection efficiency," *Energy & Environmental Science,* vol. 4, pp. 2863-2869, Aug 2011.

[11] P. Zhu, G. Liu, J. Zhang, and N. Tansu, "FDTD Analysis on Extraction Efficiency of GaN Light-Emitting Diodes With Microsphere Arrays," *J. Display Technol.,* vol. 9, pp. 317-323, 2013.

[12] X.-H. Li, P. Zhu, G. Liu, J. Zhang, R. Song, Y.-K. Ee*, et al.*, "Light Extraction Efficiency Enhancement of III-Nitride Light-Emitting Diodes by Using 2-D Close-Packed TiO_2 Microsphere Arrays," *J Disp Technol,* vol. 9, pp. 324-332, 2013.

[13] P. Zhu, J. Zhang, G. Liu, and N. Tansu, "Light Extraction Efficiency Enhancement of Thin-Film Flip-Chip LED with Microsphere Arrays, Microlens Arrays and Concave Structures," 2013.

[14] D. J. Chae, D. Y. Kim, T. G. Kim, Y. M. Sung, and M. D. Kim, "AlGaN-based ultraviolet light-emitting diodes using fluorine-doped indium tin oxide electrodes," *Appl. Phys. Lett.,* vol. 100, p. 3, Feb 2012.

[15] Y. Narukawa, M. Ichikawa, D. Sanga, M. Sano, and T. Mukai, "White light emitting diodes with super-high luminous efficacy," *J Phys D Appl Phys,* vol. 43, Sep 8 2010.

[16] S. Ye, F. Xiao, Y. X. Pan, Y. Y. Ma, and Q. Y. Zhang, "Phosphors in phosphor-converted white light-emitting diodes Recent advances in materials, techniques and properties," *Mater. Sci. Eng. R-Rep.,* vol. 71, pp. 1-34, Dec 2010.

[17] J. M. Phillips, M. E. Coltrin, M. H. Crawford, A. J. Fischer, M. R. Krames, R. Mueller-Mach*, et al.*, "Research challenges to ultra-efficient inorganic solid-state lighting," *Laser Photonics Rev.,* vol. 1, pp. 307-333, Dec 2007.

[18] C. J. Humphreys, "Solid-state lighting," *MRS Bull.,* vol. 33, pp. 459-470, Apr 2008.

[19] J. S. Wang, H. Y. Zhu, C. L. Ma, X. X. Wu, J. Zhang, D. M. Li*, et al.*, "High-Pressure Behaviors of SrF2 Nanocrystals with Two Morphologies," *Journal of Physical Chemistry C,* vol. 117, pp. 615-619, Jan 10 2013.

[20] J. McKittrick, M. E. Hannah, A. Piquette, J. K. Han, J. I. Choi, M. Anc*, et al.*, "Phosphor Selection Considerations for Near-UV LED Solid State Lighting," *ECS J. Solid State Sci. Technol.,* vol. 2, pp. R3119-R3131, 2013.

[21] E. Setiawati, K. Kawano, T. Tsuboi, and H. J. Seo, "Studies on thermal migration of Eu ion doped into TiO2 nanoparticles," *Jpn J Appl Phys,* vol. 47, pp. 4651-4657, 2008.

[22] T. Tsuboi, E. Setiawati, and K. Kawano, "Spectroscopy study on the location and distribution of Eu3+ ions in TiO2 nanoparticles," *Jpn J Appl Phys,* vol. 47, pp. 7428-7435, Sep 2008.

[23] Q. G. Zeng, Z. M. Zhang, Z. J. Ding, Y. Wang, and Y. Q. Sheng, "Strong photoluminescence emission of Eu:TiO2 nanotubes," *Scripta Mater,* vol. 57, pp. 897-900, 2007.

[24] L. Li, C. K. Tsung, Z. Yang, G. D. Stucky, L. D. Sun, J. F. Wang*, et al.*, "Rare-earth-doped nanocrystalline Titania microspheres emitting luminescence via energy transfer," *Adv Mater,* vol. 20, pp. 903-908, Mar 5 2008.

[25] K. L. Frindell, M. H. Bartl, A. Popitsch, and G. D. Stucky, "Sensitized luminescence of trivalent europium by three-dimensionally arranged anatase nanocrystals in mesostructured titania thin films," *Angew Chem Int Edit,* vol. 41, pp. 1001-1004, 2002.

[26] J. G. Li, X. H. Wang, K. Watanabe, and T. Ishigaki, "Phase structure and luminescence properties of Eu^{3+}-doped TiO_2 nanocrystals synthesized by Ar/O^{-2} radio frequency thermal plasma oxidation of liquid precursor mists," *J Phys Chem B,* vol. 110, pp. 1121-1127, Jan 26 2006.

[27] D. Pan, N. Zhao, Q. Wang, S. Jiang, X. Ji, and L. An, "Facile Synthesis and Characterization of Luminescent TiO2 Nanocrystals," *Adv. Mater.,* vol. 17, pp. 1991-1995, 2005.

[28] J. Ovenstone, P. J. Titler, R. Withnall, and J. Silver, "A Study of the Effects of Europium Doping and Calcination on the Luminescence of Titania Phosphor Materials," *J Phys Chem B,* vol. 105, pp. 7170-7177, 2001.

[29] J. Yang, Z. W. Quan, D. Y. Kong, X. M. Liu, and J. Lin, "Y2O3 : Eu3+ microspheres: Solvothermal synthesis and luminescence properties," *Cryst Growth Des,* vol. 7, pp. 730-735, Apr 2007.

[30] R. Shannon, "Revised effective ionic radii and systematic studies of interatomic distances in halides and chalcogenides," *Acta Crystallographica Section A: Crystal Physics, Diffraction, Theoretical and General Crystallography,* vol. 32, pp. 751-767, 1976.

[31] Q. G. Zeng, Z. J. Ding, and Z. M. Zhang, "Synthesis, structure and optical properties of Eu^{3+}/TiO_2 nanocrystals at room temperature," *J Lumin,* vol. 118, pp. 301-307, Jun 2006.

[32] T. Tachikawa, T. Ishigaki, J. G. Li, M. Fujitsuka, and T. Majima, "Defect-Mediated Photoluminescence Dynamics of Eu^{3+} Doped TiO_2," *Angew. Chem,* vol. 120, pp. 5428-5432, 2008.

Chapter 9 Summary and Future Outlook

9.1 Summary

During the dissertation research, several research projects have been successfully carried out. The sets of projects will be outlined below consisting of two broad classifications. The first broad classification include the methods and analysis for enabling improved light extraction efficiency in III-Nitride LEDs, and the second broad classification include the investigation of nanomaterials for applications in white LED technology.

First, finite-difference time-domain (FDTD) method was employed to calculate light extraction efficiency of GaN based light-emitting diode (LED). The effect of microsphere diameters and refractive indices on the light extraction efficiency was investigated. The results showed that the use of 400-nm anatase TiO_2 sphere arrays with refractive index of 2.5, which is matched with that of GaN, resulted in 2.4 times enhancement in light extraction efficiency.

Second, rapid convective deposition (RCD) method was employed to self-assemble microsphere/nanosphere arrays. The sphere arrays were obtained under the tradeoff between the electrostatic forces and capillary forces. Suspension concentration and deposition speed are the two key parameters to achieve monolayer sphere array deposition. Hexagonal-closed spheres arrays with diameter from 1 μm down to 100 nm have been obtained by tuning suspension concentration and deposition speed. The comprehensive study of deposition of binary sphere arrays were also carried out and binary sphere arrays with various diameters were obtained. The microlens arrays were obtained by thermal annealing the binary sphere arrays at 140 ^{0}C and the aspect ratio of microlens arrays was tuned by adjusting the annealing time.

Third, the deposition of anatase TiO_2 spheres on the GaN-based LED was carried out. The deposition conditions to form monolayer sphere arrays was optimized. The Electroluminescence showed that much high light intensity was obtained for the LED with anatase TiO_2 sphere arrays than that of planar LED, which resulted in 1.83 times enhancement in output power.

Fourth, FDTD calculation was employed to optimize the thin-film flip-chip (TFFC) LED device structure. Quantum well position and cavity thickness were tuned to obtain optimum light extraction for the planar TFFC LED. The self-assembly microsphere arrays were implemented on TFFC LED, light extraction efficiency of 75% has been predicted by tuning refractive index and diameter of spheres as well as the quantum well position and cavity thickness, which is much higher than that of planar TFFC LED. Further enhancement was achieved by embedding the microsphere arrays in planar PS layer to obtain microlens arrays. The use of microlens arrays on TFFC resulted in light extraction efficiency of 86%. This finding would result in significant improvement in quantum efficiency of LED by using cost-effective method.

Fifth, the rapid convective deposition method and nanosphere lithography were employed to fabricate organic light-emitting diodes (OLEDs) with corrugated structures. The novel device structure effectively extracted organic mode, which otherwise would be trapped in the devices. The use of defective microlens arrays led to broadband light extraction.

Further optimization was carried out employing FDTD method. We found that grating period and grating depth have significant effect on the light extraction efficiency. The optimized device structure was obtained by tuning the grating period and grating depth. Optimum light extraction of 91% has been achieved, which is 4 times higher than that of conventional OLED without grating structures.

Finally, the monodisperse TiO_2 spheres were prepared by mixed-solvent method; ammonia plays an important role in forming the spherical TiO_2 particles. The ratio of acetonitrile to acetone is the key factor to form monodisperse TiO_2 particles. In the presence of ammonia, we obtained monodisperse spherical TiO_2 particles when the ratio of acetonitrile to acetone is 3:1. The size of TiO_2 particles can be adjusted by changing the precursor's concentration and reaction temperature. We have also demonstrated that these spherical TiO_2 particles could be converted from amorphous to anatanse and then to rutile by annealed at elevated temperatures. The optical properties of Eu^{3+}-doped TiO_2 was investigated, we found that there are some strong absorption in blue region and emit red light. Especially for the anatase TiO_2. This leads to potential applications for the Eu^{3+}-doped TiO_2 in high efficiency LED devices.

9.2 Future Outlook

The topics in solid-state lighting are receiving significant attentions recently. Solid-state lighting (SSL) technology has the potential to cut lighting energy usage by nearly one half. It is anticipated that SSL will play a significant role in realizing global energy cost savings within the next several years. Manufacturing cost reductions are critical to ensure wildly spread adoption of SSL. Therefore, seeking cost-effective method to improve the quantum efficiency is vital important. The progress achieved in this work is expected to advance the field of solid state lighting, in particular for enabling wider adoption of microlens arrays methods for improving light extraction efficiency in LEDs.

CURRICULUM VITAE
(Ms.) Peifen Zhu

Education

July 2011–Nov. 2014, Lehigh University (Bethlehem, Pennsylvania, USA)
Ph.D. in Electrical Engineering

- PhD Advisor: Professor Nelson Tansu (ECE and CPN, Lehigh University)
- Research Areas: III-Nitride semiconductor nanostructures for thermoelectric, solid-state lighting, solar cell and solar hydrogen technologies.

Aug. 2009 – May. 2011, Texas Tech University (Lubbock, Texas, USA)
Master of Science (M.S.) in Electrical Engineering

- Advisors: Professor Hongxing Jiang and Professor Jingyu Lin (ECE, Texas Tech University)
- Research Areas: III-Nitride semiconductor nanostructures for solar hydrogen technologies.

Sep. 2004 – July. 2007, Jilin University (Changchun, Jilin, China)
Master of Science (M.S.) in Physics, Institute of Atomic and Molecular Physics

- Advisor: Professor Qiren Zhu (Institute of Atomic and Molecular Physics, Jilin University).
- Research Areas: Nanomaterial synthesis and characterization
- Thesis: Synthesis, Luminescence Properties and Thermal Stability of $BaMgAl_{10}O_{17}$: Eu^{2+} Blue Phosphors

Sep. 2000 – July. 2004, Liaocheng University (Liaocheng, Shandong, China)
Bachelor of Science (B.S.) in Physics

- Thesis: Discussion on the Use of Analogy in Atomic Physics

Professional Experiences

August 2014 – Present, the University of Tulsa (Tulsa, OK, USA)
Assistant Professor
Department of Physics and Engineering Physics
College of Engineering and Natural Sciences

July 2011 – August 2014, Lehigh University (Bethlehem, PA, USA)
Ph.D. Candidate and Research Assistant
Department of Electrical and Computer Engineering (ECE)
P. C. Rossin College of Engineering and Applied Science & Center for Photonics and Nanoelectronics (CPN)
Ph.D. Advisor: Professor Nelson Tansu (Lehigh, ECE and CPN)

May 2009 –May 2011, Texas Tech University (Lubbock, TX, USA)
Research Assistant
Department of Electrical and Computer Engineering (ECE) & Center for Nanophotonics
Edward E. Whitacre Jr. College of Engineering
Advisor: Professor Hongxing Jiang and Jingyu Lin

Sep. 2006 – Oct. 2008, Jilin University (Changchun, Jilin, China)
Research Assistant
College of Electronic Science and Engineering & State Key Laboratory on Integrated Optoelectronics

Advisor: Professor Weiping Qin
Received Top Ranking Graduate (1st Rank) in MS Program (July 2007)

Sep. 2005 – Sep. 2006, Chinese Academy of Science (Changchun, Jilin, China)
Research Assistant
Changchun Institute of Optics, Key Lab of Excited-State Processes
Advisor: Professor Baojiu Chen

Research Interests

My research work covers various aspects of nanomaterial synthesis and characterization, computational physics, material growth, device fabrication and characterization. The pursuit of novel materials for high thermoelectric figure of merit, solid-state lighting, solar cell and solar hydrogen applications, synthesis and characterization of photonic and electronic nanomaterials for the applications in solid-state lighting, solar cell and solar hydrogen technologies. Specifically, my research work focus on these three aspects:

1) **Computational Electromagnetics for Optoelectronic Device Applications to Achieve High Performance Devices**
   - ➔ Optimization of GaN LED device structure to achieve high extraction efficiency
   - ➔ Optimization of organic LED device structure to achieve high and broadband light extraction
   - ➔ Optimization of other photonic device structure, such as solar cell, to achieve high efficiency devices
2) **Experimental Implementation of Novel Device Structure to Achieve High Performance Devices**
   - ➔ MOCVD growth of nitride materials and optoelectronic device fabrication
   - ➔ Material characterization and device performance testing
   - ➔ Deposition of microsphere or microlens arrays on LED to achieve high efficiency LED by employing low-cost, large-scale, self- assembly method
   - ➔ Optimization of the photoelectrochemical (PEC) cell structure for achieving high-efficiency solar hydrogen generation in III-Nitride nanostructures
3) **Nanomaterial Synthesis and Characterization for Addressing Energy Efficiency and Renewable Energy Technologies**
   - ➔ Synthesis of rare earth-doped nanomaterials and investigation of their photoluminescence properties and thermal stability for the applications in solid-state lighting technology
   - ➔ Synthesis of photon-conversion nanomaterials for the applications in solar cell technology
   - ➔ Synthesis of the microspheres/nanospheres for quantum efficiency enhancement in GaN-based light-emitting diodes (LEDs), organic LEDs, and solar cells

Awards & Honors Received

- ***Sherman-Fairchild Fellowship for Solid State Studies*** (2014-2015), Lehigh University
- ***Lehigh University Research Assistantship***(July. 2011- Present), Lehigh University
- ***Lehigh University Dean's Scholarship***(Aug. 2011- Aug. 2012), Lehigh University
- ***Texas Tech University Research Assistantship*** (Sep.2009-May2011),Texas Tech University
- ***Passed Fundamental Engineering Exam (FE) for Professional Engineers***, Texas, 2010
- ***Jilin University Graduate Student Scholarship*** (Sep. 2007- July 2010), Jilin University
- ***Jilin* University *Graduate Student Scholarship*** (Sep. 2004- July 2007), Jilin University
- ***Received Top Ranking Graduate (1st Rank) in MS Program*** (July 2007), Jilin University

Professional Affiliations

2012 - Present, Student Member, Institute of Electrical and Electronics Engineers (IEEE)

2012 - Present, Student Member, International Society for Optical Engineering (SPIE)

Selected Refereed Journal and Conference Publications

1. **(Invited Conference Paper)** **P. F. Zhu**, W. Sun, C. K. Tan, and N. Tansu, "Light Extraction Efficiency Enhancement in GaN-Based LEDs with Self-Assembly Approach," Proc. of the *Progress In Electromagnetics Research Symposium (PIERS) 2014*, Guangzhou, China, August 2014.
2. **P. F. Zhu**, T. Toma, C. K. Tan, and N. Tansu, "Investigation of Solar Hydrogen Generation from the GaN and InGaN Thin Films," Proc. of the *SPIE Optics + Photonics 2014*, Solar Energy + Technology, San Diego, CA, August 2014.
3. **P. F. Zhu**, H. Y. Zhu, W. P. Qin, C. K. Tan, and N. Tansu, "Eu^{3+}-doped TiO_2 Nanospheres for GaN-based White Light-Emitting Diodes," Proc. of the SPIE Optics + Photonics 2014, *Thirteenth International Conference on Solid State Lighting and LED-based Illumination Systems*, San Diego, CA, August 2014.
4. **P. F. Zhu,** C. K. Tan, and N. Tansu, "Comparison of Extraction Efficiency for Thin-Film Flip-Chip InGaN Light-Emitting Diodes with Microsphere and Microconcave Array Structures," Proc. of the SPIE Optics + Photonics 2014, *Thirteenth International Conference on Solid State Lighting and LED-based Illumination Systems*, San Diego, CA, August 2014.
5. **P. F. Zhu**, C. K. Tan, and N. Tansu, "Extraction Efficiency Enhancement of Thin-Film Flip-Chip GaN Light-Emitting Diodes with Self-Assembled Microsphere Arrays," Proc. of the *International Conference on White LEDs and Solid State Lighting (WLED 5) Conference 2014*, Jeju, Korea, June 2014.
6. **P. F. Zhu**, G. Y. Liu, J. Zhang, and N. Tansu, "FDTD Analysis on Extraction Efficiency of GaN Light-Emitting Diodes with Microsphere Arrays", Journal of Display Technology, vol. 9, no. 5, pp. 316-322, May 2013. DOI: 10.1109/JDT.2013.2250253.
7. **P. F. Zhu**, P. O. Weigel, G. Y. Liu, J. Zhang, A. L. Weldon, T. Muangnaphor, J. F. Gilchrist, and N. Tansu, "Optimization of Deposition Conditions for Silica / Polystyrene Microlens and Nanolens Arrays for Light Extraction Enhancement in GaN Light-Emitting Diodes," Proc. of the SPIE Photonics West 2013, San Francisco, CA, January 2013.
8. **P. F. Zhu**, Q. Zhu, H. Zhu, H. Zhao, B. Chen, Y. Zhang, X. Wang and W. Di, "Effect of SiO_2 coating on photoluminescence and thermal stability of $BaMgAl_{10}O_{17}$: Eu^{2+} under VUV and UV excitation, Optical Materials, 30, pp. 930-934, 2008.
9. **P. F. Zhu**, W. Di, Q. Zhu, B. Chen, H. Zhu, H. Zhao, Y. Yang and X. Wang, "Luminescent Properties and Thermal Stability of $BaMgAl_{10}O_{17}$: Eu^{2+} Synthesized by Sol-Gel Route, Journal of Alloys and Compounds, 454, pp. 245-249, 2008.
10. **P. F. Zhu**, J. Zhang, G. Y. Liu, and N. Tansu, "FDTD Modeling of InGaN-Based Light-Emitting Diodes with Microsphere Arrays," Proc. of the IEEE Photonics Conference 2012, Burlingame, CA, September 2012.
11. H. Cui, **P. F. Zhu**, H. Y. Zhu, H. D. Li, and Q. L. Cui, "Photoluminescence Properties and Energy Transfer in Y_2O_3: Eu^{3+} Nanophosphors", Chin. Phys. B, 2014, vol.23, no.5, 57801.
12. X. H. Li, **P. F. Zhu**, G. Y. Liu, J. Zhang, R. B. Song, Y. K. Ee, P. Kumnorkaew, and J. F. Gilchrist, and N. Tansu, "Light Extraction Efficiency Enhancement of III-Nitride Light-Emitting Diodes by using 2-D Close-Packed TiO_2 Microsphere Arrays", Journal of Display Technology, vol. 9, no. 5, pp. 323-331, May 2013. DOI: 10.1109/JDT.2013.2246541.
13. C. K. Tan, **P. F. Zhu**, and N. Tansu, "Controlling the Interband Auger Recombination Mechanism in III-Nitride Based Ternary Active Regions," Proc. of the SPIE Optics + Photonics 2014, Thirteenth International Conference on Solid State Lighting and LED-based Illumination Systems, San Diego, CA, August 2014.
14. C. K. Tan, **P. F. Zhu**, and N. Tansu, "Investigation of Dilute-As GaNAs Active Regions for High Efficiency GaN-based Light-Emitting Diodes," Proc. of the International Conference on White LEDs and Solid State Lighting (WLED 5) Conference 2014, Jeju, Korea, June 2014.

15. J. Zhang, H. Cui, **P. F. Zhu**, C. L. Ma, X. X. Wu, H. Y. Zhu, Y. Z. Ma, and Q. L.Cui, Photoluminescence Studies of Y_2O_3:Eu^{3+} under High Pressure, Journal of Applied Physics, vol.115, no.3. 023502, Jan. 2014.
16. W. H. Koo, W. Youn, **P. F. Zhu**, X-H. Li, N. Tansu, F. So, Light Extraction Of Organic Light Emitting Diodes by Defective Hexagonal-Close-Packed Array. Advanced Functional Materials, vol. 22, pp. 3453-3453, 2012.
17. W. Di, X.Wang, **P. F. Zhu**, and B. Chen, Energy Transfer and Heat-Treatment Effect of Photoluminescence in Eu^{3+}-Doped $TbPO_4$ Nanowires, Journal of Solid State Chemistry, 180, pp.467-473, 2007.
18. H. Zhu, H. Yang, W. Fu, **P. F. Zhu**, M. Li, Y. Li, Y. Sui, S. Liu and G. Zou, "The Improvement Of Thermal Stability of $BaMgAl_{10}O_{17}$: Eu^{2+} Coated with MgO, Materials Letters, 62, pp. 784-786, 2008.
19. G. Wei, W. Qin, **P. F. Zhu**, R. Kim, G. Wang, D. Zhang, K. Zheng and L. Wang, "Large-Scale Synthesis and Photoluminescence Properties of Aligned Multicore SiC-SiO_2, Nanocables," Journal of Nanoscience and Nanotechnology, 10(3): pp. 1964-1968, 2010.
20. W. H. Koo, W. Youn, **P. F. Zhu**, X. H. Li, N. Tansu, and F. So, "Light Extraction From OLEDS by Defective Hexagonal-Close-Packed Silica Array," Proc. of the SPIE Optics + Photonics 2012, Organic Electronics + Photonics, San Diego, CA, August 2012.
21. W. Koo, W. Yun, **P. F. Zhu**, X. H. Li, N. Tansu, and F. So, "P‐110: Light extraction of Phosphorescent OLEDs by Defective Hexagonal‐Close‐Packed Array," SID Symposium Digest of Technical Papers, vol. 43, pp. 1474-1476, 2012.
22. **(Invited Keynote Conference Paper)** N. Tansu, C. K. Tan, **P. F. Zhu,** and W. Sun, "Physics of High Efficiency and Efficiency-Droop in III-Nitride Light-Emitting Diodes," Proc. of the Progress in Electromagnetics Research Symposium (PIERS) 2014, Guangzhou, China, August 2014.
23. **(Tutorial Conference Paper)** N. Tansu, J. Zhang, G. Y. Liu, H. P. Zhao, C. K. Tan, and **P. F. Zhu**, "Internal and External Efficiency in InGaN-Based Light-Emitting Diodes," Proc. of the *Asian Communications and Photonics (ACP) Conference 2013*, Beijing, China, Nov 2013.
24. **(Invited Conference Paper)** N. Tansu, J. Zhang, G. Y. Liu, H. P. Zhao, C. K. Tan, and **P. F. Zhu**, "Physics of High-Efficiency III-Nitride Quantum Wells Light-Emitting Diodes," Proc. of the Asian Communications and Photonics (ACP) Conference 2012, Guangzhou, China, Nov 2012.
25. **(Invited Conference Paper)** J. Zhang, G. Y. Liu, C. K. Tan, **P. F. Zhu**, H. P. Zhao, and N. Tansu, "Engineering Nanostructures in Active Regions and Devices for High-Efficiency III-Nitride Light-Emitting Diodes – Epitaxy and Physics," Proc. of the SPIE Optics + Photonics 2012, NanoEpitaxy : Materials and Devices IV, San Diego, CA, August 2012.
26. **(Invited Keynote Plenary Conference Talk)** N. Tansu, J. Zhang, G. Y. Liu, C. K. Tan, **P. F. Zhu**, and H. P. Zhao, "Physics and Technology of III-Nitride Semiconductors for Energy Efficiency Applications," Proc. of the IUMRS-ICYRAM Conference 2012, Material Research Society (MRS), Singapore, July 2012.
27. **(Invited Conference Talk)** N. Tansu, J. Zhang, G. Y. Liu, C. K. Tan, **P. F. Zhu**, and H. P. Zhao, "Advances in III-Nitride Semiconductors for Energy Efficiency Applications," Proc. of the KAUST-UCSB-NSF Solid State Lighting Workshop 2012, Thuwal, Saudi Arabia, Feb 2012.

Journal Reviewing

- ✓ **Optical Materials Express (*Optical Society of America*)**
- ✓ **IEEE Photonics Journal (*IEEE*)**
- ✓ ***IEEE/OSA* Journal of Display Technology (*IEEE/OSA*)**
- ✓ **Journal of Photonics for Energy (*SPIE*)**
- ✓ **Intenational Journal of Photoenergy**
- ✓ **Optical Materials**
- ✓ **Nanoscience and Nanotechnology letters**